Flow characteristics and clogging phenomena in granular systems involving non-spherical particles

by

A. Vamsi Krishna Reddy

Roll No: 146107034

A thesis submitted
in Partial Fulfillment of the Requirements
for the Degree of

DOCTOR OF PHILOSOPHY.

Supervisor
Dr. K. Anki Reddy

Department of Chemical Engineering
Indian Institute of Technology Guwahati
Guwahati 781039, India.

September 2020

Flow characteristics and clogging phenomena in granular systems involving non-spherical particles

by

A. Vamsi Krishna Reddy

Roll No: 146107034

A thesis submitted
in Partial Fulfillment of the Requirements
for the Degree of

DOCTOR OF PHILOSOPHY.

Supervisor
Dr. K. Anki Reddy

Department of Chemical Engineering
Indian Institute of Technology Guwahati
Guwahati 781039, India.

September 2020

DECLARATION

I hereby certify that the work compiled in this thesis is the outcome of the research work, performed by myself, else stated, under the guidance of Dr K. Anki Reddy.

Any part of this work has not been submitted for the award of any degree, diploma, associate-fellowship, fellowship or it's equivalent to any university or institution.

A. Vamsi Krishna Reddy,
Registration No: 146107034
Department of Chemical Engineering
IIT Guwahati,
Guwahati-781039, Assam, India.
DATE: .....

CERTIFICATE

It is certified that the work contained in the thesis entitled "*Flow characteristics and clogging phenomena in granular systems involving non-spherical particles*" by Mr A. Vamsi Krishna Reddy, a student of the Department of Chemical Engineering, IIT Guwahati was carried out under my supervision and has not been submitted elsewhere for the award of any degree.

Dr K. Anki Reddy,
Department of Chemical Engineering, IIT Guwahati,
Guwahati-781039, Assam, India.
DATE: .....

ACKNOWLEDGMENTS

Firstly, I would like to thank my supervisor, Dr K. Anki Reddy, without whom this thesis would not have been possible. His persistent guidance, motivation, and recommendations have shaped my basic understanding of this domain to a great extent during my research work. I have learned a lot from him during this short research career so far, and I hope to learn furthermore in the forthcoming years.

Besides my supervisor, I would like to acknowledge the doctoral committee members, Prof. Anugrah Singh, Dr Rajesh Kumar Upadhyay, Prof. Gautam Barua, and Prof. Raghvendra Gupta, for their valuable recommendations and insightful remarks throughout research activities, which has encouraged me continuously towards undertaking a meaningful thesis work. Further, special appreciation for the support staff of the Department of Chemical Engineering.

I would also like to thank IITG for providing HPC (PARAM-ISHAN) facility for performing my simulations and the Government of India. I would like to extend my sincere gratitude to the Ministry of Human Resource Development and Indian Institute of Technology Guwahati for providing financial assistance, which reinforced me to study comfortably.

I would sincerely appreciate all my fellow lab-mates-friends: Mr Swamy Sumanth Raju, Mr Manish Dhiman, Mr Bitang Kwrung Tripura, Mr Abhishek, Mr Shivam Tiwari, Mr Kranthi Kumar, Mr Prashanth Tyagi, Mr Aman, Mr Raja Sekhar, Mr Vasistha, for their contributions towards my dissertation: be it providing valuable suggestions in manuscripts or assisting me in coding or any technical issues. I would like to especially thank Mr Sonu Kumar for enriching discussions, immense contribution and valuable suggestions in two of my works. Without this group, my journey perhaps would have been of less fun.

I also owe thanks to my seniors as well as fellow mates: Dr Mallikarjun, Dr Anupoju Rajeev, Dr Jagan Mohan Rao, Miss Chouti Evangleen, Mr Vimalathithan, Mr Harish,

Mr Shivaji, Mr Nagireddy Sreenu, Mr Bharath, Mr Joy Prakash Das, Mr Kuldeep, Mr Rupam, Miss. Barnali Bhui, Mr Muni Raja, etc.

Special thanks to the following people: A.C. Bhaktivedanta Swami Prabhupada, Mahasundar Dasa Prabhuji, Chaitanya Dasa Prabhuji, Nareshwar Das Prabhuji, Ananth Govind Das Prabhuji, Krishna Prabhuji, Murali Lola Prabhuji, Venu Madhav Prabhuji, Narsimha Das Prabhuji, Loknath Das Prabhuji, Janardhan Prabhuji and all other prabhujis of Hare Krishna Movement for making my life more beautiful. I also thank Mrs Anwesha Mahantha for introducing me into the classical dance of Assam, Sattriya.

Special gratitude is due to my parents Late. Mr A. Koteswara Reddy, and Mrs A. Shanthi Sudha Devi, who have sacrificed a lot for me. I am immensely grateful to my grandparents Mr A. Bala Krishna Reddy and Late Mrs A. Madamma who nurtured me since my childhood. I wouldn't have reached so far without their love and constant support. I thank my brother A. Hari Teja Reddy whom I admire and am extremely grateful for his love, support and trust in me and special thanks to my sister- in-law, Mrs Shruthi Keerthi who supports me unconditionally. I would like to thank Lord Krishna for guiding me and supporting me all the way. Lastly and most importantly, I would like to thank Om Swamiji who is my constant inspiration. I am grateful to his brainchild, Black Lotus App, a meditation app, which transformed me in ways I have never dreamt of. I further than Swamiji for his another contribution - OS.ME platform, the kindest conrner on the internet which has become a source of inspiration, relaxation and creativity for me since an year.

A. Vamsi Krishna Reddy
Indian Institute of Technology Guwahati
September 2020

Abstract

This thesis examines the characteristics of the flow of granular systems involving non-spherical particles in a silo. The flow of an assembly of solid particles reminiscent of fluid flow can be witnessed in the form of landslides or during unloading of sand from trucks in a construction site or during the processing of raw materials in industries. Understanding the flow of solid particles or granular flow is of great importance in industries for effective plant operations and for producing desired products. Most of the experimental or numerical works dedicated to understanding the rheology of granular materials concentrated on systems consisting of either spherical or disc-shaped particles. However, the particles involved in industries are mostly non-spherical particles or mixtures involving non-spherical particles. In this regard, we studied systems involving elongated particles or a mixture of discs and elongated particles. When the orifice is slightly larger the particles flowing out of it, the flow might halt abruptly due to the formation of a stable structure of particles above the orifice. This is commonly termed as clogging phenomena, which is undesirable in industries as it leads to the stoppage of production. In our work, we varied the position and size of a circular insert above the orifice to reduce clogging. One interesting finding is the presence of two local minima in the clogging index when the height of the obstacle is increased from the orifice. Time-averaged flow fields for a mixture of elongated particles and discs revealed an increase in the stagnant zone beside the orifice with an increase in the fraction of dumbbells thus decreasing the velocity and flow rate of the mixtures. Moreover, we investigated how the flow dynamics are affected when the orifice is placed at an unconventional position: on a side wall in one case and in the other case, two orifices on the silo base. Here, we found a shift in the flowing zone towards the right-side wall with an increase in the fraction of dumbbells due to an expansion in the stagnant zone thus decreasing the velocity. The decrease in the velocity and flow rate with an increase in the fraction of dumbbells is also explained by an increase in the dynamic friction near

the orifice due to an increase in the affinity to interlock by the dumbbell particles. I observed that the flow rate is found to be maximum when the inter-orifice spacing is zero and with an increase in the inter-orifice distance, the flow rate is found to decrease and gets saturated at very large spacing. The time-averaged flow fields showed the presence of a stagnant zone on the silo base between the two orifices and with an increase in the inter-orifice distance, the stagnant zone is noticed to expand thus hindering the flow of particles through orifices. This is the reason for a decrease in the velocity and flow rate of particles with an increase in the inter-orifice spacing. Moreover, we analyzed how the increase in the size of the head of the snowman-shaped particles influence the clogging probability near the orifice.

TABLE OF CONTENTS

CHAPTER 1

INTRODUCTION

1.1 Granular materials

Granular medium is a system of distinct solid particles where the motion of an individual particle is independent of other particles and interacts only at contacts. The sand on the beach, desserts and pebbles, rocks on the mountains are a few examples of granular particles in nature. They can be seen in our daily lives in the form of food materials like rice, grains and coffee beans etc. Moreover, these materials are handled in diverse commercial industries like agriculture, mining, pharmaceutical, food, energy and many more. The size of these materials can range from fine powders to enormous meteors. The recent decades were inundated with research articles on the granular field. One reason is due to the applicability of granular physics in particulate matter, ranging from micro size to meteor size, and from mundane systems to major industrial hoppers. The second reason being the advent of numerical models and their ceaseless development regularly which opened new frontiers to tackle issues in this field. Thus researchers envisioned and applied the laws of granular physics to diversified fields including pedestrian behaviour, vehicular traffic, meteor impacts, landslides using experiments as well as numerical simulations to name a few.

Some of the major topics of interest for researchers regarding these unique particles are segregation [1, 2], pattern formation [3, 4], force chains [5, 6], meteor impacts [7, 8],

silo clogging [9, 10], artificial intelligence [11, 12] etc. The works including the flow of pedestrians [13], a flock of animals [14] or vehicular traffic [15] etc. are carried out using principles of granular matter in experiments and computations. Segregation among the particles is witnessed when they are subjected to vibration or rotation. One of the examples includes Brazil nut effect [16]. Pattern formation is one of the characteristics exhibited by these materials when they are in motion. This can be visualized in dunes. In the desert areas, quicksand acts like gas as it has less packing fraction due to fluidization. In non-cohesive granular systems, the force is transferred through a network of contacts namely force chains. Silos or hoppers are usually used in industries to accompany a large number of solid materials during storage or processing or packing. During the outflow of solids, the flow might get blocked at the orifice and this phenomenon is known as clogging. The jamming behaviour of granular material is recently applied in the manufacture of the universal gripper. “The Physics of Blown Sand and Desert Dunes”(1941) by Ralph Alger Bagnold, the pioneer in the field of granular materials, was one of the earliest books written on these omnipresent materials.

1.2 Flow of granular particles

The flow of granular particles is an interesting topic of research due to its complex behaviour, Spatio-temporal heterogeneity and the manifestation of diversified phenomena. The granular flows can be witnessed during the unloading of sand or gravel near the construction sites, during landslides or the flow of sand in an hourglass. In industries, the feeding of solid raw materials or extraction of processed solid goods is common sites. In a stationary pile of non-cohesive granular materials on a horizontal surface, the angle between the steep and the base is known as the angle of repose and it is one of the prime factors that influence the flowability of granular materials. One of the usages of the angle of repose along with the coefficient of friction is to calibrate DEM simulations. The magnitude of the angle of repose depends on many factors like static and dynamic coefficients of friction, the roughness of the surface on which the pile is placed, size and shape of the material used, the method used for measuring it etc [17]. The authors reported that the angle of repose was found to increase with an increase in the roughness of the base and particle surface, static and dynamic coefficient of friction, deviation from the spherical shape of the particle.

In granular shear flows, the volume of the granular material was noticed to increase due to shearing accompanied by the internal pressure forces among the particles and this phenomenon is known as dilatancy [18].

Granular matter exhibits versatility in the state when subjected to different flow conditions. Although they are solids individually, the particulate system as a whole behaves in a complex way. For instance, particles on an inclined plane remain stationary and manifest solid-state behaviour when the inclination angle is less than the angle of repose [19]. As the tilt angle increases beyond the angle of repose, the transition from solid to liquid-like behaviour is witnessed. When the tilt angle is further increased the system exhibits gaseous nature where interactions between particles cease to exist. In all the above cases, the matter as a whole displays unique characteristics in each of the states. Hence some researchers proposed that granular matter can itself be stated as a different state of matter instead of placing it in a solid-state or fluid state.

1.3 Silo flows

Silos or hoppers are huge cylindrical containers that are generally employed in industries while handling the flow of solid materials. Silo is a flat bottomed hopper while hopper has an inclined base with a small opening at the bottom which regulates the discharge rate of particles. There are primarily two kinds of flows in a hopper: mass flow or funnel flow. Mass flow involves a steady flow of particles through the bottleneck following "first in first out". Whereas in funnel flow, particles in the centreline discharges and those close to the walls either remain stationary or maintain insignificant velocities. Funnel flow is also an issue in industries which in some cases reduces the overall efficiency of the production. An extreme case of funnel flow is rat-holing where the flow is confined at the centre with a width equal to the orifice width throughout the silo while the particles are stagnant on either side of this central region. This kind of flow pattern has been observed [20] in the flow of elongated particles having an aspect ratio of 12.

1.4 Non-spherical particulate systems

Most of the research that has taken place was centred around spherical particles in 2D and 3D silos and hoppers. However, systems of perfect spherical granules are scarce in reality. So, comprehending the dynamics of non-spherical particulate matter is of great importance. Few researchers have attempted to understand the dynamics of non-spherical particles discharging out of a silo. Favier *et al.* [21] conducted experiments and numerical simulation of nonspherical particles with aspect ratio 1.4 for various orifice sizes. They observed a good agreement between the two methods and proposed a modified Beverloo's equation for computing flow rate. Cleary and Sawley [22] reported that the flow rate of elongated particles is 30% less than that of spherical particles. It is also observed that an increase in the blockiness decreases the discharge rate by 28%. Langston *et al.* [23] has reported that disc-shaped particles discharge 40% faster than the spherical particles in the absence of the friction between particles. Jintang li *et al.* [24] did a comparative study of the flow of spherical and disc-shaped particles using experimental and DEM method. They reported that discs flow 20-30% faster than spherical particles. They observed consistency in both the methods regarding flow pattern and clogged states. In Tao *et al.* [25] work, the mean voidage of corn-shape particles is found to be less than that of spherical particles. The mean voidage decreases with an increase in the ratio of width to length of hopper.

Jin Baosheng *et al.* [26] has reported that hexahedron particles displayed the fastest discharge rates and plug-like flow pattern. Whereas, the ellipsoidal, spherical and binary mixture of spherical and hexahedron showed parabolic profile while discharging. Liu *et al.* [27] reported that the flow rate of ellipsoidal particles is maximum when the aspect ratio is 1. It decreases with both increase or decrease in the aspect ratio. They modified Beverloo's equation by incorporating the variation of parameters C, k with aspect ratio to get the flow rate. Tamás Börzsönyi *et al.* [28] has conducted 3d experiments to determine the shape effect of granular particles on dynamics of silo discharges using X-ray tomography method. They reported that particles preferred vertical orientation in the flowing zone making small angles with the streamlines. The Dome shape of the particles is observed when they get clogged at the orifice similar to an arch formation in 2d systems. Ashour *et al.* [20] has reported that with an increase in the aspect ratio of particles, flow rate decreases whereas clogging probability increases. However, when the

aspect ratio is 12 a peculiar behaviour was observed where a vertical hole is formed from the bottom to the free surface which is termed as a rat hole.

The previous experimental and theoretical works were mostly on spherical particles in 2d and 3d inclined and normal silos and hoppers. Though there were few works dedicated to systems of non-spherical particles, they were mainly focused on flow regimes and mass flow rate analysis. It seems like there exists meagre research dedicated to analyzing the particle level dynamics for systems of non-spherical particles as well as a mixture of spherical and non-spherical particles.

1.5 Objectives

The objectives of this thesis are as follows:

- To understand the effect of position and size of the insert placed near the orifice on clogging probability.
- To assess how the fraction of dumbbells influence the flow of a mixture of discs and dumbbells.
- To analyse mixtures of dumbbells and discs at two eccentric flow conditions namely lateral orifice and multiple orifices on the silo base.
- To provide insights on the clogging phenomena in a system of asymmetric dumbbells or snow-man shaped particles.
- To probe how a continuous flow through a larger orifice helps in reducing the clogging at an adjacent smaller orifice.

The thesis is organized as follows:

Chapter 2: Simulation technique is elucidated.

Chapter 3: I studied the clogging phenomena in a two-dimensional silo consisting of dumbbells using the discrete element method (DEM) technique. The influence of the position and size of a circular insert on the clogging of particles near the orifice is analysed.

Chapter 4: Here, I reported the effect of the fraction of dumbbells on the flow dynamics of a mixture of discs and dumbbells in two flow regimes. The first one is a

steady-flow regime where we elucidated the flow dynamics through time-averaged flow fields (coarse-grained). Whereas, the other one is interrupting the flow regime, in which arch morphology is probed as the chances of the system getting clogged is more.

Chapter 5: Dynamics of granular particulate mixtures flowing through silo with orifices placed at unconventional positions are studied. In the first case, we placed the orifice on the sidewall and probed how the variation in the orifice width and in the fraction of dumbbells affect the flow dynamics. In the second case, the effect of varying distance between the two orifices placed on the silo on the flow is reported.

Chapter 6: Two different sized spheres/discs adjoined to each other is known as snowman-shaped particles. These are not uncommon in the industries due to cohesion or ineffective grinding operations etc. In this work, we studied how an increase in the size of one of the discs of the snowman influences the clogging near the orifice.

Chapter 7: The unclogging at a smaller orifice due to the continuous flow of non-spherical particles through an adjacent larger orifice is analysed. We varied the inter-orifice distance and studied how it affects the unclogging process.

Chapter 8: Conclusion and suggestions for future work.

Please note that the chapters from **3** to **7** are either published works in peer-reviewed journals or the manuscripts under preparation. So, there might be slight repetition in the simulation methodology as the discrete element method (DEM) has been employed in all the works.

BIBLIOGRAPHY

[1] J. M. Ottino and D. V. Khakhar. Mixing and segregation of granular materials. *Annual Review of Fluid Mechanics*, 32(1):55–91, 2000.

[2] K. M. Hill and J. Kakalios. Reversible axial segregation of binary mixtures of granular materials. *Phys. Rev. E*, 49:R3610–R3613, May 1994.

[3] Keiko M. Aoki and Tetsuo Akiyama. Spontaneous wave pattern formation in vibrated granular materials. *Phys. Rev. Lett.*, 77:4166–4169, Nov 1996.

[4] J.M.N.T. Gray and K. Hutter. Pattern formation in granular avalanches. *Continuum Mechanics and Thermodynamics*, 9(6):341–345, Dec 1997.

[5] M. E. Cates, J. P. Wittmer, J.-P. Bouchaud, and P. Claudin. Jamming, force chains, and fragile matter. *Phys. Rev. Lett.*, 81:1841–1844, Aug 1998.

[6] J.-P. Bouchaud, P. Claudin, D. Levine, and M. Otto. Force chain splitting in granular materials: A mechanism for large-scale pseudo-elastic behaviour. *The European Physical Journal E*, 4(4):451–457, Apr 2001.

[7] Amanda M. Walsh, Kristi E. Holloway, Piotr Habdas, and John R. de Bruyn. Morphology and scaling of impact craters in granular media. *Phys. Rev. Lett.*, 91:104301, Sep 2003.

[8] Simon J. de Vet and John R. de Bruyn. Shape of impact craters in granular media. *Phys. Rev. E*, 76:041306, Oct 2007.

[9] Angel Garcimartín Iker Zuriguel, Alvaro Janda. Silo clogging reduction by the presence of an obstacle. *Phsical review Letters*, 107:278001, 2011.

[10] C. Lozano, I. Zuriguel, and A. Garcimartín. Stability of clogging arches in a silo submitted to vertical vibrations. *Phys. Rev. E*, 91:062203, Jun 2015.

[11] Eric Brown, Nicholas Rodenberg, John Amend, Annan Mozeika, Erik Steltz, Mitchell R. Zakin, Hod Lipson, and Heinrich M. Jaeger. Universal robotic gripper based on the jamming of granular material. *Proceedings of the National Academy of Sciences*, 107(44):18809–18814, 2010.

[12] N. G. Cheng, M. B. Lobovsky, S. J. Keating, A. M. Setapen, K. I. Gero, A. E. Hosoi, and K. D. Iagnemma. Design and analysis of a robust, low-cost, highly articulated manipulator enabled by jamming of granular media. In *2012 IEEE International Conference on Robotics and Automation*, pages 4328–4333, May 2012.

[13] Dirk Helbing and Péter Molnár. Social force model for pedestrian dynamics. *Phys. Rev. E*, 51:4282–4286, May 1995.

[14] A. Garcimartín, J. M. Pastor, L. M. Ferrer, J. J. Ramos, C. Martín-Gómez, and I. Zuriguel. Flow and clogging of a sheep herd passing through a bottleneck. *Phys. Rev. E*, 91:022808, Feb 2015.

[15] Dirk Helbing and Benno Tilch. Generalized force model of traffic dynamics. *Phys. Rev. E*, 58:133–138, Jul 1998.

[16] Meheboob Alam, L. Trujillo, and H. J. Herrmann. Hydrodynamic theory for reverse brazil nut segregation and the non-monotonic ascension dynamics. *Journal of Statistical Physics*, 124(2):587–623, Aug 2006.

[17] Hamzah M. Beakawi Al-Hashemi and Omar S. Baghabra Al-Amoudi. A review on the angle of repose of granular materials. *Powder Technology*, 330:397 – 417, 2018.

[18] K. Hutter and K. R. Rajagopal. On flows of granular materials. *Continuum Mechanics and Thermodynamics*, 6(2):81–139, Jun 1994.

[19] Heinrich M. Jaeger, Sidney R. Nagel, and Robert P. Behringer. Granular solids, liquids, and gases. *Rev. Mod. Phys.*, 68:1259–1273, Oct 1996.

[20] A. Ashour, S. Wegner, T. Trittel, and 39:1045 Borzsonyi. Outflow and clogging of shape-anisotropic grains in hoppers with small apertures. *Soft Matter*, 13:402–414, 2017.

[21] M.H.Abbaspour-Fard J.F.Favier and M.Kremmer. Modeling nonspherical particles using multisphere discrete elements. *Journal of Engineering Mechanics*, 127, 2001.

[22] Paul W Cleary and Mark L Sawley. {DEM} modelling of industrial granular flows: 3d case studies and the effect of particle shape on hopper discharge. *Applied Mathematical Modelling*, 26(2):89 – 111, 2002.

[23] Feras Y. Fraige Basel N. Asmar Paul A. Langston, Mohammad A. Al-Awamleh. Discrete element modelling of non-spherical frictionless particle flow. *Chemical Engineering Science*, 59:425–435, 2003.

[24] Jintang Li, Paul A Langston, Colin Webb, and Tom Dyakowski. Flow of sphero-disc particles in rectangular hoppers—a {DEM} and experimental comparison in 3d. *Chemical Engineering Science*, 59(24):5917 – 5929, 2004.

[25] He Tao, Baosheng Jin, Wenqi Zhong, Xiaofang Wang, Bing Ren, Yong Zhang, and Rui Xiao. Discrete element method modeling of non-spherical granular flow in rectangular hopper. *Chemical Engineering and Processing: Process Intensification*, 49(2):151 – 158, 2010.

[26] Baosheng JIN, He TAO, and Wenqi ZHONG. Flow behaviors of non-spherical granules in rectangular hopper. *Chinese Journal of Chemical Engineering*, 18(6):931 – 939, 2010.

[27] S.D. Liu, Z.Y. Zhou, R.P. Zou, D. Pinson, and A.B. Yu. Flow characteristics and discharge rate of ellipsoidal particles in a flat bottom hopper. *Powder Technology*, 253:70 – 79, 2014.

[28] Tamás Börzsönyi, Ellák Somfai, Balázs Szabó, Sandra Wegner, Pascal Mier, Georg Rose, and Ralf Stannarius. Packing, alignment and flow of shape-anisotropic grains in a 3d silo experiment. *New Journal of Physics*, 18(9):093017, 2016.

CHAPTER 2

SIMULATION METHOD

We used numerical technique named discrete element method (DEM) [1] in all our works to study the particle level dynamics. One of the main advantages of the DEM technique is it stores the positions, velocities, forces, torques etc of all the particles at every timestep of the entire simulation. In this technique firstly, contacts are determined for each particle. Two particles i and j as shown in Fig 2.2 are said to be in contact if the overlap between the particles $\delta \geq 0$. In reality, the overlap of the particles is not possible however, it can be understood as the shrinking of the particle at the point of contact due to the normal force of the other particle. Once the contacts are recognised for all the particles, the normal F_n and tangential F_t components of the contact forces [2] are computed as follows:

$$F_{ij}^{n} = \sqrt{R_{\text{eff}}\delta_{ij}}(K_n\delta_{ij}\hat{\boldsymbol{r}}_{\boldsymbol{ij}} - m_{\text{eff}}\gamma_n \boldsymbol{v}_{ij}^{n})$$

$$F_{ij}^{t} = -min(\mu F_{ij}^{n}, \sqrt{R_{\text{eff}}\delta_{ij}}(K_t\boldsymbol{\Delta s}_{\boldsymbol{ij}} + m_{\text{eff}}\gamma_t \boldsymbol{v}_{ij}^{t})).$$

Then, these forces are substituted in the equations of motion where gravitational force F_g and contact forces F_c are the only forces considered.:

$$\frac{dm_i u_i}{dt} = F_g + \sum_{j=1}^{N} F_{c_j}$$

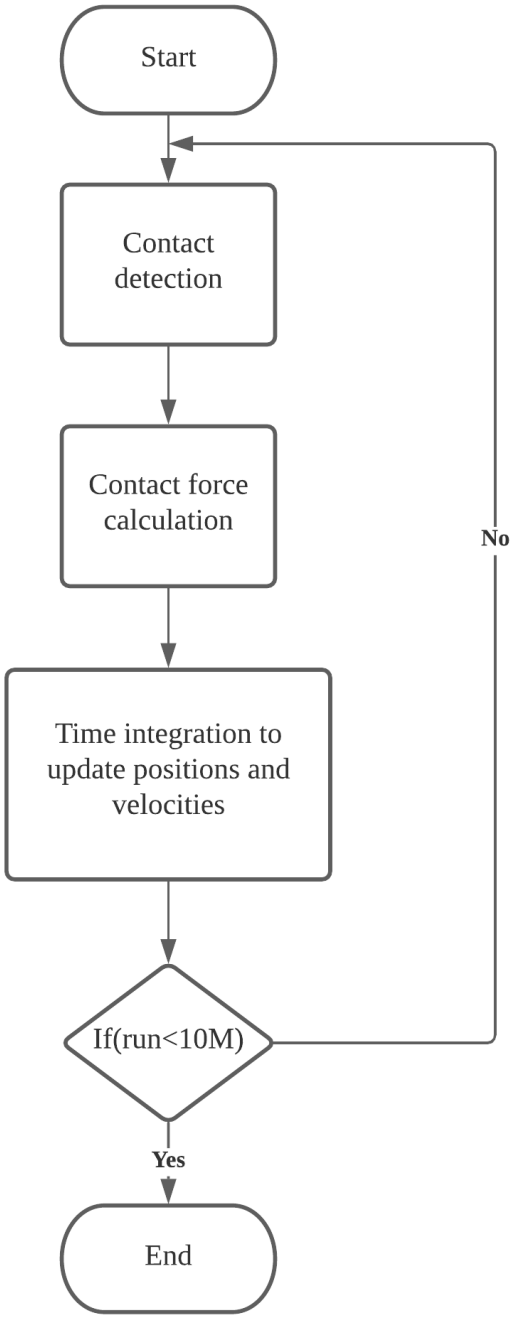

Figure 2.1: The flowchart depicting the flow of operations in a DEM technique.

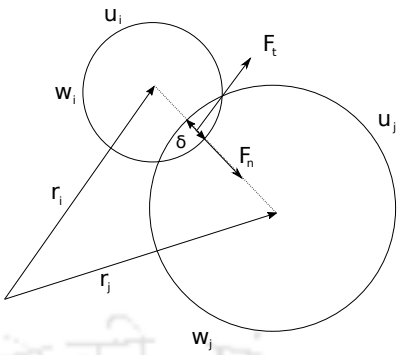

Figure 2.2: Two particles i and j in contact with r_i, r_j as their position vectors, u_i, u_j are their velocities and w_i, w_j are their rotational velocity vectors. F_n and F_t are normal and tangential forces acting at the point of contact of the two particles. Here, δ is the overlap between the two particles i and j.

The positions and velocities are updated at regular intervals of time by integrating the above equation using the velocity Verlet algorithm. The sequential flow of a DEM technique is displayed in Fig 2.1.

The subscripts or superscripts consisting of n, t corresponds to normal and tangential components of respective parameters and i, j denotes i^{th}, j^{th} particles. Here, $R_{\text{eff}} = \frac{R_i R_j}{R_i + R_j}$ is the effective radius where R is the radius of the particle. $\delta_{ij} = R_i + R_j - |\boldsymbol{R_{ij}}|$ is the overlap between the particles where $\boldsymbol{R_{ij}}$ is the position vector in the direction of line joining the centres of two particles i and j. K is the elastic constant, $\hat{\boldsymbol{r}}_{\boldsymbol{ij}}$ is the unit vector in the direction of line joining the particles i and j and $m_{\text{eff}} = \frac{m_i m_j}{m_i + m_j}$ is the effective mass where m is mass. γ is the damping coefficient, μ is the coefficient of friction, $\boldsymbol{\Delta s_{ij}}$ is the tangential displacement vector and $\boldsymbol{v}_{ij}^t$ is the tangential component of the relative velocity. For the case of dumbbells which are generated by fusing two discs, positions and velocities are computed as the centre of mass and centre of mass velocities from its two discs. The force acting on each dumbbell is calculated by adding total force acting on two discs of the dumbbell and assigning it to the centre of mass position of the dumbbell. The torque on each dumbbell is calculated in the same way as that of the force. Note that forces or torques experienced by a disc due to another disc that is part of the same dumbbell are set to zero. All of our simulations are performed in LAMMPS [3] and the visualization is done using OVITO [4].

The DEM has been an important tool to study the nature of granular particulate flow in different scenarios. Most importantly in recent decades, the usage of DEM has increased multifold due to the advent of supercomputers and good computational facili-

ties. It has been used in problems about an intruder moving through a granular media [5, 6], particles flowing over an inclined plane [7, 8], flow of particles through a hopper [9], frictional distribution in the granular media [10], analysing packing properties of particles [11, 12], contact networks in a granular media [13]. Moreover, this numerical technique has been used in determining jamming probability in confined granular systems [14–16], analysing mixing properties [17, 18], studying particle motion in rotating cylinders [19, 20], probing segregation dynamics [21–23], force chains [24, 25].

BIBLIOGRAPHY

[1] P. A. Cundall and O. D. L. Strack. A discrete numerical model for granular assemblies. *Géotechnique*, 29(1):47–65, 1979.

[2] Nikolai V. Brilliantov, Frank Spahn, Jan-Martin Hertzsch, and Thorsten Pöschel. Model for collisions in granular gases. *Phys. Rev. E*, 53:5382–5392, May 1996.

[3] Steve Plimpton. Fast parallel algorithms for short-range molecular dynamics. *Journal of Computational Physics*, 117(1):1 – 19, 1995.

[4] Alexander Stukowski. Visualization and analysis of atomistic simulation data with ovito–the open visualization tool. *Model. Simul. Mater. Sci. Eng*, 18(1):015012, 2010.

[5] Manish Dhiman, Sonu Kumar, K. Anki Reddy, and Raghvendra Gupta. Origin of the long-ranged attraction or repulsion between intruders in a confined granular medium. *Journal of Fluid Mechanics*, 886:A23, 2020.

[6] Sonu Kumar, Manish Dhiman, and K. Anki Reddy. Magnus effect in granular media. *Phys. Rev. E*, 99:012902, Jan 2019.

[7] Stanislav Parez, Einat Aharonov, and Renaud Toussaint. Unsteady granular flows down an inclined plane. *Phys. Rev. E*, 93:042902, Apr 2016.

[8] Anurag Tripathi and D. V. Khakhar. Rheology of binary granular mixtures in the dense flow regime. *Physics of Fluids*, 23(11):113302, 2011.

[9] Amlan Datta, B. K. Mishra, S. P. Das, and A. Sahu. A dem analysis of flow characteristics of noncohesive particles in hopper. *Materials and Manufacturing Processes*, 23(2):195–202, 2008.

[10] V. S. Akella, M. M. Bandi, H. George E. Hentschel, Itamar Procaccia, and Saikat Roy. Force distributions in frictional granular media. *Phys. Rev. E*, 98:012905, Jul 2018.

[11] Jieqing Gan and Aibing Yu. Dem simulation of the packing of cylindrical particles. *Granular Matter*, 22(1):22, Jan 2020.

[12] Q. Li, V. Rudolph, F.Y. Wang, and M. Horio. A study of particle packing compression under fluid drag force by dem simulations. *Developments in Chemical Engineering and Mineral Processing*, 13(5-6):693–708, 2005.

[13] A. Sufian, A. R. Russell, and A. J. Whittle. Anisotropy of contact networks in granular media and its influence on mobilised internal friction. *Géotechnique*, 67(12):1067–1080, 2017.

[14] Su-San Park and Eung Soo Kim. Jamming probability of granular flow in 3d hopper with shallow columns: Dem simulations. *Granular Matter*, 22(4):77, Sep 2020.

[15] Ya Zhao, Ray A. Cocco, Shiliang Yang, and Jia Wei Chew. Dem study on the effect of particle-size distribution on jamming in a 3d conical hopper. *AIChE Journal*, 65(2):512–519, 2019.

[16] Michel Tsukahara, Lionel Pournin, and Thomas M. Liebling. Simple probabilistic modeling of granular jamming and validation using dem. *AIP Conference Proceedings*, 1145(1):507–510, 2009.

[17] F. Bertrand, L.-A. Leclaire, and G. Levecque. Dem-based models for the mixing of granular materials. *Chemical Engineering Science*, 60(8):2517 – 2531, 2005. 5th International Symposium on Mixing in Industrial Processes (ISMIP5).

[18] Steffen Schmelzle and Herrmann Nirschl. Dem simulations: mixing of dry and wet granular material with different contact angles. *Granular Matter*, 20(2):19, Feb 2018.

[19] J. R. Third, D. M. Scott, S. A. Scott, and C. R. Müller. Tangential velocity profiles of granular material within horizontal rotating cylinders modelled using the dem. *Granular Matter*, 12(6):587–595, Dec 2010.

[20] S.S. Shirsath, J.T. Padding, H.J.H. Clercx, and J.A.M. Kuipers. Dynamics of granular flows down rotating semi-cylindrical chutes. *Procedia Engineering*, 102:731 – 740, 2015. New Paradigm of Particle Science and Technology Proceedings of The 7th World Congress on Particle Technology.

[21] Shiliang Yang, Liangqi Zhang, Kun Luo, and Jia Wei Chew. Dem study of the size-induced segregation dynamics of a ternary-size granular mixture in the rolling-regime rotating drum. *Physics of Fluids*, 29(12):123301, 2017.

[22] Wenguang Wang, Zhigang Zhou, Jin Zong, and Meiying Hou. DEM simulation of granular segregation in two-compartment system under zero gravity. *Chinese Physics B*, 26(4):044501, apr 2017.

[23] Ahmed Jarray, Hao Shi, Bert J. Scheper, Mehdi Habibi, and Stefan Luding. Cohesion-driven mixing and segregation of dry granular media. *Scientific Reports*, 9(1):13480, Sep 2019.

[24] Wei Wang, Wei Gu, and Kun Liu. Force chain evolution and force characteristics of shearing granular media in taylor-couette geometry by dem. *Tribology Transactions*, 58(2):197–206, 2015.

[25] Lingran Zhang, Nho Gia Hien Nguyen, Stéphane Lambert, François Nicot, Florent Prunier, and Irini Djeran-Maigre. The role of force chains in granular materials: from statics to dynamics. *European Journal of Environmental and Civil Engineering*, 21(7-8):874–895, 2017.

CHAPTER 3

GRANULAR SILO FLOW OF INELASTIC DUMBBELLS: CLOGGING AND ITS REDUCTION[1]

3.1 Introduction

Clogging is a common, and unwanted phenomenon during the discharge of granular material from a silo or hopper. It is also observed in active matter like a herd of sheep passing through a narrow door[1–3], in a crowd of pedestrians[4], panic escape [5, 6] and traffic jams [7, 8]. Clogging is typically the result of the particles forming an arch in two dimensions [9, 10] or a dome in three dimensions [11, 12] next to the orifice. Cates *et al.* [13] have termed clogged particles as fragile matter since an entire assemblage can be collapsed by applying a small external force at particular points of the arch. Various methods, including hitting or vibrating the silo[14–16], poking, or aiming compressed air at, the arches, have been proposed as practical methods to unclog silos. These solutions, however, have certain limitations in practice. For instance, vibrating a silo is not economical since it requires energy from an external source.

A recently proposed method to prevent, or reduce, clogging is to place an obstacle above the orifice [2, 17, 18]. Zuriguel *et al.* [18] have reported that a well-placed obstacle

[1]The article based upon the work reported in this chapter is published in *Phys. Rev. E*, vol. 98, 022904, year 2018; title: Granular silo flow of inelastic dumbbells: clogging and its reduction; authors: AVK Reddy, S Kumar, KA Reddy, J Talbot.

can reduce the clogging probability (CP) by up to a hundredfold. They proposed that the underlying mechanism is the pressure difference between the particles that are flowing below the obstacle and those that are flowing above. A similar phenomenon can be observed in active matter. In particular, Zuriguel *et al.* studied the effect of an obstacle on the flow properties of sheep passing through a narrow door [2]. They observed an increase in CP when the obstacle is close to the orifice as temporary clogging occurs between the obstacle and the bottom wall. On the other hand, when the obstacle is placed far from the orifice, it does not affect the clogging. Time taken for the egress of sheep was noticed to be minimum at an intermediate position of the obstacle. This suggests the existence of an optimum position where clogging is minimum. Recently, the effect of the shape of the obstacle on the clogging of spherical particles has been reported[17]. The authors have considered three different shapes of obstacle namely circular, triangular and inverted triangular. They reported that triangle-shaped obstacle is more effective than the circular one in reducing the clogging probability of a system of spherical particles.

Most of the 2D and 3D experimental and numerical studies of clogging in silos and hoppers were carried out for systems of spherical particles. However, most granular materials processed in industry, as well as those that occur in natural processes, are aspherical to some degree. So, understanding the flow dynamics of non-spherical particles is of great importance. In this regard, Börzsönyi *et al.* [11] conducted 3D experiments to determine the shape effect of granular particles discharging out of a silo using X-ray tomography. They reported that particles with a greater aspect ratio prefer to align vertically in the flowing zone. Ashour *et al.* [12] have analyzed the shape and size effect of non-spherical particles on clogging probability, flow rate and avalanche statistics. Until now, most investigations of non-spherical particulate systems [19–25] have focused mainly on modelling and computing flowrate. Few studies try to understand the physical mechanism above the orifice, where clogging occurs. Moreover, the effect of an obstacle on the flow of non-spherical particulate systems has not yet been investigated to the best of our knowledge. Therefore, here we present results of 2D numerical simulations of dumbbell-shaped particles discharging from a silo to analyze how the position and size of an obstacle affect the flow dynamics in the region above the orifice. Firstly, we performed numerical simulations in the absence of an obstacle for varying orifice width (W). Then, we placed a circular obstacle at various axial (H) and lateral (L) positions

while maintaining the orifice width (W) and diameter (D) of the obstacle constant. Later, we compared four different D's at $H = 10d$ and $L = 0d$.

The organization of the chapter is as follows. Section 3.2 outlines the simulation methodology and the force models used. In section 3.3, results and corresponding interpretations are discussed and section 3.4 presents our conclusions.

3.2 Simulation Methodology

In our study, we employed the Discrete Element Method (DEM)[26, 27] to simulate the gravity-driven flow of granular matter. We performed the simulations in quasi two-dimensions, i.e., the equations of motions are integrated along two dimensions with consideration of the third dimension for calculation of parameters such as the moment of inertia. An inelastic dumbbell consists of two fused, tangential spheres each of diameter d forming a rigid body. The simulation technique is explained in chapter 2.

The values of the various constants used in the simulations are $K_n = 2 \times 10^6 \rho dg$ and $K_t = 2.45 \times 10^6 \rho dg$ for a particle of density ρ (mass per unit volume). For a particle of density $\rho = 5000 kg/m^3$ and diameter $20mm$ in a gravitational field of $g = 9.8 m/s^2$, this represents roughly a material with Young's modulus of 1 GPa and Poisson's ratio of 0.3 [28]. Moreover, if we take K_n as high as 100 times its current value to represent materials such as steel, the instantaneous flow rate and the number of particles discharged as a function of time barely changes (see Fig. 3.2). Thus, we can use $K_n = 2 \times 10^6 \rho dg$ to represent realistic materials. In our simulations, we choose a damping coefficient $\gamma_n = \gamma_t = 2500\sqrt{g/d^3}$ to represent a realistic coefficient of restitution curve with respect to collision velocity. The coefficient of friction is chosen as 0.5 and a time-step of $10^{-4}\sqrt{d/g}$ is taken in our simulations. The positions and velocities of the dumbells are defined as the centre of mass positions and centre of mass velocities of the two adjoining spheres. Forces between the two fused spheres are turned off and by considering the force and torque on the dumbbell as the sum of the forces and torque on each of the constituent spheres, i.e., $\boldsymbol{F}_I = \sum_{n_i=1}^{2} \boldsymbol{F}_{I,n_i}$ for force along x on I^{th} dumbbells consisting of spheres $n_i = 1$ and 2 where $\boldsymbol{F}_{I,n_i}$ is the force vector on the n_i sphere of the I^{th} dumbbell while $\boldsymbol{F}_I$ is the net force vector acting on the dumbbell. Each simulation is carried out for the time it takes the system to fully discharge or until clogging occurs. The initial configurations are generated independently of each other.

We simulated $N = 8000$ dumbbells in a system of size $100d \times 150d$ along x and y,

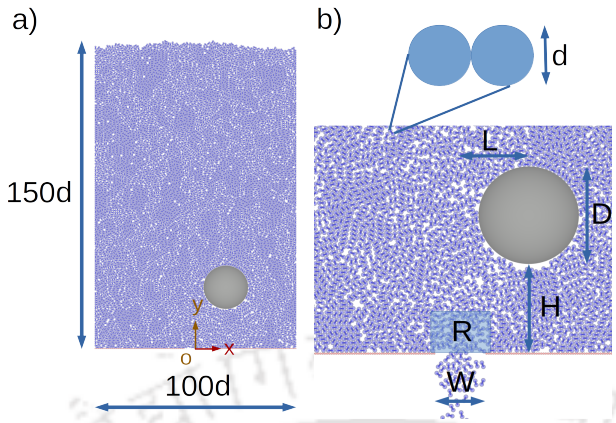

Figure 3.1: a) One of the configurations of our simulation box with dimensions $100d \times 150d$. b) View near the orifice. W is the orifice width, H is height of the obstacle and L is the horizontal distance from axis to the centre of the obstacle. In this image dumbbells are represented by lines to indicate their orientation.

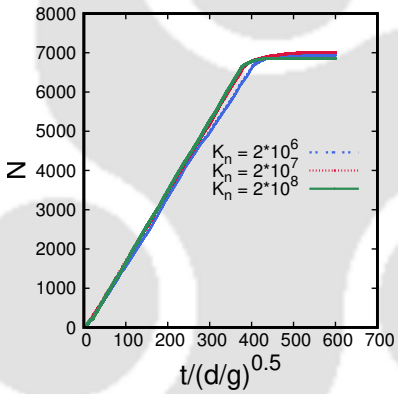

Figure 3.2: Number of dumbbells discharged N as a function of time t for different values of the normal elastic constant K_n at $W = 14d$.

respectively, enclosed by walls at $x = \pm 50d$ and $y = 0d$. A gravitational force of magnitude g acts in the negative-y direction. The initial configuration is generated by placing particles randomly in space with random orientations and letting them settle in the presence of gravity. This fills the system to a height of roughly $y = 150d$. The stress at a depth roughly equal to the silo width remains unchanged even when more particles are added into a silo because the frictional forces between the particles and lateral walls shift the additional stress towards the wall instead of the silo base through force chains. This behaviour is known as the Janssen effect [29]. The height of the granular bed in our system is taken as 1.5 times that of the silo width to maintain a constant pressure at the orifice during the discharge of particles. Fig. 3.1 shows the initial configuration for one of

the many cases we have considered in the study. Two spheres joined by a line represents a single dumbbell. We open the orifice at the beginning of each simulation to allow the flow of particles in the presence of gravity. The origin in our study represents the centre of the orifice located symmetrically between the two vertical walls.

All the simulations are carried out in LAMMPS [30] and the post visualizations are carried out in OVITO [31] and VMD [32].

3.3 Results and Discussions

In this section, we present the main results of our numerical simulations and their interpretation. We have considered four different variables in our study: the orifice width W, the axial height H, the lateral position L and diameter D of the obstacle (see Fig. 3.1(b)). In subsection 3.3.1, we present the results for the case without any obstacle for varying orifice widths. In subsection 3.3.2, the results for various values of H for $L = 0$ are discussed, while in subsection 3.3.3, the results for various values of L for a fixed H are discussed. In subsection 3.3.4, we report results for various values of D for constant H and $L = 0$.

We calculate the clogging index Ψ for a given run i as the ratio of undischarged particles to the initial number of particles. The particles that cannot undergo motion in a silo, such as the those in the stagnant zone next to the orifice, are subtracted. The number of particles in stagnant zone corresponds to the number of undischarged particles when clogging doesn't happen.

$$\Psi = \frac{1}{n} \sum_{i=1}^{n(\approx 15)} \frac{N_{\text{undis},i} - \overline{N}_u}{N_{\text{total}} - \overline{N}_u} \tag{3.1}$$

Here, $\overline{N}_u = (\overline{N}_{\text{undis},i}) = \sum_i N_{\text{undis},i}/m$, where m is the number of cases in which clogging does not occur, $N_{\text{total}} = 8000$ is the total number of dumbbells in our system and $N_{\text{undis},i}$ is the total number of particles that remain in the silo before the system's kinetic energy approaches zero for a given run i. Naturally, $N_{\text{undis},i} \approx \overline{N}_u$ for the case of full discharge.

Region R is defined above the orifice as shown in Fig. 3.1(b) with a length of $(W + 2d)$ along x and $10d$ along y as used in Ref. [17]. The packing fraction Φ of the particles in the region R is calculated as the ratio of the volume of particles lying in the region R to the total volume of the region R. Since this system is quasi two-dimensional, its thickness is taken as d for calculating the volume of the region R. The granular temperature is computed for region R as $T_g = \frac{1}{2}\langle (v_x - < v_x >)^2 + (v_y - < v_y >)^2 \rangle$ where $< . >$ denotes the

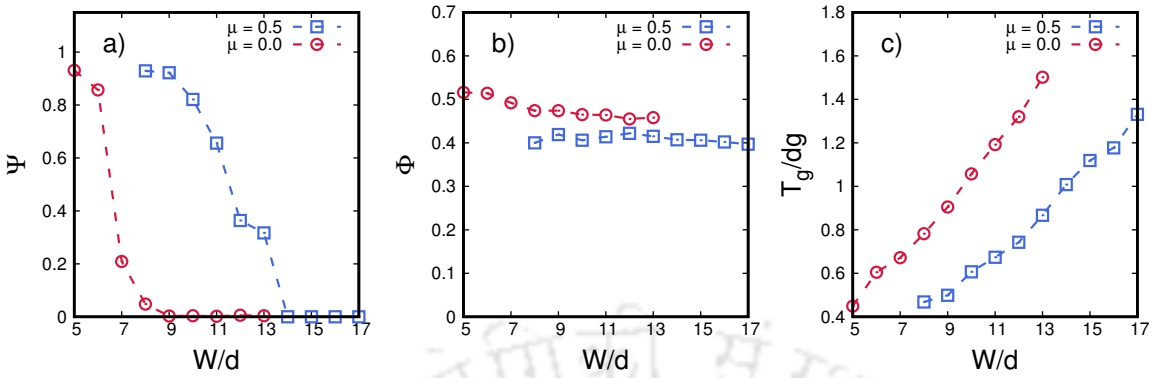

Figure 3.3: The variation of (a) Clogging index Ψ, (b) Packing fraction Φ and (c) Granular temperature T_g with respect to an orifice width of W for a silo without an obstacle.

spatiotemporal mean. All the results presented, including the velocity distributions, are averaged for approximately 15 independent runs using different initial configurations. We calculate all the quantities of interest by averaging over time until clogging, or full discharge occurs. We neglected any run in which clogging occurs before a minimum of 100 dumbbells discharge out of the silo. They correspond to those which are just above the orifice which will anyway flow when the orifice is opened.

3.3.1 Without Obstacle

In this subsection, clogging of dumbbells in the absence of an obstacle is discussed for various orifice widths W. The discharge of the dumbells is initiated by opening the orifice at time $t = 0$.

In Fig. 3.3(a), we show the clogging index Ψ as a function of the orifice width W for frictional (μ = 0.5) and frictionless (μ = 0.0) particles. One observes that the clogging index of frictional particles is almost unity for $W \leq 9d$, while it is approximately zero for $W \geq 14d$. Börzsönyi *et al.* [11, 12] have considered the critical orifice width ratio W_c/l_{eq}, where W_c is critical width and l_{eq} is the equivalent diameter of a spherical particle of volume equal to that of an aspherical particle. For disks in two dimensions, this ratio is found to lie between 4 to 5 [33]. In our case, however, we observe the critical width W_c to lie between $13d$ to $14d$ corresponding to a critical ratio in the range $10.3 < W_c/l_{\text{eq}} < 11.1$. This is in huge contrast to what is observed in the case of circular particles. Even if we consider, the longest dimension of the dumbbells $2d$, still W_c/l_{max} comes out to be around $6.5d$ to $7.0d$. Moreover, for frictionless dumbells, critical orifice width lies between $8d$

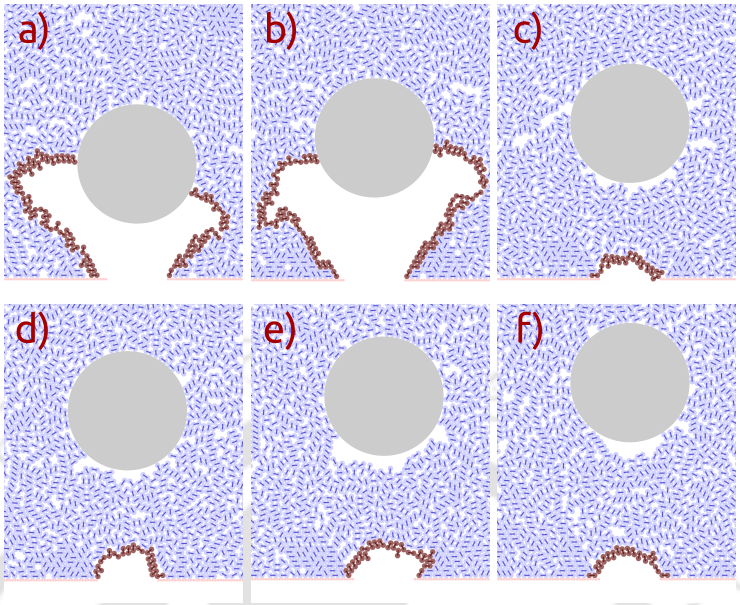

Figure 3.4: Clogged states at H = a) $10d$, b) $15d$, c) $17.5d$, d) $20d$, e) $22.5d$ and f) $25d$ with an orifice width of W =$11d$.

and $9d$ while it is slightly larger than $1d$ for hydrogel particles used in [34]. This high critical width ratio is due to many factors such as an orientational barrier, geometrical interlocking and a larger surface area of interaction compared to disks. Clogging can be induced due to an orientational barrier if a particle that has enough space to flow gets clogged due to improper orientation. An example of this in real life would be attempting to get a couch through a door. If the couch is improperly oriented it will not pass through. Similarly, an aspherical particle will experience the same difficulty. This, in turn, also induces anisotropy in the system as seen in [11]. Geometrical interlocking plays a role not just in enhancing clogging but also in stabilizing the clogging arch that is formed. Spherical particles have the least interlocking of all the particle shapes.

In Fig. 3.3 (b) and (c), we plot the packing fraction Φ and the granular temperature T_g (non-dimensionalized by dg), respectively, of the dumbbells contained in region R as a function of W. We notice that Φ is almost constant indicating that Ψ remains independent of Φ in the absence of an obstacle. The granular temperature T_g, however, increases with the orifice width. This can be explained by the increase in fluctuations of the velocity components as W increases which are due to an increase in the collision rate between the particles when particles on either side of the silo meet at the orifice as W is increased. This increase in T_g with W can also be explained by plotting the horizontal and vertical velocity distributions, v_x and v_y, respectively as shown in Fig. 3.5.

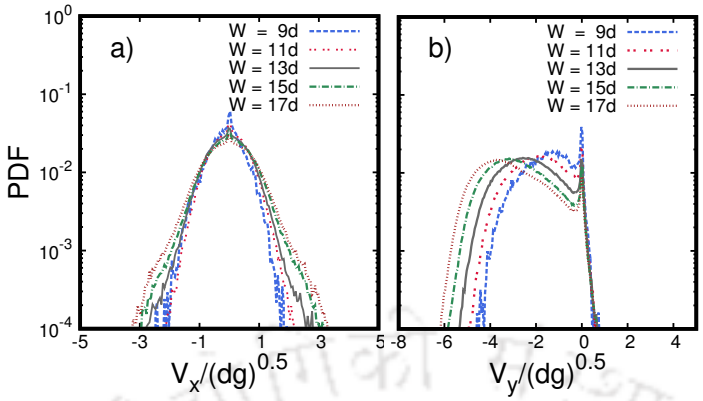

Figure 3.5: The probability distribution of (a) velocity component along x and (b) velocity component along y in region of analysis R for a silo without an obstacle .

The width of the distribution of horizontal and vertical components of particles in region R increases as W is increased, thus, justifying the increase in T_g.

3.3.2 Axial variation of the obstacle position

This subsection examines the clogging of dumbbells in the presence of a circular obstacle situated at a height H above an orifice of width $W = 11d$. We chose this width, as the clogging index at $W = 11d$ in the absence of an obstacle is approximately $\Psi = 0.66$ and hence can be used to study the increase or decrease in Ψ in the presence of an obstacle. Zuriguel *et al.* [18] observed that placing an obstacle at an appropriately chosen height greatly decreased the clogging of circular particles. In Fig. 3.6(a), we see that the clogging index is very high when the obstacle is close to the orifice exit. In this case, clogging is enhanced by the ability of the obstacle to forming arches with the exiting particles. On the other hand, we see that when the obstacle is positioned sufficiently far above the exit, the clogging index tends to approach that of the no obstacle case. This is explained by the fact that as the height of the obstacle increases, the more of its effect on the flow at the exit dissipate, thus mimicking no obstacle case. At intermediate heights, however, low values of the clogging index are observed. We see two local minima in Ψ (see Fig. 3.6(a)) at which $\Psi \approx 0.2$. i.e., about a three-fold reduction compared to a silo with no obstacle. However, another intriguing thing to notice is the maxima at $H = 20d$. This behaviour is explainable in terms of the type of clogging arch that is formed.

We observe that in the presence of an obstacle two types of clogging arches occur, namely one that involves and one that does not involve the obstacle. When the obstacle

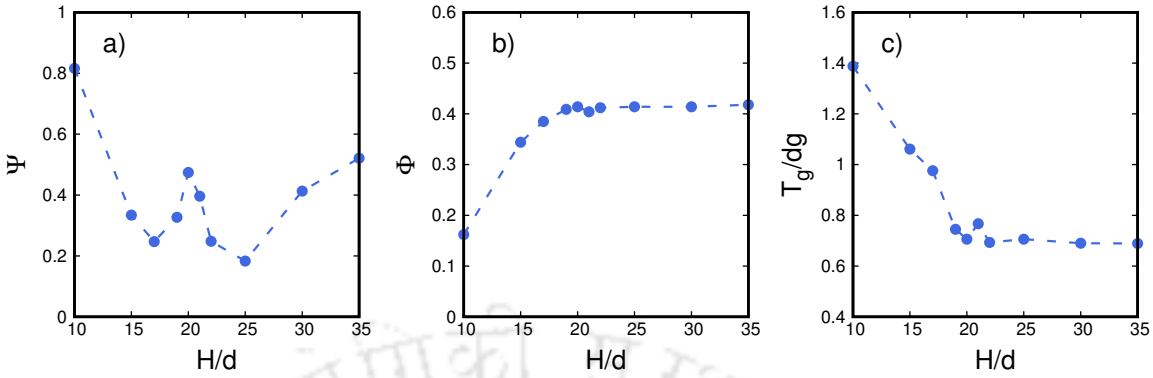

Figure 3.6: The variation of (a) Clogging index Ψ, (b) Packing fraction Φ, (c) Granular temperature T_g with respect to the vertical position of obstacle H at $L = 0d$ and $W = 11d$. All parameters are computed for particles in region R.

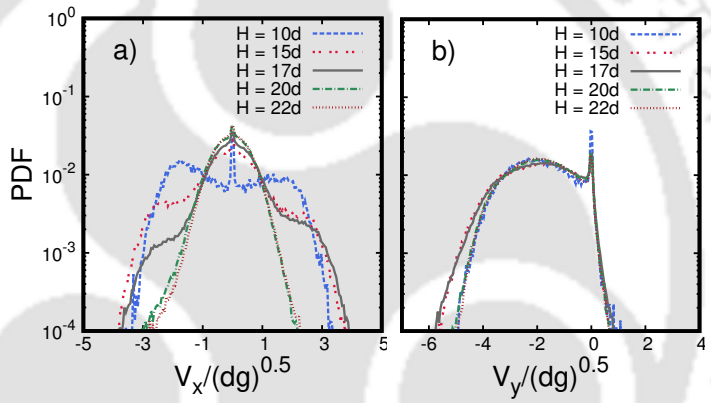

Figure 3.7: The probability distribution of the (a) horizontal and (b) vertical velocity component of particles in region R for a silo with $W = 11d$ containing an obstacle.

is very close to the orifice, clogging is mostly due to the first type while when it is far away, the clogging arches are formed only by the particles. The decrease and spike in the clogging index (see Fig. 3.6(a)) is for the obstacle's position in which transition from the first type of clogging arc to the second type takes place. Both types of arches are displayed in as in Fig. 3.4. When H = 10d, only the first type of arch is observed and for $H = 15d$ and $17.5d$ both types are witnessed. Whereas, for $H \geq 20d$, the only second type of arches is observed. This can be explained by the huge standard deviations in vertical heights of the arches for $H = 15d$ and $17.5d$ as shown in Table. 3.1. Figures 3.6(b) and (c) show the variation of Φ and T_g in region R with respect to H of the obstacle. We see that the packing fraction increases gradually while the granular temperature decreases with respect to H. Both saturate after a certain H. The presence of an obstacle close to the orifice reduces Φ due to the wake formed below the obstacle. Similarly, it increases

Table 3.1: Average width $\bar{w}$ and height $\bar{h}$, standard deviation of width σ_w and height σ_w of the arches averaged over n runs. The first row represents the case without an obstacle, the next set of rows are runs with an an obstacle present. The final set is with frictionless ones.

W/H	w_{avg}	σ_w	h_{avg}	σ_h	n
$W = 11d$	12.43	0.54	8.47	2.22	10
$H = 10d$	12.75	0.76	18.99	4.19	14
$H = 15d$	12.26	1.15	18.08	10.59	10
$H = 17.5d$	11.74	0.68	9.31	8.91	12
$H = 19d$	12.19	1.02	8.47	7.73	10
$H = 20d$	11.84	0.77	6.59	2.23	12
$H = 21d$	11.54	0.75	7.13	2.22	13
$H = 22.5d$	12.23	0.68	7.94	1.95	10
$H = 25d$	12.25	0.9	7.86	3.61	10
$H = 30d$	12.12	0.7	8.13	2.07	15
$H = 35d$	12.04	0.65	6.96	1.5	14
$W = 7d$	8.5	1.33	4.75	2.35	14
$W = 6d$	6.6	0.72	3.81	2.02	10

the fluctuation in velocities of particles in the region R as the particles moving on the alternate side of the obstacle collide in the region R giving rise to high fluctuations. This can be seen in Fig. 3.7 which shows the distributions of the horizontal and vertical velocity components. The width of the distribution decreases with an increase of H.

Interestingly, both Φ and T_g saturate at $H \approx 20d$. Although, this may indicate that the effect of obstacle ceases to exist in the region R, however, the spike in the clogging index is because of the transition from the first type of clogging arch to the second. At $H = 20d$, the clogging arcs are formed without the obstacle. The decrease in Ψ beyond that point may be related to the stability of the clogging arches which might be affected by the obstacle.

3.3.3 Lateral variation(L) of the obstacle

Earlier studies have shown the existence of optimal location of an obstacle for reducing clogging in the discharge of spherical particles from a silo [17], as well as for sheep passing through a narrow door [2]. In the present work, we examine if a *lateral* displacement of the obstacle leads to the reduction in the clogging. It should be noted that two stagnant zones (one on each side of the orifice) exist in our system. When the obstacle is displaced laterally, particles flowing on either side of it interact with the stagnant zones differently

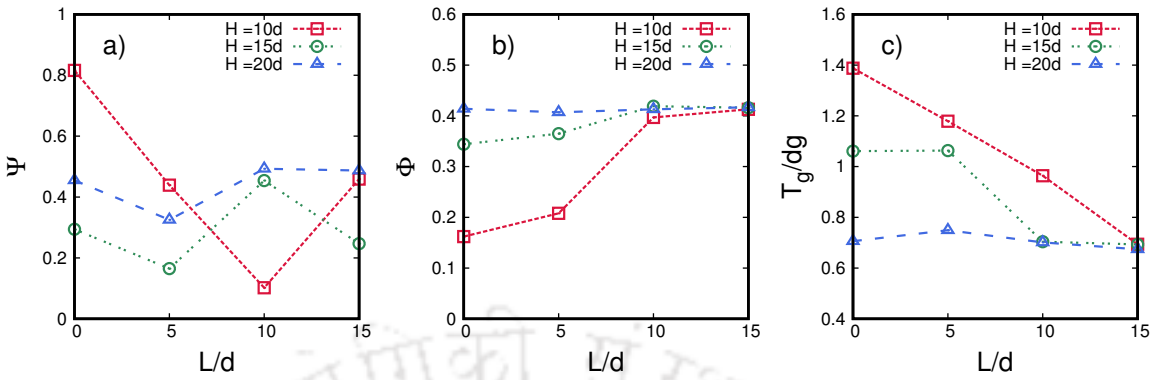

Figure 3.8: Variation of (a) clogging index Ψ, (b) packing fraction Φ, (c) granular temperature T_g for particles in region R with respect to the lateral position L of the obstacle with $W = 11d$ and constant H.

and this may lead to a change in the clogging index Ψ.

We observe that displacing the obstacle laterally may reduce clogging. Although the clogging index as shown in Fig. 3.8(a) shows variability it does show that there exists at least one location at which the clogging index Ψ is lower than for $L = 0$. Moreover, the presence of an obstacle away from the central vertical axis also increases the packing fraction of the particles in the region R up until $L/d \approx 10$ beyond which there is no dependence. The wake formed below the obstacle lies completely inside the region R for $L = 0d$ and $H = 10d$. However, for $L \geq 5d$, only a part of the wake lies in the region R thus providing more room for particles to fill.

The granular temperature T_g decreases with L (see Fig. 3.8(c)). When an obstacle is located symmetrically, i.e., $L = 0$, then the flow is separated into two halves that collide below the obstacle. However, as we increase L the flow rates on the right side of the obstacle decreases thereby reducing the collision rate as shown in Fig. 3.10. This is the reason behind the decrease in granular temperature.

The distribution of the horizontal velocity component at $H = 10d$ is shown in Fig. 3.9a. The plot is symmetric and widest at $L = 0$ since in this position the obstacle forces the particles to flow on either side of the obstacle. However, for $L \geq 5d$, the left part of the plot is very steep since the obstacle blocks particles flowing from the right side. Thus at $L = 5d$, even the particles on the right side are forced to flow from the left side. This results in additional stress on the particles corresponding to those in the stagnant zone on the left side of the orifice. The above phenomena coupled with the absence of collisions with particles flowing on the right side results in high horizontal and vertical

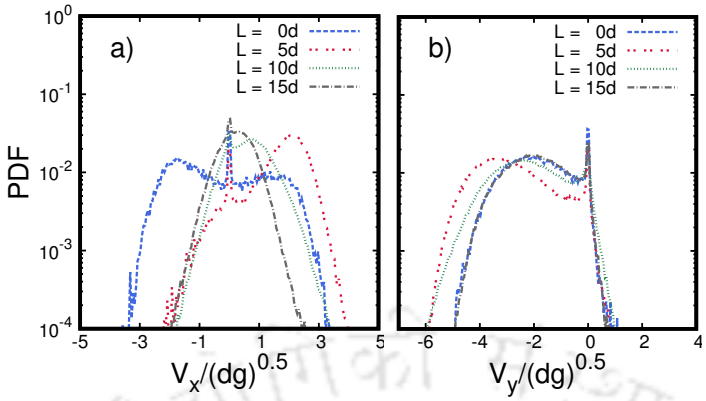

Figure 3.9: The probability distribution of the (a) horizontal and (b) vertical velocity component of particles in region R for a silo containing an obstacle with $H = 10d$, $W = 11d$ at various values of L.

velocities. This is consistent with the large width on the right side of the plot for $L = 5d$ in horizontal velocity distributions. However, for $L \geq 10d$, the width of the plot on the right side decreases gradually. As the obstacle is displaced further towards the right, most of the particles can reach the orifice without detouring around the obstacle. As a result lateral collisions, which are responsible for major variations in velocities, are almost absent for $L \geq 10d$ explaining the smaller widths on the right side of the plots. The distribution of the vertical velocity component for different values of L is displayed in Fig. 3.9 b. The width of the plot is least at $L = 0d$ indicating that the obstacle hinders the free flow of particles, thus reducing the vertical velocities in the region R. Whereas, the plots are slightly broader for $L \geq 5d$ as the interference of the obstacle in the free flow of particles gradually decreases.

3.3.4 Variation of the obstacle size

Here we consider the effect of varying the obstacle size D (for $L = 0$ and three different values of H) on the clogging index. Fig. 3.11 displays Ψ, Φ and T_g as a function of D at $W = 11d$ and constant H. Ψ increases with increase in D for $H \leq 15d$. During the discharge of the particles from the silo, a stagnant zone on either side of the orifice is present. As D increases, the distance between the obstacle and the stagnant zone(S_d) decreases. Moreover, the surface exposed to the stagnant zone increases. This coupled effect enhances the resistance to the free flow of particles at $D = 10d$ as displayed by high values of Ψ. At $D = 15d$, arches are primarily formed between the obstacle and

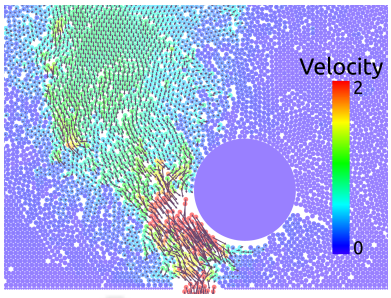

Figure 3.10: Velocity magnitude and vector field for the case of $H = 10d$ and $L = 10d$ (see Fig. 3.1 to get a clear idea about the location of the orifice and the obstacle) at a particular instant. The figure shows the interaction of obstacle with the stagnant zone as well. The reduction in T_g with L is a consequence of the reduced collision rate due to the blocking of the flow on the right. Note that, the dimensions of the silo shown here are the same as that of the one shown in figure 3.1 however, I have shown only the zoomed-in image close to the orifice.

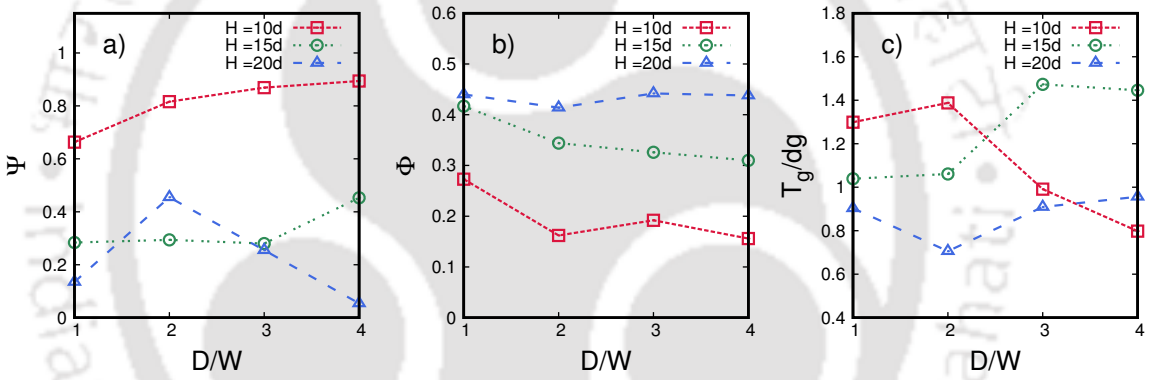

Figure 3.11: The variation of (a) Clogging index Ψ, (b) Packing fraction Φ and (c) Granular temperature T_g with respect to diameter of the obstacle D for various H at $W = 11d$ and $L = 0d$.

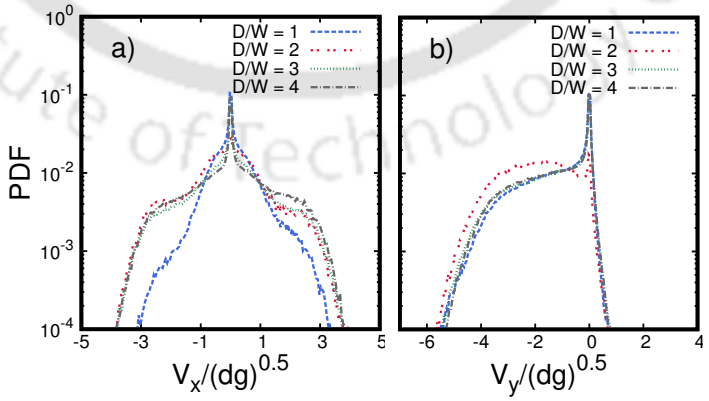

Figure 3.12: The probability distribution of (a) velocity component along x and (b) velocity component along y in region R for obstacle position $H = 15d$, $L = 0d$ in a silo having an orifice width $W = 11d$.

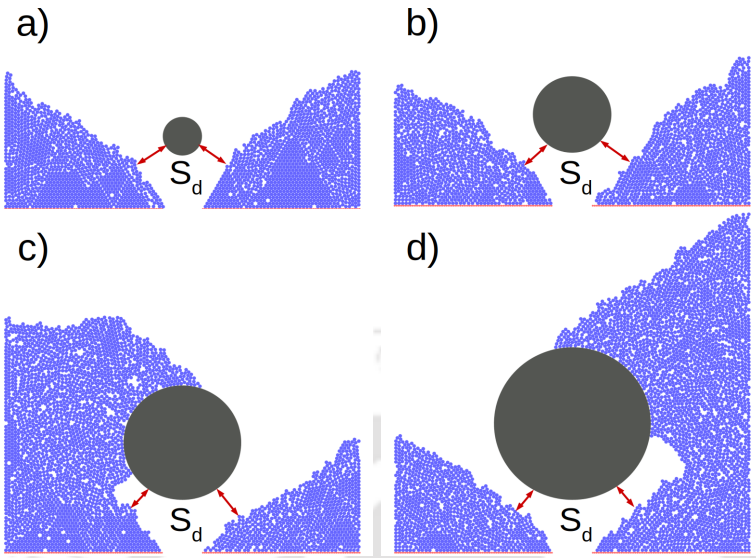

Figure 3.13: The distance between the stagnant zone and the obstacle at an orifice width W= a) 11d, b) 22d, c) 33d and d) 44d. Please note that, the dimensions of the silo shown here is same as that of the one shown in figure 3.1. However, I have shown only the part of the silo which is close to the orifice.

the bottom wall. This requires the arch height to be at least $15d$, which involves more particles to align in a particular way to resist the huge stress from the particles above. The other possibility of arch formation at $H = 15d$ is between obstacle and stagnant zone when particles pile up so that S_d is close to $5d$. Thus Ψ increases with an increase in D due to an increase in the exposed curvature of the obstacle to the stagnant zone and due to a decrease in S_d. However, Ψ exhibits a non-monotonic variation with D at $H = 20d$ rather than the steady rise observed for $H \leq 15d$. At $H = 20d$, arch formation involving the obstacle is almost negligible as $S_d > 15d$. So, the only possibility of arch formation is by particles near the orifice. Moreover, an increase in D creates a larger wake region below the obstacle due to its large curvature. Thus particles colliding below the wake region are less likely to be clogged for $H \geq 33d$. Ψ decreases with increasing D due to large wakes created below the obstacle for $H \leq 15d$. However, it remains almost constant for $H \geq 20d$ as, in this case, the wake is formed above region R. T_g increases as D increases for $H \geq 15d$. High horizontal velocities observed in the region R for $D \geq 33d$ due to the increase in the curvature of the obstacle. The distributions of the horizontal and vertical velocity components are displayed in Fig. 3.12.

3.4 Conclusion

In the present work, we studied the flow of a monolayer of dumbbells through an orifice at the bottom of a silo. We performed simulations of discharge flow for several orifice widths and observed that the clogging probability is close to zero when the orifice width is greater than 13d. This is equivalent to 6.5 times the particle length (major dimension of the dumbbell). We also studied the effect of placing an obstacle in the vicinity of the orifice on the granular flow. The size and position of the obstacle have a marked influence on the probability of clogging. While a previous study examined the effect of changing the vertical position only, we also considered changes in the lateral position. Even small displacements away from the vertical axis can substantially lower the clogging probability.

Compared with spherical particles, the clogging probability of the aspherical dumbbells is markedly higher, though velocity distributions of particles in the vicinity of the orifice, which characterize the particle dynamics, are qualitatively similar. It would be interesting to understand the particle dynamics near the orifice for aspherical particles of larger aspect ratios and complex shapes and to investigate whether we can relate their dynamics to the clogging. Another important observation from the present study is the nonmonotonicity of the clogging index as a function of the height of the the obstacle which is not observed in the case of spherical particles.

BIBLIOGRAPHY

[1] A. Garcimartín, J. M. Pastor, L. M. Ferrer, J. J. Ramos, C. Martín-Gómez, and I. Zuriguel, Phys. Rev. E **91**, 022808 (2015).

[2] I. Zuriguel, J. Olivares, J. M. Pastor, C. Martín-Gómez, L. M. Ferrer, J. J. Ramos, and A. Garcimartín, Phys. Rev. E **94**, 032302 (2016).

[3] J. M. Pastor, A. Garcimartín, P. A. Gago, J. P. Peralta, C. Martín-Gómez, L. M. Ferrer, D. Maza, D. R. Parisi, L. A. Pugnaloni, and I. Zuriguel, Phys. Rev. E **92**, 062817 (2015).

[4] D. Helbing, A. Johansson, and H. Z. Al-Abideen, Phys. Rev. E **75**, 046109 (2007).

[5] D. Elliott and D. Smith, Industrial & Environmental Crisis Quarterly **7**, 205 (1993), https://doi.org/10.1177/108602669300700304 .

[6] N. R. Johnson, Soc. Probl **34**, 362 (1987).

[7] B. S. Kerner and H. Rehborn, Phys. Rev. E **53**, R1297 (1996).

[8] Y. Sugiyama, M. Fukui, M. Kikuchi, K. Hasebe, A. Nakayama, K. Nishinari, S. ichi Tadaki, and S. Yukawa, New J. Phys **10**, 033001 (2008).

[9] A. Garcimartín, I. Zuriguel, L. A. Pugnaloni, and A. Janda, Phys. Rev. E **82**, 031306 (2010).

[10] R. C. Hidalgo, C. Lozano, I. Zuriguel, and A. Garcimartín, Granular Matter **15**, 841 (2013).

[11] T. Börzsönyi, E. Somfai, B. Szabó, S. Wegner, P. Mier, G. Rose, and R. Stannarius, New J. Phys **18**, 093017 (2016).

[12] A. Ashour, S. Wegner, T. Trittel, T. Borzsonyi, and R. Stannarius, Soft Matter **13**, 402 (2017).

[13] M. E. Cates, J. P. Wittmer, J.-P. Bouchaud, and P. Claudin, Phys. Rev. Lett. **81**, 1841 (1998).

[14] C. Lozano, G. Lumay, I. Zuriguel, R. C. Hidalgo, and A. Garcimartín, Phys. Rev. Lett. **109**, 068001 (2012).

[15] C. Lozano, I. Zuriguel, and A. Garcimartín, Phys. Rev. E **91**, 062203 (2015).

[16] Guerrero, Bruno, Lozano, Celia, Zuriguel, Iker, and Garcimartín, Angel, EPJ Web Conf. **140**, 03016 (2017).

[17] K. Endo, K. A. Reddy, and H. Katsuragi, Phys. Rev. Fluids **2**, 094302 (2017).

[18] I. Zuriguel, A. Janda, A. Garcimartín, C. Lozano, R. Arévalo, and D. Maza, Phys. Rev. Lett. **107**, 278001 (2011).

[19] S. Liu, Z. Zhou, R. Zou, D. Pinson, and A. Yu, Powder Technol **253**, 70 (2014).

[20] J. Li, P. A. Langston, C. Webb, and T. Dyakowski, Chem. Eng. Sci **59**, 5917 (2004).

[21] J. F. Favier, M. H. Abbaspour-Fard, and M. Kremmer, J Eng Mech **127**, 971 (2001).

[22] B. Jin, H. Tao, and W. Zhong, Chin. J. Chem. Eng **18**, 931 (2010).

[23] P. W. Cleary and M. L. Sawley, Appl. Math. Model **26**, 89 (2002).

[24] H. Tao, B. Jin, W. Zhong, X. Wang, B. Ren, Y. Zhang, and R. Xiao, Chem Engineer Process.ens **49**, 151 (2010).

[25] P. A. Langston, M. A. Al-Awamleh, F. Y. Fraige, and B. N. Asmar, Chem. Eng. Sci **59**, 425 (2004).

[26] P. A. Cundall and O. D. L. Strack, Géotechnique **29**, 47 (1979), https://doi.org/10.1680/geot.1979.29.1.47 .

[27] N. V. Brilliantov, F. Spahn, J.-M. Hertzsch, and T. Pöschel, Phys. Rev. E **53**, 5382 (1996).

[28] H. P. Zhang and H. A. Makse, Phys. Rev. E **72**, 011301 (2005).

[29] H. A. Janssen, Zeitschr. d. Vereines deutscher Ingenieure **39**, 1045 (1895).

[30] S. Plimpton, J. Comput. Phys **117**, 1 (1995).

[31] A. Stukowski, Model. Simul. Mater. Sci. Eng **18**, 015012 (2010).

[32] W. Humphrey, A. Dalke, and K. Schulten, J Mol Graph Model **14**, 33 (1996).

[33] A. Janda, I. Zuriguel, A. Garcimartín, L. A. Pugnaloni, and D. Maza, EPL (Europhysics Letters) **84**, 44002 (2008).

[34] X. Hong, M. Kohne, M. Morrell, H. Wang, and E. R. Weeks, Phys. Rev. E **96**, 062605 (2017).

CHAPTER 4

GRANULAR PARTICLE-SHAPE HETEROGENEOUS MIXTURES DISCHARGING THROUGH A SILO[1]

4.1 Introduction

A large assembly of randomly amassed solid particles, commonly termed as granular particles, is ubiquitous in both industries and nature. Granular particles discharging through silos or hoppers exhibit interesting phenomena like spatio-temporal heterogeneities [1], jamming [2], funnel flow [3], etc. This along with its applications in industries has garnered interest among the researchers to explore the characteristics of dense granular media flowing out of a silo. Some works [4–6] have been dedicated to comprehending the dynamic behaviour of spherical particles in silos or hoppers. However, solid particles involved in either industry or nature are often non-spherical. The shape of the flowing particles induces more complexity into the system, thus yielding yet new phenomena like ratholing [7] or local jamming because of strong interlocking among the particles. In non-spherical particulate flow, the shear-induced orientation of the particles at different depths also plays a crucial role in flow dynamics. Tamás Börzsönyi *et al.* [8] noticed that the longer axis of elongated particles or rods were not oriented parallel to the streamlines but encloses small angles

[1]The article based upon the work reported in this chapter is published in *J. Fluid Mech* vol. 912, year 2021; title: Granular particle-shape heterogeneous mixtures discharging through a silo; authors: AVK Reddy, S Kumar and KA Reddy.

during silo flow. The solid materials in practice are often heterogeneous mixtures due to imperfect processing while grinding or milling. So, a basic understanding of the flow dynamics of heterogeneous mixtures of particles, which vary in shape and size, is of great importance. Binary mixtures of spherical and non-spherical particles flowing out of a silo is a special case. Adding spherical particles to a system of non-spherical particles or vice versa shows a wide variety of phenomena such as lubricating effects, stratification and segregation. Wambaugh *et al.* [9] has observed lubrication effect by adding monomers to a collection of trimers (glueing three spherical particles side by side in a single line). Here, monomers or spherical particles acted as a lubricant, thus increasing the velocity of trimers on a vibrating ratchet-shaped base. The critical angle of repose of a sandpile consisting of spherical monomer grains was found [10] to increase with the addition of dimers. However, Zhiguo Guo *et al.* [11] has observed "needle particle effect" where the addition of elongated particles has enhanced the flow of fine granules. They argued that elongated particles played a major role in reducing cohesion and adhesion among fine granules, thus improving the flow conditions. A comprehensive understanding of the flow of mixtures helps in predicting flow rates which aid in effective handling of operations in industries.

One of the most widely accepted laws that predicts flow rate of grains discharging through silo proposed by Beverloo *et al.* [12] is $Q = C\rho_b\sqrt{g}(W - kD)^{n-\frac{1}{2}}$. Here Q, W, D are mass flow rate, orifice width and particle diameter, ρ_b is bulk density and C, k are empirical discharge and shape coefficients and $n = 2,3$ corresponds to the two-dimensional and three-dimensional system. The major limitation of this model is that it is valid for $W >> D$ and it fails to predict flow rates for small orifice widths where clogging is evidenced. To bridge this gap, Mankoc *et al.* [13] has proposed a modified expression for the number of beads discharged per unit time which is valid for orifice widths ranging from $2 < W/D < 100$ as $Q_b = C'(1 - \frac{1}{2}e^{-b(\frac{W}{D}-1)})(\frac{W}{D} - 1)^{n-\frac{1}{2}}$. Here, $C, \rho_b, \sqrt{g}$ of Beverloo's expression are clubbed into a single term C' and k is set to one which is obtained from the fit. Further, they reported that the introduced correction factor (exponential term) most possibly corresponds to the variation in grain density in the region above the orifice. The above-mentioned models apply to monodisperse particles. In reality, the granular systems are hardly monodisperse. In this light, modified Beverloo expressions were proposed for different binary mixtures. For instance, Artega and Tüzün *et al.* [14] has proposed a model for the flow rate of binary mixtures of equal density granules in cylindrical and conical hoppers. Whereas, for binary mixtures of fine particles flowing through a

sieve, Chevoir *et al.* [15] has proposed an alternative model. Recently, Benyamine *et al.* [16] empirically generated a flow rate expression for the binary mixture of glass beads. Researchers [17, 18] have proposed analytical expressions for flow rate which mostly apply to the large orifice width to particle size ratios $W/d >> 1$. In industries, often regulated flow of solid particles is essential during processing or packing. In regulated flows involving narrow outlets, particle flow might encounter hindrance or it might abruptly stop because of the blockage at the orifice. This phenomenon is commonly termed as clogging. In the flow of mono layered spherical particles, it has been noticed that clogging might occur at the orifice of the silo or in the bulk [19–21]. The latter type of clogging slightly hinders the flow, whereas the former one yields in complete stoppage of the flow. This issue of clogging at bottlenecks has been addressed in different ways like understanding the arch geometry [22], the stability of arches when subjected to external force [23] or placing an obstacle just above the orifice [24, 25] to alleviate clogging. The clogged structures of mutually stabilized particles formed above the orifice were found to be close to a semicircle or dome shape in two-dimensional and three-dimensional silos. To *et al.* [22] proposed that arches are convex everywhere by showing the angle Φ made by any arch particle with its two adjacent arch particles as less than 180^o for the case of mono layered spherical particles in a silo. However, Garcimartín *et al.* [26] proved the existence of local concavities in arches, namely defects ($\Phi > 180^o$), although they observed the ratio of height and half-width of the arch as close to one. Defects were found to be the weakest portions of an arch. Lozano *et al.* [27] observed that the resistance of the arch to vibrations of the silo is determined by Φ_{max}. The geometry of the arch gets more complex for the case of nonspherical particles [7, 28] such as elongated particles or dumbbells. However, to the best of our knowledge, there is hardly any work that deals with the geometry of arches in the case of heterogeneous mixtures. The flow of heterogeneous mixtures through silos has been a topic of interest due to its wide variety of applications in industries. Binary mixtures are a special case comprising only two types of particles that differs in either their shape or size. Experimental [16] and simulation [29] works were carried out for analysing bi-disperse mixtures of spherical particles varying in size. However, the dense solid mixtures in practice often consist of particles varying in shape. In the present work, we have analysed how the presence of dumbbell-shaped particles affects the flow of a mixture of disc and dumbbell particles in two-dimensional silos using numerical simulations. We have analysed flow characteristics by varying the orifice width W and the fraction of dumbbells X_{db} in the mixture. Two regimes

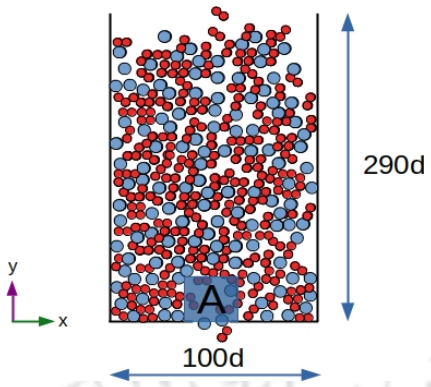

Figure 4.1: Schematic diagram representing a mixture of dumbbells (red circles) and discs (blue circles) in a two-dimensional silo. Here, d is the diameter of each circle of a dumbbell. Few parameters in our work are computed in the region A whose width is $W + 2\sqrt{2}d$ and height is $5\sqrt{2}d$, where W is orifice width. The origin is located at the centre of the orifice which is equidistant from both the side walls.

were analyzed namely, the free flow regime and interrupted flow regime. Firstly, in the free flow regime, flow is characterized by using various parameters like flow rate, area fraction, granular temperature. We plotted mean flow fields for various parameters to analyse the region above the orifice. In the interrupted flow regime, unlike the free flow one, the orifice might get blocked after some time because of the formation of mesoscopic structures of mutually stabilising particles. In this case, we focussed on the morphology of arches for different particle mixtures. Moreover, we determined the deviation of the arch shape from semicircle with the addition of dumbbells. The paper is organised as follows: Simulation methodology is explained in Section 4.2. The results obtained from numerical simulations for the free flow regime are explained in Section 4.3.1 and those of interrupted flow regime in Section 4.3.2. In Section 4.4, concluding remarks of the work are reported.

4.2 Simulation Methodology

We employed the Discrete Element Method (DEM) [30] to study the dynamics of granular mixtures of dumbbells and discs in a two-dimensional silo. Figure 4.1 shows the schematic representation of our system. Dumbbells are rigid particles created by fusing two circles, each of diameter d, adjacent to each other. The diameter of the disc is $D = \sqrt{2}d$ which is computed by considering the area of the dumbbell same as that of the disc. The total number of particles is $N = 15000$ for all fractions of dumbbells X_{db}. Firstly, dumbbells

and discs are placed at arbitrary positions with random orientations in a silo confined by walls at $x = \pm 50d$ and $y = 0$ while ensuring that there are no overlaps among them. Then, a gravity of magnitude g is applied in the negative-y direction. Once the particles get settled, the height of the assembly of particles reaches close to $290 \pm 10d$, which slightly depends on X_{db}. The origin is located at the centre of the silo base, which is also the centre of the orifice. At time $t = 0$, the orifice of width W on the silo base is opened to let the particles discharge out of the silo. Periodic boundary conditions are applied in y-direction and the particles discharged out of the silo are placed at random positions with reduced velocities at the top. The DEM technique is explained in chapter 2. The values of the constants used in the simulations such as elastic constants K_n and K_t are $2.0 \times 10^6 \rho d g$ and $2.45 \times 10^6 \rho d g$. The damping coefficients γ_n and γ_t are $1000\sqrt{g/d^3}$ and the subscripts n and t represents normal and tangential components of respective parameters. The coefficient of friction μ is taken as 0.5 and the timestep t_s is set to $10^{-4}\sqrt{d/g}$.

4.3 Results and Discussion

In this section, we will present numerical simulation results for our system of dumbbells and discs. Flow dynamics of mixtures that varied in the fraction of dumbbells X_{db} are analysed at different orifice widths W. The results pertaining to the free flow regime ($W/d \geq 15$) are explained in Section. 4.3.1. Time-averaged flow fields of various parameters in the absence of an obstacle are demonstrated in Section. 4.3.1.1 and we discuss the flow fields in the presence of an obstacle in Section. 4.3.1.2. In Section 4.3.2, results corresponding to interrupted flow regime ($W/d \leq 10$) are elucidated and in the next subsection, the morphology of arches are presented. We examine the flow characteristics at different orifice widths W using various parameters like flow rate Q, area fraction ϕ and granular temperature T_g. Flow rate Q is the average number of particles discharged per unit time before a clogging event or during the free flow of particles. Area fraction ϕ and granular temperature T_g are computed in the region A as shown in figure 4.1 which lies just above the orifice and whose length is $W + 2\sqrt{2}d$ in x direction and $5\sqrt{2}d$ in y direction respectively. Area fraction ϕ is calculated as the ratio of area occupied by all the particles in the region A and the area of region A. Granular temperature is a measure of fluctuations in translation and rotation velocities [34, 35] and is computed as $T_g = \frac{1}{3}\langle m\{(v_x - < v_x >)^2 + (v_y - < v_y >)^2\} + I(\Omega_z - < \Omega_z >)^2\rangle$. Here, v_x, v_y are the instan-

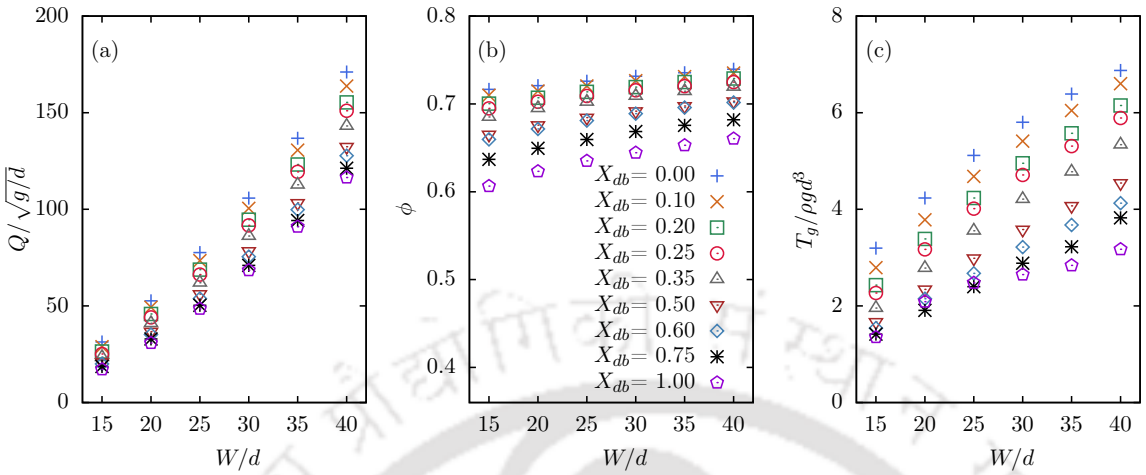

Figure 4.2: a) Flow rate Q, b) area fraction ϕ and c) granular temperature T_g as a function of normalised orifice width W/d for different fractions of dumbbells X_{db}. Here, d is the diameter of each of the circles in a dumbbell.

taneous velocities in x, y direction and Ω_z is the instantaneous angular velocity in z direction. Moreover, $< . >$ denotes spatio-temporal average over the region A and from time $t = 0$ to $t = T$. The mass and moment of inertia of the particles are indicated by m and I.

4.3.1 The flow of a mixture of discs and dumbbells in the freeflow regime

In this subsection, we will elucidate the numerical results for large orifice widths $W/d \geq 15$ where the free flow regime is observed. We analyse the flow characteristics at six different orifice widths W/d ranging from 15 to 40. To examine how the total number of dumbbells in the mixture affects the flow dynamics, we have considered nine different fractions of dumbbells X_{db} at each W/d. Figure 4.2 shows flow rate Q, area fraction ϕ and granular temperature T_g as a function of W/d. Q is noticed to increase monotonically with W/d for all X_{db}. Interestingly, at each W/d, Q is observed to decrease with an increase in the fraction of dumbbells X_{db}. We tried to find whether the average orientation of dumbbells is almost zero with the horizontal in the flowing zone which might hinder the flow. Figure 4.3 shows the average orientation of dumbbells θ at different horizontal positions x/D from the centre of the orifice $x, y = 0$ and θ at various angular positions

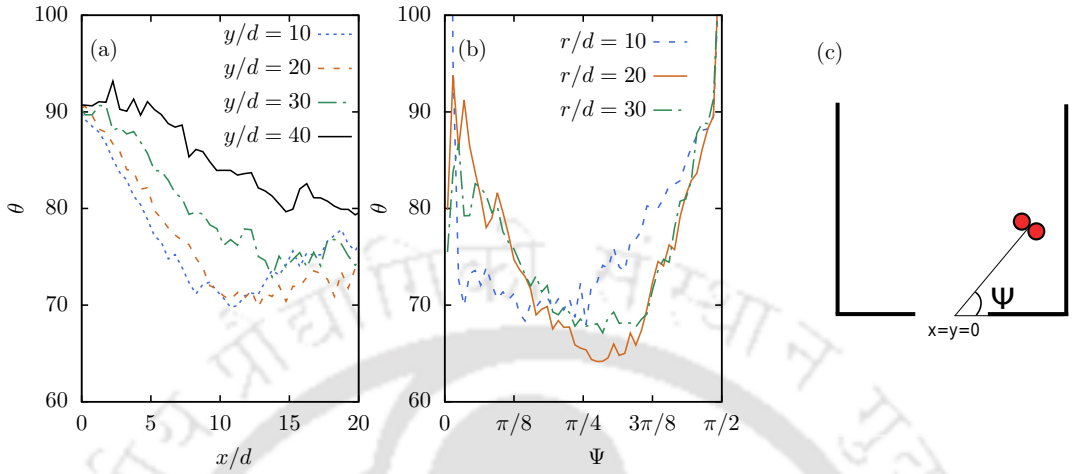

Figure 4.3: The mean orientation of dumbbells θ with respect to a) horizontal position x at different heights and with respect to b) angular position Ψ for different radii from the centre of the orifice. c) The angular position Ψ of the dumbbells is represented. The orientation of a dumbbell θ is computed as the angle between the larger axis of the dumbbell and the horizontal axis $x = 0$. The angular position Ψ is measured as the angle made by the line joining the centre of the orifice $x, y = 0$ and centre of the dumbbell with horizontal axis $x = 0$.

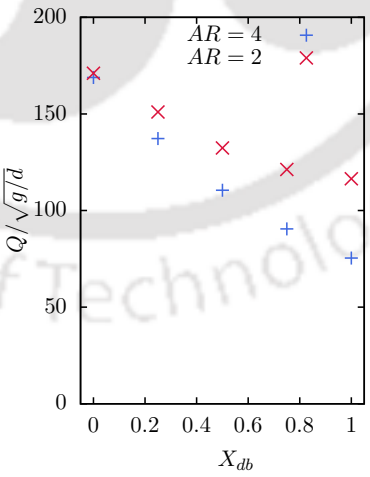

Figure 4.4: Flow rate Q as a function of the fraction of elongated particles X_{db} at an orifice width of $W/d = 40$ for a mixture of discs and elongated particles. AR corresponds to aspect ratio of the elongated particle.

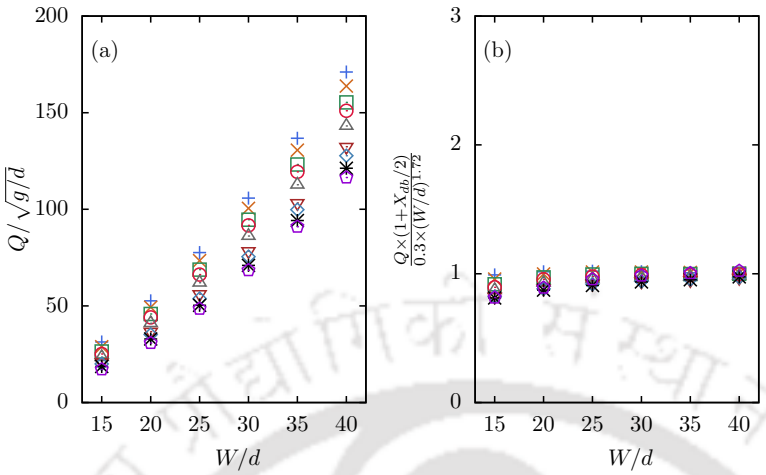

Figure 4.5: a) Flow rate Q and b) the flow rate Q scaling with the orifice width W and the fraction of dumbbells X_{db}, as a function of W/d for different X_{db}. Here, d is the diameter of each of the circles in a dumbbell.

Ψ of the dumbbells with $x, y = 0$ as the center. Both plots show that the longer side of the dumbbells is almost vertically oriented $\theta \approx 90^o$ at the centre line of the silo, $x = 0$ and $\Psi = 90^o$. As the position of the dumbbells shifts from the centerline, θ is observed to decrease, which can be seen in both plots. These results show that the dumbbells do not orient horizontally in the flowing zone, suggesting that the orientation of dumbbells is not the reason behind the decrease in Q with an increase in X_{db}. Tamás Börzsönyi *et al.* [8] observed that in a system of elongated particles, the longer side of the particles align to the flow and their average orientation makes small angles with streamlines. However, in our case, for $x/d > 10$, there is no correlation in the orientation of dumbbells due to the stagnant zone where velocities of the particles are almost zero. The reason for the decrease in Q with an increase in X_{db} could be due to the interlocking of particles. Spheres or discs can not interlock among themselves, but particles with higher aspect ratio are more prone to interlocking. An example of this is a robust bird's nest created by interlocking feeble twigs of high aspect ratios. In our case, dumbbells with an aspect ratio of 2 can interlock among themselves and hinders the flow. Moreover, dumbbells experience a much higher hindrance in their rotational degree of freedom, i.e., the spheres have their rotational freedom resisted by just the frictional forces as their rotation does not occupy any space. However, rotation of dumbbells entail particles surrounding them to undergo complete rearrangement. There may be these two namely

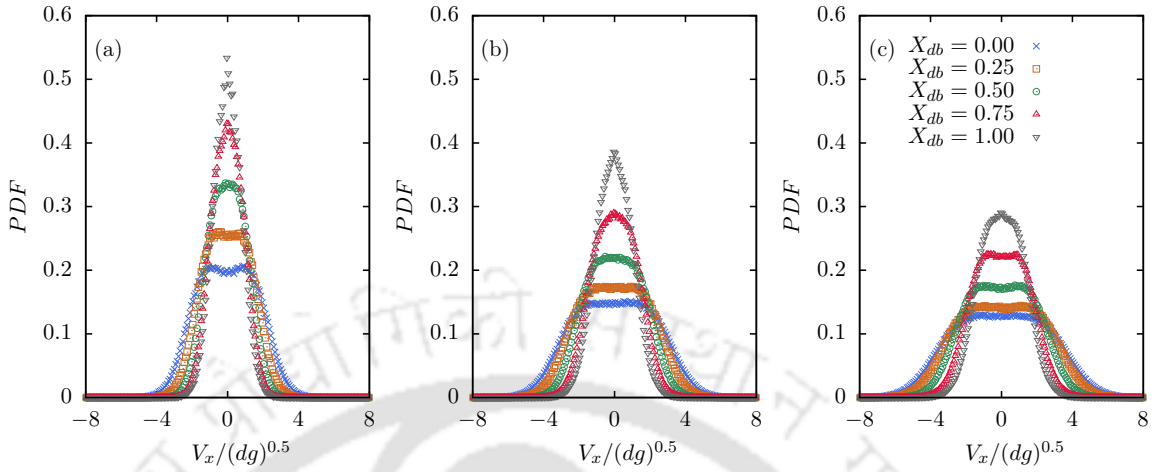

Figure 4.6: Probability distribution of horizontal velocities V_x of particles in region A at orifice widths W/d = a) 15, b) 25 and c) 35 for various fractions of dumbbells X_{db}.

geometrical interlocking and hindrance to the rotation that may compete or possibly one of the two may dominate in reducing the flow rate of the mixture with an increase in X_{db}. To validate whether the flow rate of the mixture decreases with an increase in the fraction of particles with a higher aspect ratio, we performed simulations with a mixture of discs and elongated particles with an aspect ratio of 4. The elongated particles (AR = 4) are generated by fusing four circles adjoining each other. Here, the mass and area of the elongated particles are taken the same as that of the discs so that the diameter of each circle of the elongated particle(AR=4) is $d_{AR=4} = 0.707$. The variation of flow rate Q in figure 4.4 shows a decreasing trend with an increase in the fraction of elongated (AR=4), (AR=2) particles X_{db} at $W/d = 40$. This indicates that adding elongated particles to a system of discs decreases the flow rate of the mixture provided the particles are non-cohesive and their areas are equal. The flow rate scaling with the orifice width as $0.3 \times (W/d)^{1.72}$ and with the fraction of dumbbells as $1 + X_{db}/2$ is shown in the figure 4.5.

Area fraction ϕ in the region A increases with W/d for all X_{db} as shown in figure 4.2b. As the orifice width increases, the flowing zone above the orifice increase and facilitates better rearrangement of the particles increasing the area fraction. However, ϕ decreases with an increase in X_{db} at all W/d because the void space formed inside a set of interconnected dumbbells is more than the void space formed inside a set of interconnected discs. Similar behaviour was observed previously [10] in a mixture of dimers and monomers. Granular temperature T_g increases steadily with W/d as shown

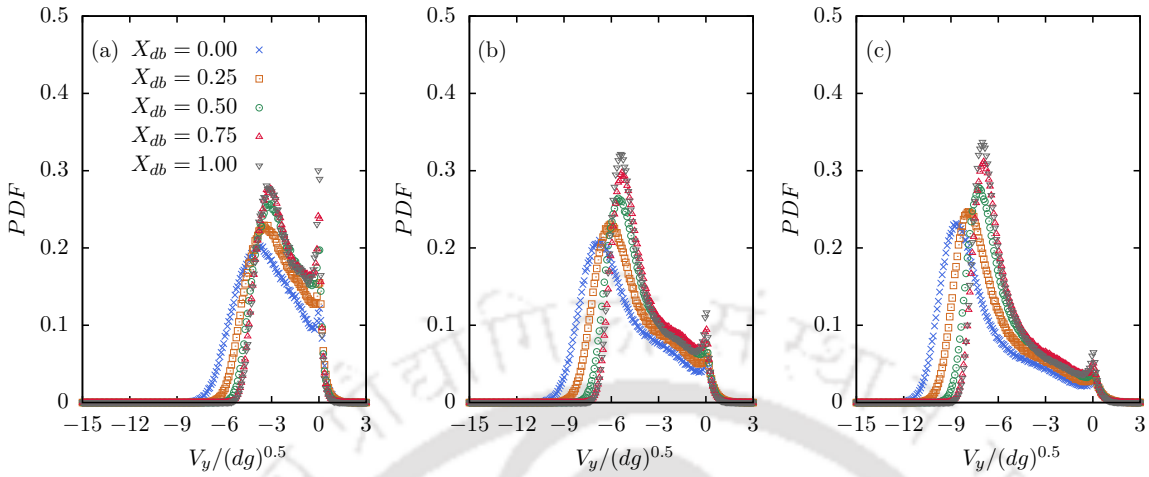

Figure 4.7: Probability distribution of vertical velocities V_y of particles in region A at orifice widths W/d = a) 15, b) 25 and c) 35 for various fractions of dumbbells X_{db}.

in figure 4.2c due to increase in the fluctuations of velocity components. This is due to an increase in the collision rates among the particles flowing from either side of the orifice resulting from an increase in the particle velocities with W/d. The increase in V_x with W/d is shown by an increase in the width of the probability distributions in figure 4.6a, 4.6b and 4.6c which corresponds to $W/d = 15, 25$ and 35. In figure 4.7, V_y is observed to increase with an increase in W/d in the form of first maxima whereas the maxima at $V_y = 0$ corresponds to those particles present on the silo base. Moreover, in each of the three plots of V_y distribution, the magnitude of the first maxima decrease with an increase in X_{db}. Consequently, T_g at all W/d is noticed to decrease with an increase in X_{db} as shown in figure 4.2c. Figure 4.8 shows velocity profiles as a function of horizontal position in the region A. Self similar profiles were observed when normalised horizontal $V_x/V_{x_{max}}$ and vertical velocities $V_y/V_{y_{max}}$ are plotted against normalised horizontal position x/W. In an earlier study [29], similar trends of velocity profiles were observed in the case of binary mixtures of spherical particles of two different sizes. The maximum velocity V_{max} in the region above the orifice increases gradually with W/d as shown in figure 4.8c. However, V_{max} decreases with an increase in X_{db} at all W/d because the addition of dumbbells hinders the flow as dumbbells can interlock more effectively among themselves than that of discs.

4.3.1.1 Mean flow fields

In this subsection, we will illustrate the spatial distributions of various parameters like area fraction ϕ, angular velocity Ω and its fluctuation Ω_{fl}^2, granular temperature T_g, shear stress τ, pressure P and velocity $\boldsymbol{v}$. The parameters at various spatial locations are computed using Gaussian coarse-graining function as implemented in [36]. The aforementioned parameters are computed at any position p with position vector $\boldsymbol{r_p}$ as follows:

$$\mathscr{W}(\boldsymbol{r}) = \frac{1}{\pi w^2} e^{-\boldsymbol{r}^2/w^2} \tag{4.1}$$

$$\phi(t) = \left[\sum_{i=1}^{n} \frac{\rho \pi d_i^2}{4} \mathscr{W}(\boldsymbol{r_p} - \boldsymbol{r_i(t)}) \right] / \rho \tag{4.2}$$

$$\Omega(t) = \left[\sum_{i=1}^{n} \frac{\rho \pi d_i^2}{4} \Omega_{z_i} \mathscr{W}(\boldsymbol{r_p} - \boldsymbol{r_i(t)}) \right] / \rho\phi \tag{4.3}$$

$$\Omega_{fl}^2(t) = \left[\sum_{i=1}^{n} \frac{\rho \pi d_i^2}{4} (\Omega_{z_i} - \Omega)^2 \mathscr{W}(\boldsymbol{r_p} - \boldsymbol{r_i(t)}) \right] / \rho\phi \tag{4.4}$$

$$\boldsymbol{v}(t) = \left[\sum_{i=1}^{n} \frac{\rho \pi d_i^2}{4} \boldsymbol{v_i} \mathscr{W}(\boldsymbol{r_p} - \boldsymbol{r_i(t)}) \right] / \rho\phi \tag{4.5}$$

$$T_g(t) = \frac{\sum_{i=1}^{n} \frac{\rho \pi d_i^2}{4} |\boldsymbol{v_i} - \boldsymbol{v}|^2 \mathscr{W}(\boldsymbol{r_p} - \boldsymbol{r_i(t)})}{2\rho\phi} \tag{4.6}$$

$$\boldsymbol{\sigma_{ij}(t)} = \sum_{\boldsymbol{i=1}}^{\boldsymbol{n}} \sum_{\boldsymbol{j=i+1}}^{\boldsymbol{n}} (\boldsymbol{F^{ij}} \times \boldsymbol{r_{ij}}) \int_{\boldsymbol{s=0}}^{\boldsymbol{1}} \mathscr{W}(\boldsymbol{r_p} - \boldsymbol{r_i(t)} + \boldsymbol{s r_{ij}}) \boldsymbol{ds} \tag{4.7}$$

$$P(t) = \frac{-tr(\sigma_{ij}(t))}{2} \tag{4.8}$$

Here, ϕ(t), Ω(t), Ω_{fl}^2(t), $\boldsymbol{v}$(t), T_g(t), $\boldsymbol{\sigma_{ij}}$(t) and P(t) corresponds to area fraction, rotational velocity, fluctuations in rotational velocity, velocity, granular temperature, stress tensor and pressure at time t. Whereas, ϕ, Ω, Ω_{fl}^2, $\boldsymbol{v}$, T_g, $\boldsymbol{\sigma_{ij}}$ and P are the time-averaged values of respective parameters over approximately 5000 frames. $\mathscr{W}(\boldsymbol{r})$ is Gaussian coarse-graining function with w = 1.414. Gaussian coarse-graining function at any position p is measured for all the particles i = 0 to n which satisfy $|\boldsymbol{r_p} - \boldsymbol{r_i}| < 3w$, where r_i is the position vector of a particle i. For each parameter, we have plotted flow fields corresponding to a different fraction of dumbbells X_{db} starting from 0.0 to 1.0. For all cases, the distributions are plotted in the space range of $-40d < x < 40d$ and $1.414d < y < 148.414d$ and the orifice width is W/d = 15. Figure 4.10 shows spatial

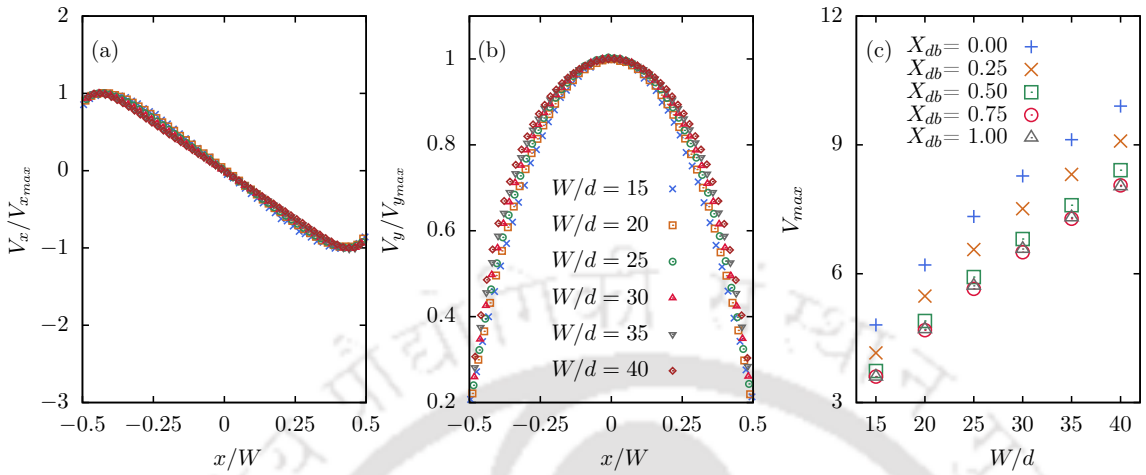

Figure 4.8: a) Normalised horizontal velocity V_x and b) normalised vertical velocity V_y profiles as a function of normalised horizontal position x/W at various widths W/d of the orifice. These plots correspond to $X_{db} = 0.5$. Similar trends were observed for all other X_{db}.

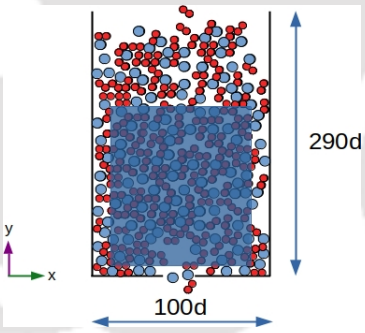

Figure 4.9: The region of interest for plotting flow fields is demonstrated. The shaded region corresponds to $-40d < x < 40d$ and $1.414d < y < 148.414d$.

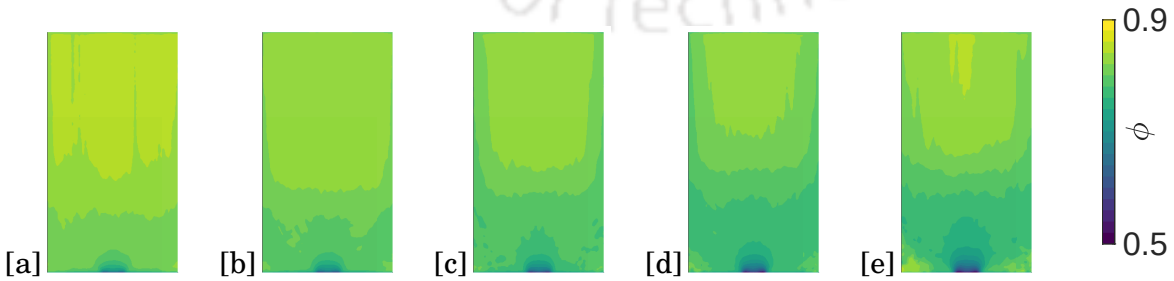

Figure 4.10: Spatial variation of area fraction at X_{db} = a) 0.0, b) 0.25, c) 0.5, d) 0.75 and e) 1.0 and width of the orifice is $W/d = 15$. The plots are averaged over approximately 5000 frames.

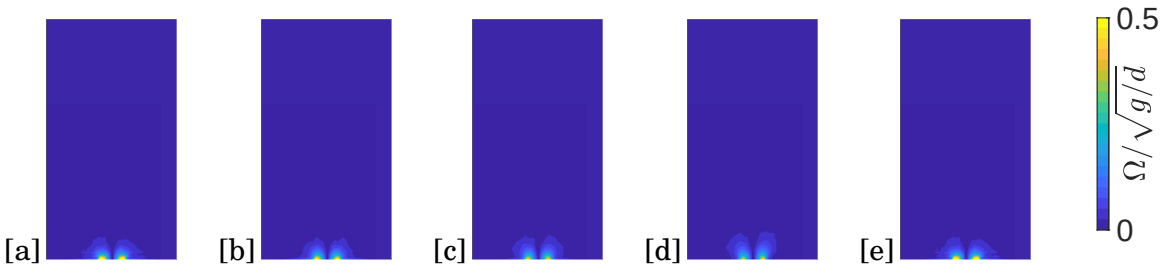

Figure 4.11: Spatial variation of rotational velocity Ω at X_{db} = a) 0.0, b) 0.25, c) 0.5, d) 0.75 and e) 1.0 and width of the orifice is $W/d = 15$. The plots are averaged over approximately 5000 frames.

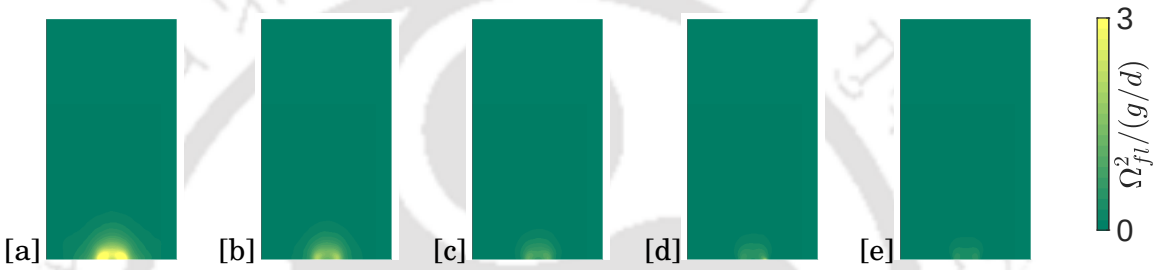

Figure 4.12: Spatial variation of fluctuations in rotational velocities Ω_{fl}^2 at X_{db} = a) 0.0, b) 0.25, c) 0.5, d) 0.75 and e) 1.0 and width of the orifice is $W/d = 15$. The plots are averaged over approximately 5000 frames.

distribution of area fraction ϕ at different X_{db}. Area fraction is less in the region above the orifice as compared to the bulk due to shear-induced dilation. Moreover, as X_{db} increases, ϕ is observed to decrease in the bulk as well as in the region above the orifice. This can be explained by an increase in the void space formed inside a set of three or more particles with the addition of dumbbells. This is due to the longer side of the dumbbells, which results in larger void spaces when the particles are randomly packed. Similar behaviour has been observed by Tamás Börzsönyi *et al.* [8] where they found a strong dilation in the case of elongated particles as compared to that of spherical particles. The angular velocity Ω as displayed in figure 4.11 is almost negligible in the bulk because the particles hardly rotate due to space constraint. However, small rotational velocities are observed near the orifice for all X_{db} because of the availability of space due to shear-induced dilation as observed in figure 4.10. Interestingly, the addition of dumbbells has very little effect on the angular velocities of the particles near the orifice. Fluctuations in rotational velocities Ω_{fl}^2 are almost negligible in the bulk for all X_{db} as shown in figure 4.12. However, as X_{db} increases, Ω_{fl}^2 near the orifice decrease. To rotate, discs require less space around them than that of a dumbbell. Thus discs can rotate easily, leading to

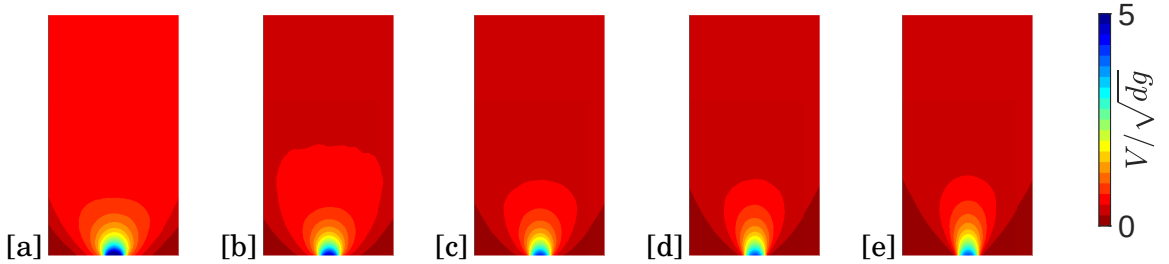

Figure 4.13: Spatial variation of velocities V at X_{db} = a) 0.0, b) 0.25, c) 0.5, d) 0.75 and e) 1.0 and width of the orifice is W/d = 15. The plots are averaged over approximately 5000 frames.

higher fluctuations in rotational velocity than that of dumbbells. The velocity V fields are shown in figure 6.12. Velocities of the particles are lower and almost constant in the entire bulk for all X_{db}. Higher velocities of the particles are observed only above the orifice because the particle motion is less obstructed by the surrounding particles in this region than that in the bulk. The regions of dark red beside the orifice corresponds to the stagnant zone or dead zone where the particles remain stationary or move with negligible velocities. The stagnant zone is found to expand with an increase of X_{db} due to the interlocking among the dumbbells. Thus, the flow pattern deviates from mass flow to semi-mass flow as X_{db} increases from 0.0 to 1.0. In a previous study [37], the size of the stagnant zone was found to increase with an increase in the aspect ratio of the particles. The stagnant zone beside the orifice hinders the movement of the particles flowing adjacent to it. This phenomenon coupled with geometrical interlocking results in the decrease of the velocity with an increase in X_{db} in the region above the orifice. Figure 4.14 demonstrates spatial distributions of granular temperature T_g. In the bulk, T_g is almost negligible because the particle velocities are almost constant as noticed in figure 6.12. However, in the region above the orifice, T_g decreases with an increase in X_{db}. With the addition of dumbbells, velocities of the particles approaching from either side of the orifice decrease resulting in a decrease in the velocity fluctuations. T_g is negligible in the region beside the orifice due to the presence of the stagnant zone. Moreover, the size of the stagnant zone where T_g is negligible is found to increase with an increase in X_{db} which is similar to that observed in figure 6.12. Pressure fields P are demonstrated in figure 6.13. In the bulk, pressure P is observed to be higher near the sidewalls than in the centre because the particles near the walls experience more stress as force chains are supported by the side walls. Figure 4.16 displays the force chains where its strength is found to be more near the walls as compared to that in the

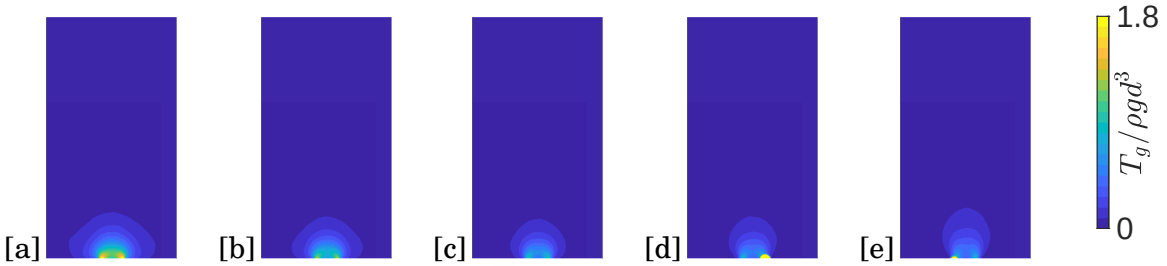

Figure 4.14: Spatial variation of granular temperature T_g at X_{db} = a) 0.0, b) 0.25, c) 0.5, d) 0.75 and e) 1.0 and width of the orifice is W/d = 15. The plots are averaged over approximately 5000 frames.

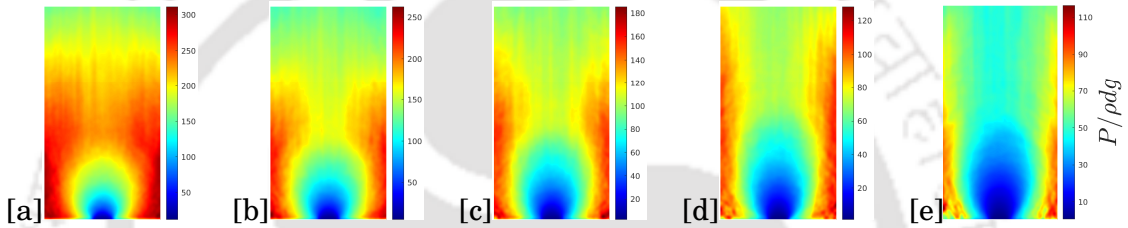

Figure 4.15: Spatial variation of pressure P at X_{db} = a) 0.0, b) 0.25, c) 0.5, d) 0.75 and e) 1.0 and width of the orifice is W/d = 15. The plots are averaged over approximately 5000 frames.

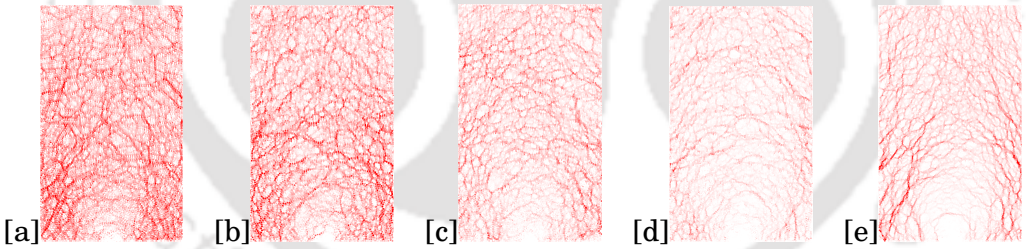

Figure 4.16: Fore chains inside the silo at X_{db} = a) 0.0, b) 0.25, c) 0.5, d) 0.75 and e) 1.0 and width of the orifice is W/d = 15.

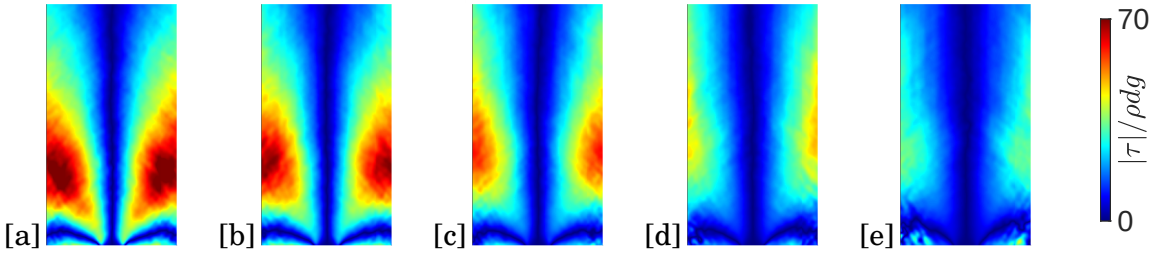

Figure 4.17: Spatial variation of shear stress τ at X_{db} = a) 0.0, b) 0.25, c) 0.5, d) 0.75 and e) 1.0 and width of the orifice is W/d = 15. The plots are averaged over approximately 5000 frames.

centre. In the region above the orifice, the pressure is least due to shear-induced dilation as observed in figure 4.10. However, P increases gradually as we go away from the orifice in the vertical direction due to an increase in the number density of the particles and thus the particles experience the load from the above particles. Similar behaviour has been observed previously [38] for pressure fields near the orifice. The pressure is found to be higher in the stagnant zone as compared to that of the flowing zone because of the presence of strong force chains supported by the side walls as well as the bottom wall. As X_{db} increases, the strength of force chains is noticed to decrease leading to a decrease in P. Figure 6.14 illustrate shear stress fields $|\tau|$ at different X_{db}. At the centre of the silo, as it is the flowing zone, interparticle shear stress $|\tau|$ is observed to be very less, which is similar to that observed in the flowing zone of liquids. However, $|\tau|$ increases close to the wall for all X_{db}. In the region beside the orifice, $|\tau|$ is noticed to be very less due to the presence of a stagnant zone. As X_{db} increases, $|\tau|$ is noticed to decrease because elongated particles hinder the movement of particles adjacent to them more effectively than that of the discs.

4.3.1.2 Mean flow fields in the presence of an obstacle

An obstacle placed at a proper position above the orifice has been proved [24, 25] to decrease the probability of clogging near the silo orifice. Zuriguel *et al.* [24] proposed that a pressure decrease in the region above the orifice due to the presence of an obstacle is the reason for the decrease in clogging probability. However, Endo *et al.*[39] proposed that placing an obstacle results in less packing fraction in the region of arch formation which causes a decrease in clogging probability. In both cases, it is evident that obstacle can dramatically influence the flow dynamics inside a silo. In this subsection, we will explain how the presence of an obstacle affects the mean flow fields of the mixtures. For all cases, the orifice width is $W/d = 12$ and the obstacle of diameter $D_{obs}/d = 24$ is placed with its centre at a height of $h_{obs}/d = 27$ from the base of the silo. Figure 4.18 displays the spatial distributions of area fraction ϕ at different fractions of dumbbells X_{db} in the presence of an obstacle. The obstacle impels those particles in its vicinity to detour around it to reach the orifice. It results in a wake formation downstream to the obstacle provided the particles are reaching the obstacle with high velocities as is the case in [40]. However, in our case, as velocities of the particles approaching the obstacle are less, the wake region is not evident for $X_{db} \leq 0.5$. A small wake is observed for $X_{db} \geq 0.75$ despite

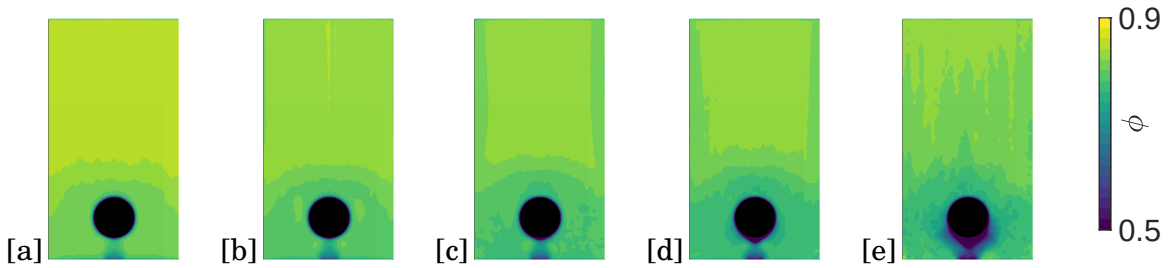

Figure 4.18: Spatial variation of area fraction at X_{db} = a) 0.0, b) 0.25, c) 0.5, d) 0.75 and e) 1.0 and width of the orifice is $W/d = 12$. The plots are averaged over approximately 5000 frames for a silo with an obstacle of diameter $D_{obs}/d = 24$ placed at height $h_{obs}/d = 27$.

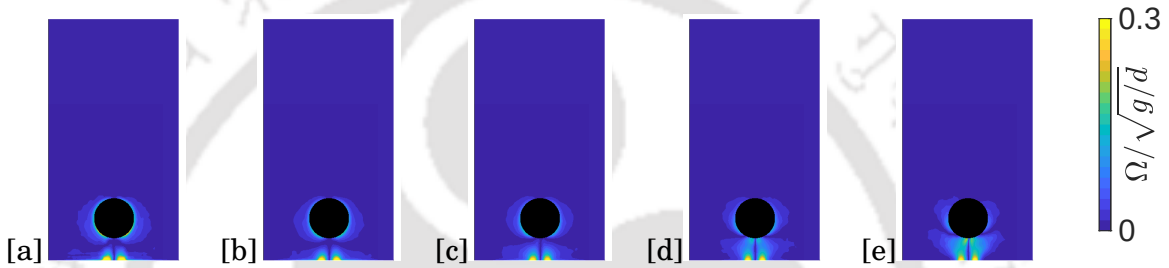

Figure 4.19: Spatial variation of rotational velocity Ω at X_{db} = a) 0.0, b) 0.25, c) 0.5, d) 0.75 and e) 1.0 is $W/d = 12$. The plots are averaged over approximately 5000 frames for a silo with an obstacle of diameter $D_{obs}/d = 24$ placed at height $h_{obs}/d = 27$.

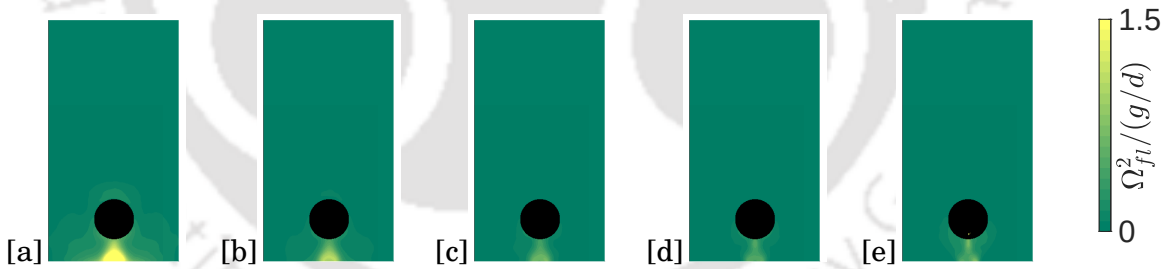

Figure 4.20: Spatial variation of fluctuations in rotational velocities Ω_{fl}^2 at X_{db} = a) 0.0, b) 0.25, c) 0.5, d) 0.75 and e) 1.0 and width of the orifice is $W/d = 12$. The plots are averaged over approximately 5000 frames for a silo with an obstacle of diameter $D_{obs}/d = 24$ placed at height $h_{obs}/d = 27$.

the low velocities of the particles because dumbbells can not move into the wake region due to their longer side. For the case of $X_{db} = 1.0$, a region of dark purple just below the obstacle signifies the presence of wake. In the region above the orifice, ϕ is observed to be small because of the presence of an obstacle in the flowing zone. Similar behaviour was noticed in [39] for the case of a system of spherical particles in a two-dimensional silo. The spatial distributions of the rotational velocities Ω are shown in figure 4.19.

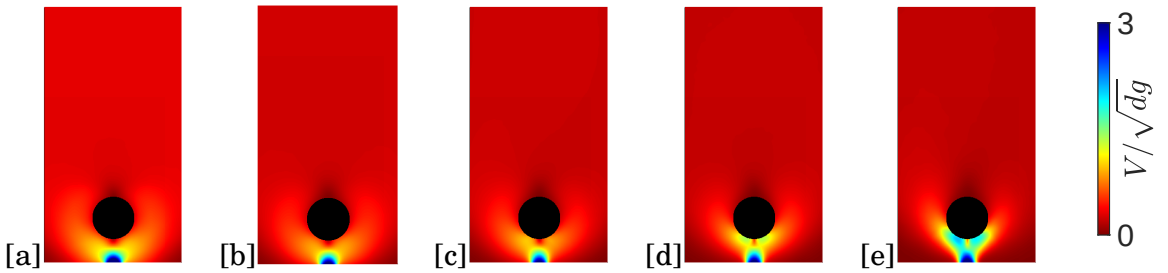

Figure 4.21: Spatial variation of velocities V at X_{db} = a) 0.0, b) 0.25, c) 0.5, d) 0.75 and e) 1.0 and width of the orifice is $W/d = 12$. The plots are averaged over approximately 5000 frames for a silo with an obstacle of diameter $D_{obs}/d = 24$ placed at height $h_{obs}/d = 27$.

In the bulk, Ω is almost negligible as the particles are closely packed. The areas of light cyan around the obstacle are due to the particles rolling over the obstacle. In the region above the orifice, the rotational velocities of the particles are significant due to the availability of space to rotate. As X_{db} increases, there is no significant variation in Ω. Figure 4.20 shows spatial variations in the fluctuations of rotational velocity Ω_{fl}^2. In the region above the orifice, Ω_{fl}^2 decreases with an increase in X_{db} similar to that of the without obstacle case. The velocity fields at different X_{db} are displayed in figure 4.21. The velocity V just above the obstacle is observed to be almost negligible, and it increases gradually in the region beside the obstacle. The flowing zone expands in the region beside the obstacle and covers almost the entire width of the silo as the particles traverse around the obstacle. This leads to a smaller stagnant zone beside the orifice as compared with that of the without obstacle case. In the region above the orifice, V is maximum as compared with the other regions of the silo. However, V is observed to be less as compared with that of the without obstacle case because of the hindrance to the flow due to the presence of an obstacle. The spatial variations of granular temperature T_g are shown in figure 4.22. In the region above the obstacle, T_g is negligible as the particles are closely packed and their velocities are almost constant. T_g is significant in the region below the obstacle because the particles detouring from either side of the obstacle collide in this region and result in the fluctuations of the velocities. As X_{db} increases, T_g varies slightly. The obstacle has a significant effect on the pressure P fields as shown in figure 4.23. The particles lying just above the obstacle experience a higher P as compared to that of the other regions of the silo. This can be explained by the presence of strong force chains supported by the obstacle as shown in figure 4.24. The zones of dark blue below the obstacle and extending up to the base of the silo indicate that of a

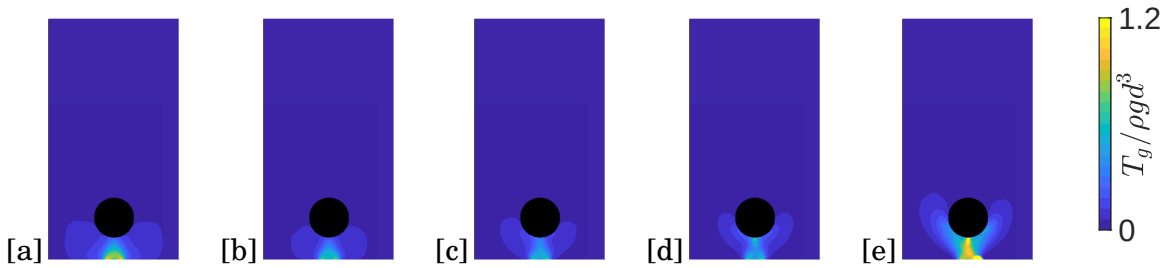

Figure 4.22: Spatial variation of granular temperature T_g at X_{db} = a) 0.0, b) 0.25, c) 0.5, d) 0.75 and e) 1.0 and width of the orifice is $W/d = 12$. The plots are averaged over approximately 5000 frames for a silo with an obstacle of diameter $D_{obs}/d = 24$ placed at height $h_{obs}/d = 27$.

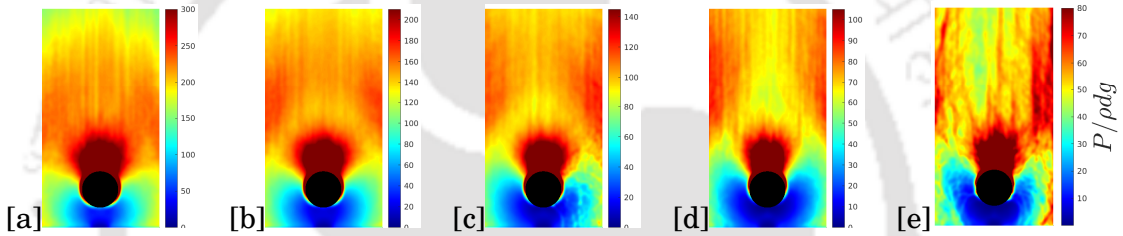

Figure 4.23: Spatial variation of pressure P at X_{db} = a) 0.0, b) 0.25, c) 0.5, d) 0.75 and e) 1.0 and width of the orifice is $W/d = 12$. The plots are averaged over approximately 5000 frames for a silo with an obstacle of diameter $D_{obs}/d = 24$ placed at height $h_{obs}/d = 27$.

low P. This is due to the absence of a strong contact network of force chains in those particles that are lying below the obstacle. The reduction of pressure in the region above the orifice due to the presence of an obstacle is observed previously [24] in the system of spherical particles. As X_{db} increases, the magnitude of pressure decreases due to a decrease in the strength of the force chains as seen in figure 4.24. The spatial variations of shear stress at different X_{db} are shown in figure 4.25. At upstream of the obstacle, a large $|\tau|$ is noticed on either side of it due to detouring of particles around the obstacle. Shear stress beside the obstacle is due to the flowing zone as observed in figure 4.21. However, $|\tau|$ is almost negligible beside the orifice due to the presence of a stagnant zone. The magnitude of $|\tau|$ decreases with an increase in X_{db} because the addition of dumbbells leads to the hindrance of flow as dumbbells can interlock with the adjacent particles.

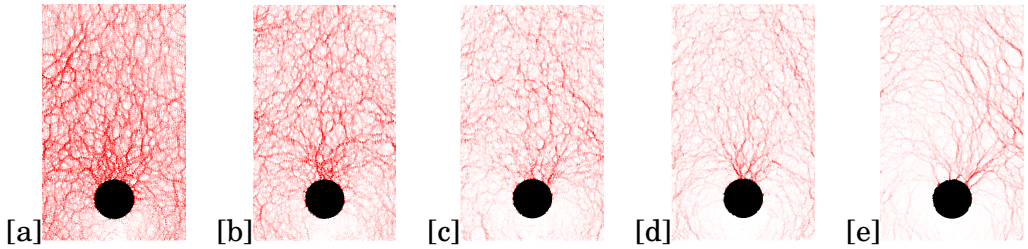

Figure 4.24: Fore chains inside the silo at X_{db} = a) 0.0, b) 0.25, c) 0.5, d) 0.75 and e) 1.0 in the presence of an obstacle of diameter $D_{obs}/d = 24$ placed at height $h_{obs}/d = 27$. The width of the orifice is $W/d = 12$.

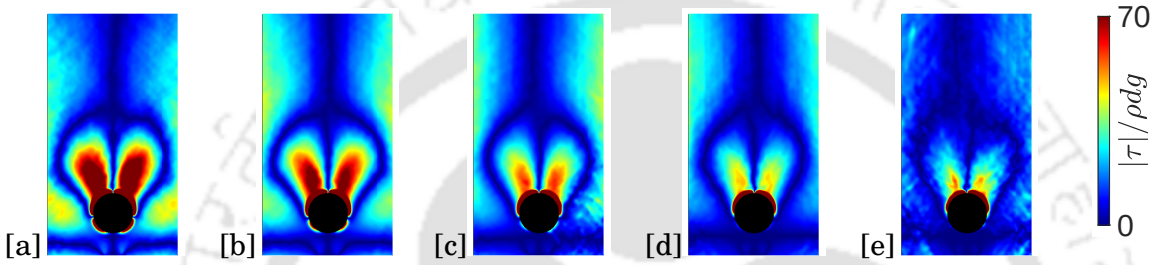

Figure 4.25: Spatial variation of shear stress τ at X_{db} = a) 0.0, b) 0.25, c) 0.5, d) 0.75 and e) 1.0 and width of the orifice is $W/d = 12$. The plots are averaged over approximately 5000 frames for a silo with an obstacle of diameter $D_{obs}/d = 24$ placed at height $h_{obs}/d = 27$.

4.3.2 The flow of a mixture of discs and dumbbells in the interrupted-flow regime

The results explained in the previous sections pertain to large orifice widths $W/d \geq 15$ where a free flow of particles is mostly observed. However, if the silos are operated at less W, the flow might get blocked due to the formation of self-stable structures at the orifice. This phenomenon is commonly termed as clogging. In this section, flow characteristics are investigated at narrow orifice widths $W/d \leq 10$ where clogging of particles is mostly noticed. We have considered four different orifice widths W/d ranging from 7 to 10. At each W/d, four mixture concentrations ($0.25 \leq X_{db} \leq 1.0$) are analysed. Figure 4.26 display clogged states of the system at different W/d where blue circles denote discs, the red ones indicate dumbbells and black ones represent clogged particles. Figure 4.27 show flow rate Q, area fraction ϕ and granular temperature T_g with respect to orifice width W/d at different X_{db}. The trends are qualitatively similar to those observed in a free flow regime. As X_{db} increases, Q is observed to decrease at all W/d because non-spherical particles present either in the flowing zone or in the stagnant zone provides more resistance to the flow than the discs as non-spherical particles can interlock among

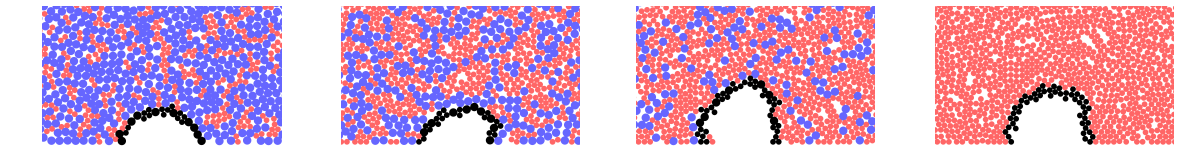

[a] [b] [c] [d]

Figure 4.26: Representative arches of the clogged outlets for the fraction of dumbbells X_{db} = a) 0.25, b) 0.5, c) 0.75 and d) 1.0. Here, blue circles correspond to discs, red ones to dumbbells and black ones to clogged particles.

themselves. Area fraction ϕ slightly increases with W/d, whereas it decreases with an increase in X_{db} because an empty space formed within a structure of particles increases with an increase in the number of dumbbells due to the longer side of the dumbbells. This yields a poor tessellation of elongated particles. The particles in the region above the orifice can rearrange more effectively when there is a large flowing zone. This is the reason for a slightly larger ϕ in the free flow regime than that of the interrupted flow regime. Granular temperature T_g increases gradually with W/d for all X_{db} because of an increase in the velocities of the colliding particles flowing from either side of the orifice resulting in more velocity fluctuations. The variation of average avalanche size $< s >$ with W/d is displayed in figure 4.28. Avalanche size s is the number of particles discharged out of a silo before the system gets clogged. We have computed $< s >$ by taking the average of a minimum of 100 avalanches s for each case. Average avalanche size $< s >$ increases gradually as a function of orifice width W/d for all X_{db}. However, $< s >$ decreases with an increase in X_{db} due to the geometrical interlocking of dumbbell particles. One of the main factors which determine the clogging and the subsequent unclogging due to external force is the stability of the arch. The stability of the arch mainly depends on its geometry, which is hardly explored [26]. In the next section, arch geometry is analysed.

4.3.2.1 Morphology of arches at the orifice

In this subsection, we will discuss the morphology of arches near the orifice by using different parameters like the fraction of dumbbells X_{db}^{arch} and the number of particles N_t in the arch, width w, height h and perimeter p of the arch. During a clogging event, the particles radially closest to the centre of the orifice are considered as particles belonging to an arch. The horizontal distance between the centres of two arch particles each lying on either side of the orifice on the silo base is the width of the arch w. The difference

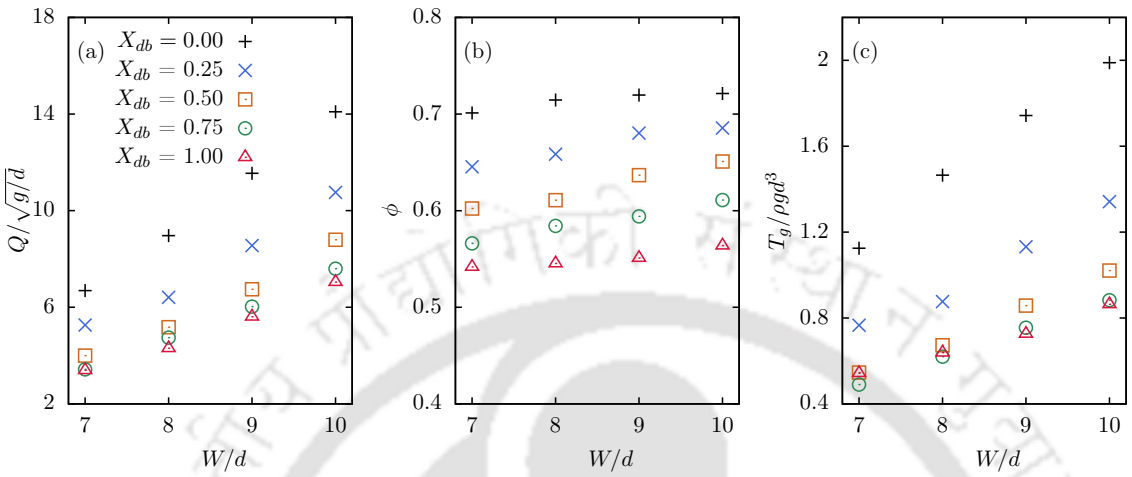

Figure 4.27: The variation in a) flow rate Q, b) area fraction ϕ and c) granular temperature T_g as a function of orifice width W/d for various fractions of dumbbells X_{db}. Here, d is the diameter of each of the circles in a dumbbell.

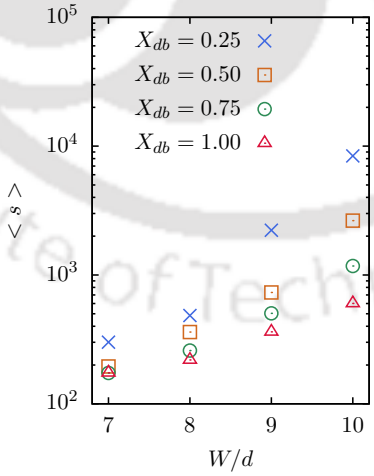

Figure 4.28: The variation in average avalanche size $< s >$ with respect to orifice width W/d for various fractions of dumbbells X_{db}.

in the y position of an arch particle with a maximum y value and the one lying on the base is the height of arch h. The perimeter of the arch p is computed by calculating the distance between centres of the adjacent particles in the arch and summing them up. The value of each parameter is an average over a minimum of 100 clogged states. We have shown the variation of the fraction of dumbbells X_{db}^{arch} and the number of particles N_t in an arch, the ratio of circular arc length to arch perimeter c/p in figure 4.29. Fraction of dumbbells in the arch X_{db}^{arch} is observed to be more than X_{db} (black horizontal lines) at all W/d and for all X_{db} except for that of $X_{db} = 1.0$. This indicates that elongated particles play a major role in arch formation when a mixture of circular and elongated particles are considered. The number of particles in an arch N_t increases gradually with W/d. However, N_t is observed to increase even with an increase of X_{db}. This can be explained by the shear-induced alignment of dumbbells to the flow direction in the flowing part as observed in the past [8] which results in more particles in an arch. The deviation of arch shape from semicircle is analysed using c/p. Here, c is the length of the arc that passes through the centres of two arch particles on the silo base and the arch particle with the highest y and p denotes the perimeter of the arch. Figure 4.29c shows that c/p is close to one for $X_{db} = 0.25$ which indicates that the arch shape is close to a semicircle. Similar behaviour was observed for the case of spherical particles ($X_{db} = 0.0$) in a two-dimensional silo, where Garcimartín *et al.* [26] found that the arch shape is close to a semicircle. A semicircle arch is more stable due to an isotropic loading. As X_{db} increases, c/p is found to decrease suggesting a deviation from semicircle shape or the presence of local concavities in the arch. Lozano *et al.* [27] found that local concavities in an arch are the weakest portions in a system of spherical particles. However, if an arch involves non-spherical particles, the local concavities might not be the weakest portions. Determining the stability of the arch based on the arch shape in a system involving non-spherical particles is still an unanswered question. Figure 4.30 displays width W/d, height h/d and perimeter p/d of an arch as a function of orifice width W/d. As X_{db} increases, W/d is noticed to vary slightly. However, h/d and p/d of the arch increases with X_{db} at all W/d. This can be due to the coupled effect of an increase in the number of arch particles with an increase in X_{db} and the length of a longer side in the case of dumbbells (2.0d) is more than that of a disc (1.414d).

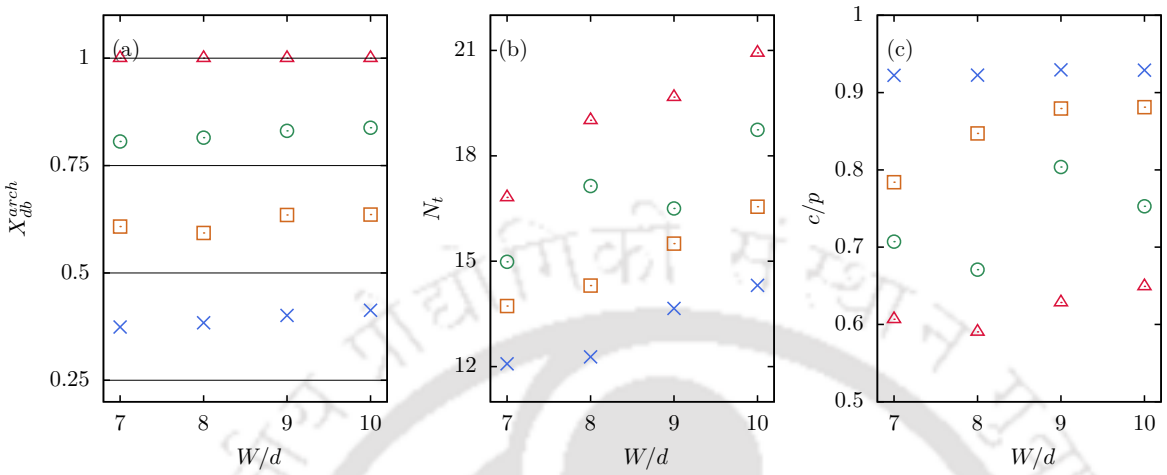

Figure 4.29: The variation in a) fraction of dumbbells in arch X_{db}^{arch}, b) number of particles in arch N_t and c) arc to perimeter ratio of the arch c/p as a function of orifice width. The symbols represent same X_{db} values as that of figure 4.28. The black horizontal lines represent $X_{db} = 0.25, 0.5, 0.75$ and 1.0 in the system.

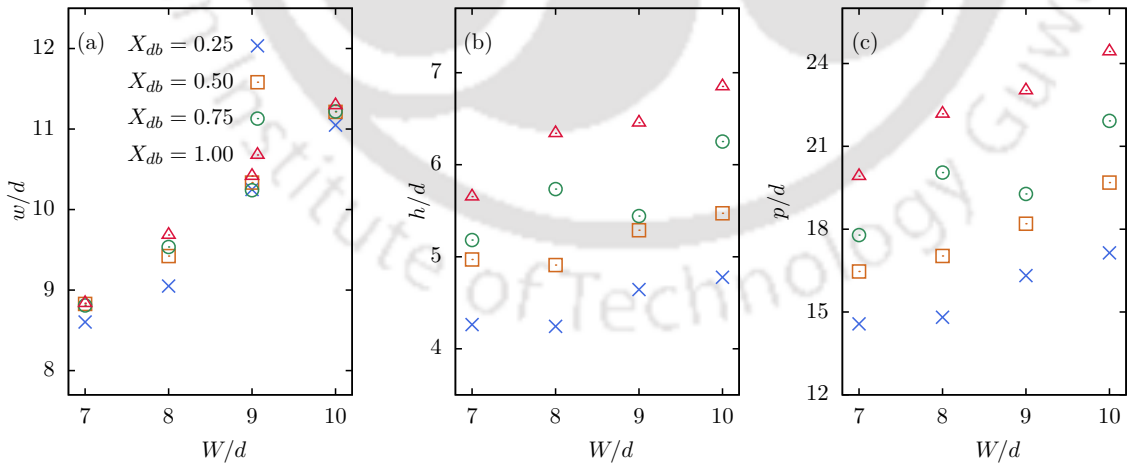

Figure 4.30: The variation in the a) width w, b) height h and c) perimeter p of the arches as a function of orifice width W/d. The arch is formed by mutually stable clogged particles at the outlet.

4.4 Conclusion

In this work, we performed numerical simulations to study the heterogeneous mixtures of dumbbells and discs flowing out of a silo. We have analysed the flow characteristics for various fractions of dumbbells as well as at different orifice widths and found that the flow rate of the mixture decreases with an increase in X_{db}. This could be due to the geometrical interlocking or hindrance to the rotation of dumbbells offered by the surrounding particles. In the flowing zone of the silo, we found that the longer side of the dumbbells is oriented along the flow even in the case of mixtures. Self-similar velocity profiles with horizontal positions are observed for all mixture concentrations. Mean flow fields are plotted for various parameters at different X_{db}. We noticed that as X_{db} increases, there is a decrease in the area fraction in the region above the orifice. Rotational velocity is observed to remain constant with a variation in X_{db} whereas fluctuations in rotational velocity decrease with an increase in X_{db} in the region above the orifice. The stagnant zone was found to expand beside the orifice where the particle velocities are found to be almost negligible. The effect of the obstacle on mean flow fields is also studied. The obstacle has a dramatic effect on the pressure and shear stress flow fields where maximum pressure is observed upstream of the obstacle. This can be attributed to the strong network of force chains supported by the obstacle. Along with the free-flow regime at large orifice widths $W/d \geq 15$, we studied the mixture flow at small orifice widths $W/d \leq 10$ where the system might get clogged after a certain time. We analysed the arch geometry at different orifice widths and for various fractions of dumbbells. The number of particles in an arch is found to increase with X_{db} because the elongated particles are mostly aligned to the flow direction in the region of the arch formation. A parameter c/p is introduced which measures the deviation of arch structure from semicircle shape ($c/p = 1.0$). As X_{db} increases, c/p is found to decrease indicating the presence of local concavities. In previous studies, local concavities were found to be the weakest portions of an arch in the case of spherical systems. However, whether the same definition works for an arch involving non-spherical particles hasn't addressed yet. The weakest location of an arch is ideally the particle that experiences the least stress, however, determining it is a very tedious task. Moreover, evaluating the continuum model with $\mu(I)$ rheology on a mixture of spherical and non-spherical particles could be interesting work.

BIBLIOGRAPHY

[1] Anita Mehta. Spatial, dynamical and spatiotemporal heterogeneities in granular media. *Soft Matter*, 6:2875–2883, 2010.

[2] Iker Zuriguel, Angel Garcimartín, Diego Maza, Luis A. Pugnaloni, and J. M. Pastor. Jamming during the discharge of granular matter from a silo. *Phys. Rev. E*, 71:051303, May 2005.

[3] J. Kozicki and J. Tejchman. Application of a cellular automaton to simulations of granular flow in silos. *Granular Matter*, 7(1):45–54, Apr 2005.

[4] L. Pournin, M. Ramaioli, P. Folly, and Th. M. Liebling. About the influence of friction and polydispersityon the jamming behavior of bead assemblies. *The European Physical Journal E*, 23(2):229, Jun 2007.

[5] R. C. Hidalgo, C. Lozano, I. Zuriguel, and A. Garcimartín. Force analysis of clogging arches in a silo. *Granular Matter*, 15(6):841–848, Dec 2013.

[6] Diego López-Rodríguez, Diego Gella, Kiwing, Diego Maza, Angel Garcimartín, and Iker Zuriguel. Effect of hopper angle on granular clogging. *Phys. Rev. E*, 99:032901, Mar 2019.

[7] A. Ashour, S. Wegner, T. Trittel, T. Börzsönyi, and R. Stannarius. Outflow and clogging of shape-anisotropic grains in hoppers with small apertures. *Soft Matter*, 13:402–414, 2017.

[8] Tamás Börzsönyi, Ellák Somfai, Balázs Szabó, Sandra Wegner, Pascal Mier, Georg Rose, and Ralf Stannarius. Packing, alignment and flow of shape-anisotropic grains in a 3d silo experiment. *New Journal of Physics*, 18(9):093017, sep 2016.

[9] J. F. Wambaugh, C. Reichhardt, and C. J. Olson. Ratchet-induced segregation and transport of nonspherical grains. *Phys. Rev. E*, 65:031308, Mar 2002.

[10] Deniz Ertaş, Thomas C. Halsey, Alex J. Levine, and Thomas G. Mason. Stability of monomer-dimer piles. *Phys. Rev. E*, 66:051307, Nov 2002.

[11] Zhiguo Guo, Xueli Chen, Yang Xu, and Haifeng Liu. Enhancing the linear flow of fine granules through the addition of elongated particles. *Sci. Rep.*, 5(1), nov 2015.

[12] W.A. Beverloo, H.A. Leniger, and J. van de Velde. The flow of granular solids through orifices. *Chemical Engineering Science*, 15(3-4):260–269, sep 1961.

[13] C. Mankoc, A. Janda, R. Arévalo, J. M. Pastor, I. Zuriguel, A. Garcimartín, and D. Maza. The flow rate of granular materials through an orifice. *Granular Matter*, 9(6):407–414, Nov 2007.

[14] P. Artega and U. Tüzün. Flow of binary mixtures of equal-density granules in hoppers—size segregation, flowing density and discharge rates. *Chemical Engineering Science*, 45(1):205–223, 1990.

[15] F Chevoir, F Gaulard, and N Roussel. Flow and jamming of granular mixtures through obstacles. *Europhysics Letters (EPL)*, 79(1):14001, jun 2007.

[16] M. Benyamine, M. Djermane, B. Dalloz-Dubrujeaud, and P. Aussillous. Discharge flow of a bidisperse granular media from a silo. *Phys. Rev. E*, 90:032201, Sep 2014.

[17] A. Medina, D. Cabrera, A. López-Villa, and M. Pliego. Discharge rates of dry granular material from bins with lateral exit holes. *Powder Technology*, 253:270 – 275, 2014.

[18] D.A. Serrano, A. Medina, G. Ruiz Chavarria, M. Pliego, and J. Klapp. Mass flow rate of granular material flowing from tilted bins. *Powder Technology*, 286:438 – 443, 2015.

[19] S. Harada, T. Mitsui, and K. Sato. Particle-like and fluid-like settling of a stratified suspension. *The European Physical Journal E*, 35(1):1, Jan 2012.

[20] Roberto Arévalo, Diego Maza, and Luis A. Pugnaloni. Identification of arches in two-dimensional granular packings. *Phys. Rev. E*, 74:021303, Aug 2006.

[21] Y. X. Cao, B. Chakrabortty, G. C. Barker, A. Mehta, and Y. J. Wang. Bridges in three-dimensional granular packings: Experiments and simulations. *EPL (Europhysics Letters)*, 102(2):24004, apr 2013.

[22] Kiwing To and Pik-Yin Lai. Jamming pattern in a two-dimensional hopper. *Phys. Rev. E*, 66:011308, Jul 2002.

[23] C. Lozano, I. Zuriguel, and A. Garcimartín. Stability of clogging arches in a silo submitted to vertical vibrations. *Phys. Rev. E*, 91:062203, Jun 2015.

[24] Iker Zuriguel, Alvaro Janda, Angel Garcimartín, Celia Lozano, Roberto Arévalo, and Diego Maza. Silo clogging reduction by the presence of an obstacle. *Phys. Rev. Lett.*, 107:278001, Dec 2011.

[25] Celia Lozano, Alvaro Janda, Angel Garcimartín, Diego Maza, and Iker Zuriguel. Flow and clogging in a silo with an obstacle above the orifice. *Phys. Rev. E*, 86:031306, Sep 2012.

[26] Angel Garcimartín, Iker Zuriguel, Luis A. Pugnaloni, and Alvaro Janda. Shape of jamming arches in two-dimensional deposits of granular materials. *Phys. Rev. E*, 82:031306, Sep 2010.

[27] Celia Lozano, Geoffroy Lumay, Iker Zuriguel, R. C. Hidalgo, and Angel Garcimartín. Breaking arches with vibrations: The role of defects. *Phys. Rev. Lett.*, 109:068001, Aug 2012.

[28] Börzsönyi, Tamás, Somfai, Ellák, Szabó, Balázs, Wegner, Sandra, Ashour, Ahmed, and Stannarius, Ralf. Elongated grains in a hopper. *EPJ Web Conf.*, 140:06017, 2017.

[29] Y. Zhou, P. Ruyer, and P. Aussillous. Discharge flow of a bidisperse granular media from a silo: Discrete particle simulations. *Phys. Rev. E*, 92:062204, Dec 2015.

[30] P. A. Cundall and O. D. L. Strack. A discrete numerical model for granular assemblies. *Géotechnique*, 29(1):47–65, 1979.

[31] Nikolai V. Brilliantov, Frank Spahn, Jan-Martin Hertzsch, and Thorsten Pöschel. Model for collisions in granular gases. *Phys. Rev. E*, 53:5382–5392, May 1996.

[32] Steve Plimpton. Fast parallel algorithms for short-range molecular dynamics. *Journal of Computational Physics*, 117(1):1 – 19, 1995.

[33] Alexander Stukowski. Visualization and analysis of atomistic simulation data with OVITO–the open visualization tool. *Modelling and Simulation in Materials Science and Engineering*, 18(1):015012, dec 2009.

[34] Sonu Kumar, Manish Dhiman, and K. Anki Reddy. Magnus effect in granular media. *Phys. Rev. E*, 99:012902, Jan 2019.

[35] K. Anki Reddy, J. Talbot, and V. Kumaran. Dynamics of sheared inelastic dumbbells. *Journal of*

Fluid Mechanics, 660:475–498, 2010.

[36] B. J. Glasser and I. Goldhirsch. Scale dependence, correlations, and fluctuations of stresses in rapid granular flows. *Physics of Fluids*, 13(2):407–420, 2001.

[37] S.D. Liu, Z.Y. Zhou, R.P. Zou, D. Pinson, and A.B. Yu. Flow characteristics and discharge rate of ellipsoidal particles in a flat bottom hopper. *Powder Technology*, 253:70 – 79, 2014.

[38] S. M. Rubio-Largo, A. Janda, D. Maza, I. Zuriguel, and R. C. Hidalgo. Disentangling the free-fall arch paradox in silo discharge. *Phys. Rev. Lett.*, 114:238002, Jun 2015.

[39] K. Endo, K. Anki Reddy, and H. Katsuragi. Obstacle-shape effect in a two-dimensional granular silo flow field. *Phys. Rev. Fluids*, 2:094302, Sep 2017.

[40] D. Chehata, R. Zenit, and C. R. Wassgren. Dense granular flow around an immersed cylinder. *Physics of Fluids*, 15(6):1622–1631, 2003.

CHAPTER 5

GRANULAR MIXTURES DISCHARGING THROUGH A SILO WITH ECCENTRIC ORIFICE LOCATION

5.1 Introduction.

The flow of an assembly of solid particles reminiscent of fluid flow can be witnessed in the form of landslides or during unloading of sand from trucks in a construction site or the flow of sand in an hourglass. In industries, the handling of solid raw materials is involved mainly during production or storage. Understanding the flow of a collection of solid particles or the rheology of granular particles is of great importance in industries for effective plant operations and for producing desired products. The common scenarios of granular particulate flow are the flow of particles on an inclined surface [1] or particles discharging through an orifice of a silo [2] or hopper [3].

The flow of particles through an orifice entails interesting phenomena like ratholing, clogging, pressure saturation etc, based on the material properties, the shape of the particles and the silo geometry. During a silo discharge, two types of flow patterns [4] can occur namely mass flow and funnel flow depending upon the inter-particle friction and the shape of the particles. In mass flow, there is little difference in the velocities of the particles that are flowing in the centre and those near the walls. Whereas, in a funnel type flow, the flow is mainly concentrated in the central part of a silo with a significant difference in the velocities of particles in the centre and those near the wall. An extreme

situation of funnel type flow is rat-holing [5] where the flow occurs only in a small section at the centre of the silo and in the other regions, the particles are completely stationary. This type of flow has been witnessed in the systems of elongated particles with high aspect ratios. Clogging phenomena [6, 7] or a sudden stoppage of the flow due to the formation of a stable structure of particles that blocks the orifice is common in silo flows involving small orifices. The average major dimension of the elongated particles was found to align almost along the streamlines of the flow due to the shear-induced orientation of the particles [8]. The pressure is found to get saturated at depths greater than the width of the silos [9] as the load of the particles is partially taken by the side walls through force chains and this is named as Janssen effect. The above-mentioned are some of the phenomena observed during the flow of particles through a silo. Beverloo *et al.* [10] proposed a model to compute flow rate for a system of spherical particles discharging through a silo as $Q = C\rho_b\sqrt{g}(W-kD)^{n-\frac{1}{2}}$. Here, Q is the flow rate, C is a constant whose value depends on the material properties, ρ_b, g and W are bulk density, acceleration due to gravity and orifice width. Moreover, k, D are dimensionless coefficient, particle diameter and $n = 2,3$ corresponds to a two-dimensional and three-dimensional silo. In recent decades, many models have been proposed for computing flow rate [2, 11–13] of particles discharging through an orifice on the silo base depending on the particle shapes, mixtures of particles or the range of orifice widths considered.

In silos, the orifice is usually placed at the centre of the base due to the practical applications in industries. One of the unconventional orifice positionings in a silo is on the sidewall which can be witnessed during an accidental leakage. In the silos with lateral exits, wall thickness plays a significant role which is not the case in silos having bottom apertures. With an increase in the wall thickness outflow capacity was found to decrease in a cylindrical tube [14]. The flow rate dependence on the diameter/hydraulic diameter of the orifice and the wall thickness has been experimentally investigated [15] for an assembly of particles discharging through circular, rectangular and triangular orifices on the vertical walls. Recently, Serrano *et al.* [16] proposed a correlation for computing flow rate Q as a function of D and w of dry cohesionless particles discharging through circular orifices of diameter D on a vertical wall of thickness w. Further, the authors showed that Hagen-law ($\mathrm{Q} \; \alpha \; \mathrm{D}^{5/2}$) can be used for computing the flow rate of particles discharging through orifices placed on very thin vertical walls. Zhou *et al.* [17] performed experiments, discrete and continuous simulations and proposed an empirical relation for computing flow rate based on the dimensions of the lateral orifice of a silo

with thin walls. Moreover, clogging phenomena at lateral orifice for a variety of granular materials was studied and the minimum orifice width where the continuous flow can be expected was proposed by Davies and Desai [18].

Granular particles discharging through $multiple$ orifices placed on the base of the silo is another eccentricity in the silo flows apart from a $lateral$ orifice. The usage of multiple orifices is one of the practical industrial solutions for mitigating the clogging of particles discharging through narrow orifices. Before the system gets clogged, the average number of particles discharged from each of the two small orifices as compared with a single orifice silo was found to increase by an order of magnitude [19] just by varying the inter-orifice distance. The fluctuations due to an intermittent flow from an orifice resulted in the resumption of the flow in another jammed orifice thus increasing the time before the system gets clogged. In another study [20], the effect of inter-particle friction has been investigated on the flow and jamming behaviour of the particles exiting through multiple orifices. Correlations for the flow rate of the particles discharging out of two orifices placed on the base considering various outlet sizes and inter-orifice distances has been proposed by performing simulations [21] as well as experiments [22]. Fullard *et al.*[23] noticed a non-monotonic dependence of flow rate on the inter-orifice distance. The authors reported that inter-particle friction is the reason for this kind of behaviour. Maiti *et al.* [24] studied the influence of inter-orifice distance between symmetrically as well as asymmetrically placed orifices on the base. Further, they reported the existence of a neutral axis between the two orifices which bifurcates the flow fields due to each orifice inside a silo when the orifices are wide apart. Kamath *et al.*[25] studied mixing characteristics in a silo having multiple orifices where it is noticed that an intermittent flow through a narrow orifice due to its small size influences the mixing of particles discharged.

In the silo problems involving either lateral orifice or multiple orifices, mostly the systems were involving spherical particles or disc particles. However, understanding the dynamics of mixtures involving non-spherical particles is more useful for practical applications since in reality, the systems involve mixtures of particles varying in size and shape. In this work, we studied the flow of a mixture of dumbbells and discs in two eccentric silo flow situations. In the first case, we analyzed how the fraction of dumbbells influence the dynamics of the particles flowing through a lateral orifice. Whereas in the second case, we studied how the distance between the two orifices placed on the silo base affects the flow dynamics. Moreover, we have presented time-averaged flow fields of

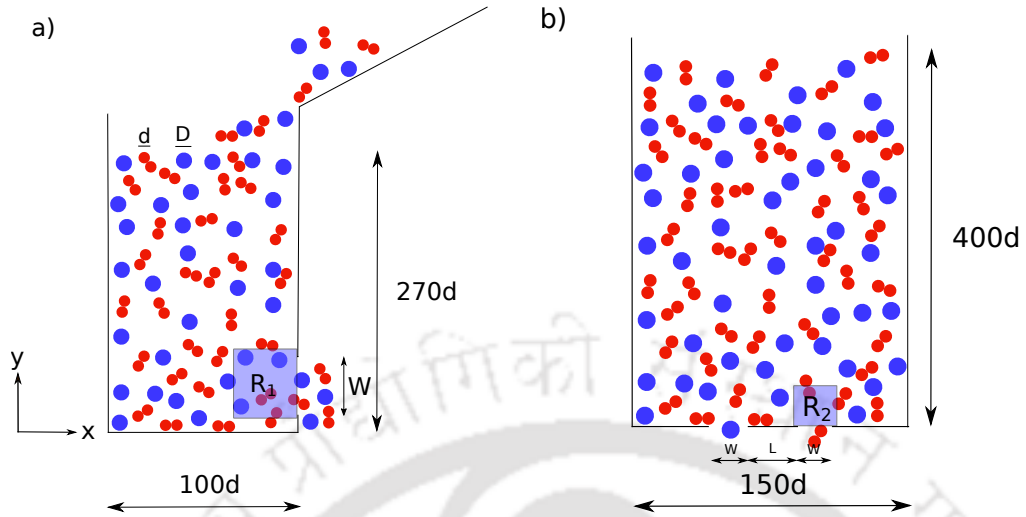

Figure 5.1: a) Schematic representation of a silo with a) an orifice placed on the *sidewall* and b) *multiple orifices* placed on the silo base. Here, the blue circles indicate discs and the red ones that of dumbbells. We have taken the area of the disc same as that of the dumbbell. The diameter of each circle of a dumbbell is d and the diameter of each disc is $D = \sqrt{2}d$. The orifice width is given by W in both the images and L is the distance between two orifices. Few parameters in our work are analysed in the regions R_1 and R_2. The region R_1 has a length of $5\sqrt{2}d$ in x direction and $W + 2\sqrt{2}d$ in y-direction and the region R_2 has a length of $W + 2\sqrt{2}d$ in x direction and $5\sqrt{2}d$ in y-direction. Please note that the orifice on the $sidewall$ is placed at a height of $3.5d$ from the silo base to avoid the effect of the base. Origin is located at the centre of silo base for both the cases.

various parameters in both cases which can be verified with the results obtained from the continuum models using $\mu(I)$ rheology. The paper is organised in the following way: in the next section, geometries of both the silos and the simulation technique are explained. In Section 5.3.1, the results pertaining to the $lateral$ orifice case are discussed and in section 5.3.2, the results obtained for the $multiple$ orifice case are elucidated. Finally, in section 5.4, our important findings are summarized.

5.2 Simulation Methodology

We used the discrete element method (DEM) [26] to study the influence of the orifice location and the fraction of dumbbells on the dynamics of granular mixtures. Figure 5.1 shows the schematic representation of two-dimensional silos differing in orifice positioning. In the first case, a single orifice is placed on the sidewall whereas, in the other one, two orifices are placed on the silo base. In both cases, mixtures of discs and dumbbells (two circles are fused to form a rigid body) are analysed. The area of each

Table 5.1: The constants used in our numerical simulations

Simulation parameters	Values
K_n	$2.00 \times 10^6 \rho dg$
K_t	$2.45 \times 10^6 \rho dg$
γ_n	$1000\sqrt{g/d^3}$
γ_t	$1000\sqrt{g/d^3}$
μ	0.5
$timestep$	$10^{-4}\sqrt{d/g}$

disc is taken the same as that of a dumbbell. Thus, the diameter of the disc is $D = \sqrt{2}d$, where d is the diameter of a single circle of a dumbbell. In figure 5.1a case, $N = 15000$ particles are placed at arbitrary locations with random orientations inside a silo confined by the walls at $x = \pm 50d$ and $y = 0$. We ensured that there are no overlaps among the particles. A gravity of magnitude g is applied in the negative y direction. Consequently, the particles got settled (KE ≈ 0.0) and the bed height was found to be close to $270d$. At time $t = 0$, an orifice of width W is placed on the sidewall so that particles can discharge out of the silo. Please note that the orifice is placed on the right side wall of the silo and at a height of $3.5d$ to lessen the effect of the silo base on the flow dynamics. Periodic boundary conditions (PBC) were applied in y direction and the particles discharging out of the silo were placed on top of the granular bed at random positions with reduced velocities. In our work, few parameters are analysed in the region R_1 which is just beside the orifice and having a length of $5\sqrt{2}d$ in x-direction and $W + 2\sqrt{2}d$ in y-direction. In figure 5.1b case, the silo is confined by the walls at $x = \pm 75d$ and $y = 0$ and it consists of $N = 33750$ particles with a bed height close to $400d$. The same procedure is employed for creating the initial configurations of both silos. At time $t = 0$, two orifices on the silo base separated by a distance of L and each of width W were opened and PBC was applied in the y direction. A few parameters are calculated in the region R_2 which is having a length of $W + 2\sqrt{2}d$ in the x direction and $5\sqrt{2}d$ in y direction and is located just above one of the orifices.

One of the main advantages of the DEM technique is it stores individual data of each particle which helps in understanding particle level dynamics. In this technique, positions and velocities of each particle are updated at regular intervals by integrating equations of motion using the velocity Verlet algorithm. In the equations of motion, gravitational and contact forces are the only forces that are considered. The normal and tangential components F^n_{ij}, F^t_{ij} of contact forces on a particle i due to particle j is

computed by using contact force model [27] as

$$F_{ij}^{n} = \sqrt{R_{\text{eff}}\delta_{ij}}(K_n\delta_{ij}\hat{\boldsymbol{r}}_{\boldsymbol{ij}} - m_{\text{eff}}\gamma_n\boldsymbol{v}_{\boldsymbol{ij}}^{\boldsymbol{n}})$$

$$F_{ij}^{t} = -\min\left(\sqrt{R_{\text{eff}}\delta_{ij}}(K_t\boldsymbol{\Delta s}_{\boldsymbol{ij}} + m_{\text{eff}}\gamma_t\boldsymbol{v}_{\boldsymbol{ij}}^{\boldsymbol{t}}), \mu F_{ij}^{n}\right)$$

Here, $R_{\text{eff}} = \sqrt{\frac{R_iR_j}{R_i+R_j}}$ and $m_{\text{eff}} = \sqrt{\frac{m_im_j}{m_i+m_j}}$ are the effective radius and effective mass of the particles i, j in contact where R_i, R_j are radii and m_i, m_j are masses of respective particles. The overlap $\delta_{ij} = R_i + R_j - |R_{ij}|$ must be non-negative for two particles to be in contact. Here, $|R_{ij}|$ is the distance between the centres of two particles. The subscripts or superscripts consisting of n, t represents the normal or tangential components of the respective parameters. The elastic constant and damping coefficient are denoted by K and γ and $\hat{\boldsymbol{r}}_{\boldsymbol{ij}}$ is the unit vector in the direction of line joining the centres of two particles. Moreover, $\boldsymbol{v}_{\boldsymbol{ij}}$ is the relative velocity, $\boldsymbol{\Delta s}_{\boldsymbol{ij}}$ is the tangential displacement vector and μ is the coefficient of friction. The values of various constants used in our numerical simulations are shown in Table 5.1. The positions and velocities of dumbbells are the centres of mass and centre of mass velocities. The force on each dumbbell is computed by adding the forces on both the circles of a dumbbell. The torques on each dumbbell are calculated in the same way as that of the forces. The force acting on each circle of a dumbbell due to the other circle of the same dumbbell is ignored. All simulations were performed using LAMMPS [28] package and the progress of the simulations were visualized using OVITO [29] package.

5.3 Results and Discussion

In this section, we will explain the results obtained for a mixture of discs and dumbbells flowing out of a two-dimensional silo. This section consists of two subsections. In Section. 5.3.1, we elucidated the effect of fraction of dumbbells on the dynamics of particles flowing through a lateral orifice and in Section. 5.3.2, we explained how the flow dynamics is influenced by the spacing between the orifices placed on the silo base. In this regard, the flow is characterized by parameters like mass flow rate Q, area fraction ϕ, granular temperature T_g etc. In this paper, wherever we use the term flow rate it means mass flow rate. The flow rate is calculated by using the least-square fitting method on the total mass of particles discharged versus time data. Area fraction is the ratio of the area occupied

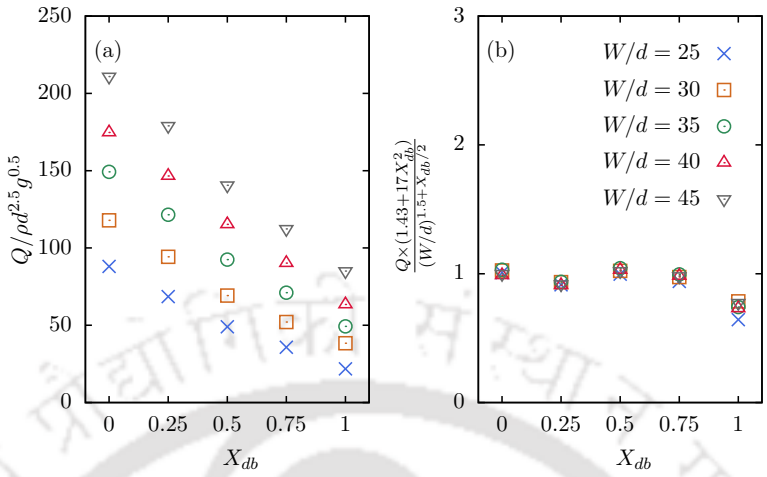

Figure 5.2: a) Flow rate Q as a function of the fraction of dumbbells X_{db}. b) Flow rate normalised by $(W/d)^{1.5+X_{db}/2}$ with respect to X_{db} and c) Flow rate normalised by $1-0.65\times X_{db}$ as a function of various widths W/d of an orifice placed on the sidewall. Here, "d" corresponds to the diameter of each of the circles of a dumbbell.

by the particles in a region of interest and the area of the region. Granular temperature T_g, a measurement of velocity fluctuations of particles [30, 31], in a region of interest is computed as $T_g = \frac{1}{3}\langle m\{(v_x - < v_x >)^2 + (v_y - < v_y >)^2\} + I(\Omega_z - < \Omega_z >)^2\rangle$. Here, m is mass of a particle, v_x and v_y are instantaneous velocities in x and y directions respectively. Moreover, I is the moment of inertia, Ω_z is the rotational velocity in z direction and $< . >$ corresponds to a spatio-temporal average over a specified region of interest.

5.3.1 Lateral orifice

In this subsection, we explained how the fraction of dumbbells influences the flow dynamics while particles are flowing out of an orifice placed on the $sidewall$ of a silo. In this regard, the particulate flow is analysed for five different fractions of dumbbells X_{db} ranging from 0.0 to 1.0. Moreover, five different widths of the orifice positioned on the sidewall ranging from W/d = 25 to 45 are considered. Flow rate is observed to decrease with an increase in the fraction of dumbbells at all orifice widths (figure 5.2a). This is due to an increase in the dynamic friction ($\overline{\mu}$ = shear stress/pressure) in the region beside the orifice R_1 with an increase in the fraction of dumbbells X_{db} as shown in figure 5.3a. The increase in the geometrical interlocking among the particles with an increase of X_{db} or the addition of dumbbells might be the reason behind an increase in $\overline{\mu}$. The shear stress

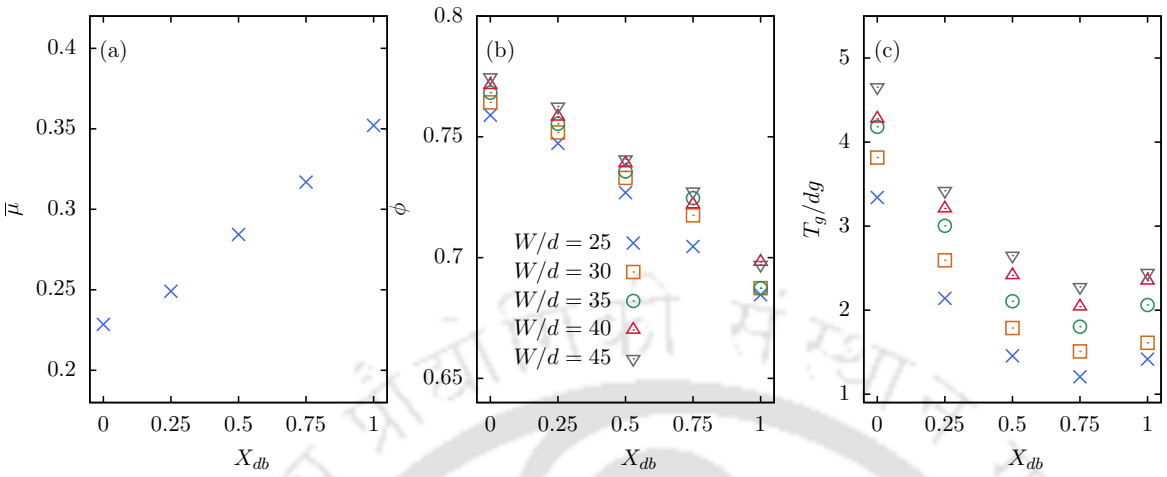

Figure 5.3: Dynamic friction $\overline{\mu}$ with respect to the fraction of dumbbells X_{db} in the region R_1 beside the lateral orifice having a width $W/d = 25$.

and pressure are obtained from the time-average flow fields which are explained in detail in the next section. Lattanzi and Stickel [3] found an increase in the flow rate with an increase in the number of rods in a rod-sphere mixture discharging through an orifice in the silo base. Beverloo's law [10] states that the mass flow rate scales with $(W-kd)^{5/2}$ for a system of spherical particles flowing out of a three-dimensional silo, where W, k, d are orifice width, shape coefficient and diameter of the disc. For a two-dimensional case, it can be derived as $(W-kd)^{3/2}$ and k was found to be 1 for spherical or disc particles. In our case which involves a mixture of dumbbells and discs, we tried to find some scaling for orifice width so that all the data collapse. Beverloo's law was fitting reasonably well only when $X_{db} = 0.0$ which involves only discs. So, we tried with a modified Beverloo's law to collapse the data. The flow rate is found to scale with orifice width as $(W/d)^{1.5+X_{db}/2}$ and with the fraction of dumbbells as $1/(1.43 + 17 \times X_{db}^2)$ as shown in figure 5.2b.

Area fraction and granular temperature are analysed in the region R_1 which lies just beside the orifice as shown in figure 5.1a. With an increase in the fraction of dumbbells, the voids formed among the particles increases resulting in a decrease in the area fraction (figure 5.3b). Recently, Lattanzi and Stickel [3] noticed a similar result where the packing fraction was found to decrease with an increase in the fraction of rod-like particles of a spherical-rod mixture flowing through the silo base. Granular temperature is found to decrease with an increase in X_{db} as shown in figure 5.3c due to a decrease in the velocity fluctuations of the particles in the region R_1. This can be

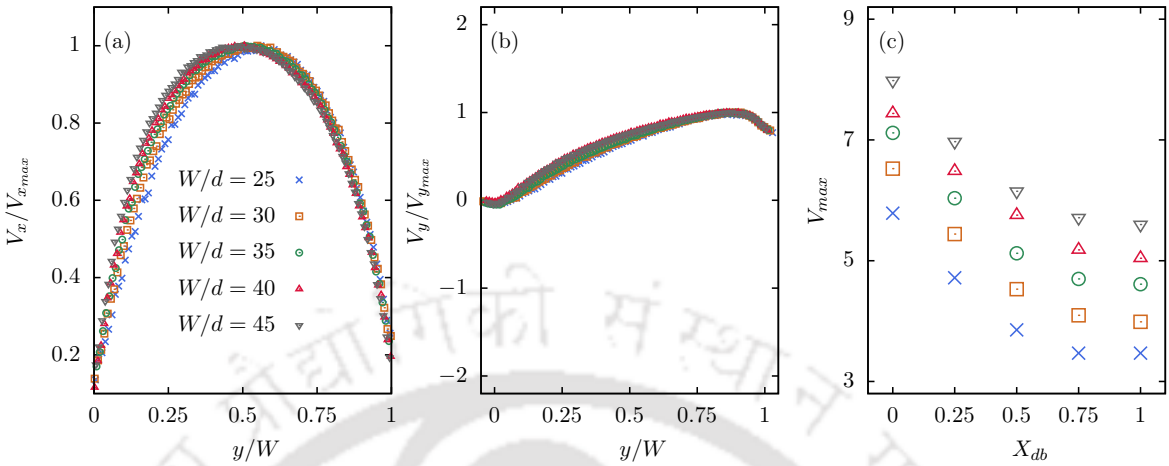

Figure 5.4: a) Normalized horizontal $V_x/V_{x_{max}}$ and b) normalized vertical $V_y/V_{y_{max}}$ velocities as a function of normalized vertical positions y/W where, W is orifice width on the sidewall of the silo. c) Maximum velocity V_{max} at different orifice widths W/d and for various fractions of dumbbells X_{db}.

explained by a decrease in the velocities and collisions of the particles with an increase in X_{db} due to geometrical interlocking among the particles. Self-similar velocity profiles are noticed when normalized horizontal and normalized vertical velocities are plotted against normalized vertical position (figure 5.4a, 5.4b). Zhou *et al.* [32] noticed self-similar velocity profiles for a system of bidisperse spherical particles discharging out of an orifice placed on the silo base. Moreover, Janda *et al.* [33] reported self-similar velocity profiles in a system of monodispersed spherical beads discharging out of a two-dimensional silo from an aperture on a silo base. The stagnant zone or a set of almost stationary particles that are present below the lateral orifice [17] hinders the free-flow of particles. Moreover, with an increase in the fraction of dumbbells, the stagnant zone offers more resistance to the flow resulting in a decrease in the flowing zone (Please refer to the supplementary information†). This yields in a decrease in the maximum velocity V_{max} (figure 5.4c) in the region beside the orifice (R_1) with an increase in X_{db}. This result complements a decrease in the flow rate of particles with an increase of X_{db} (figure 5.2a). We computed the orientational order parameter to check whether the particles are aligned in a particular direction at three different regions. The first region is beside the orifice ($35 < x < 45$ and $10 < y < W - 5$), the second one is slightly away from the orifice ($15 < x < 25$ and $W - 5 < y < W + 5$) and the third one is taken in the bulk ($5 < x < 15$

and $60 < y < 70$). The orientational order parameter S is computed as $S = 2 < cos^2\theta > -1$ where θ is the difference of the orientation of the dumbbell and the director vector which indicates the flow direction. The orientational order parameter is noticed to decrease with an increase in the fraction of dumbbells in the region close to the orifice (figure 5.5a). A disordered packing of elongated particles result in more voids and consequently lower area fraction. In our case, this decrease in the area fraction might be another reason for a decrease in the flow rate with an increase in the fraction of dumbbells. In the bulk, as the particles are closely packed, the orientational order parameter is found to increase with an increase in the fraction of dumbbells (figure 5.5c). However, in the intermediate region, the ordering of particles is almost unaffected by the fraction of dumbbells. To explore the flow dynamics at various lateral orifice widths W/d we have analysed spatial flow fields of various parameters by using the coarse-graining method [34, 35] in the next subsection.

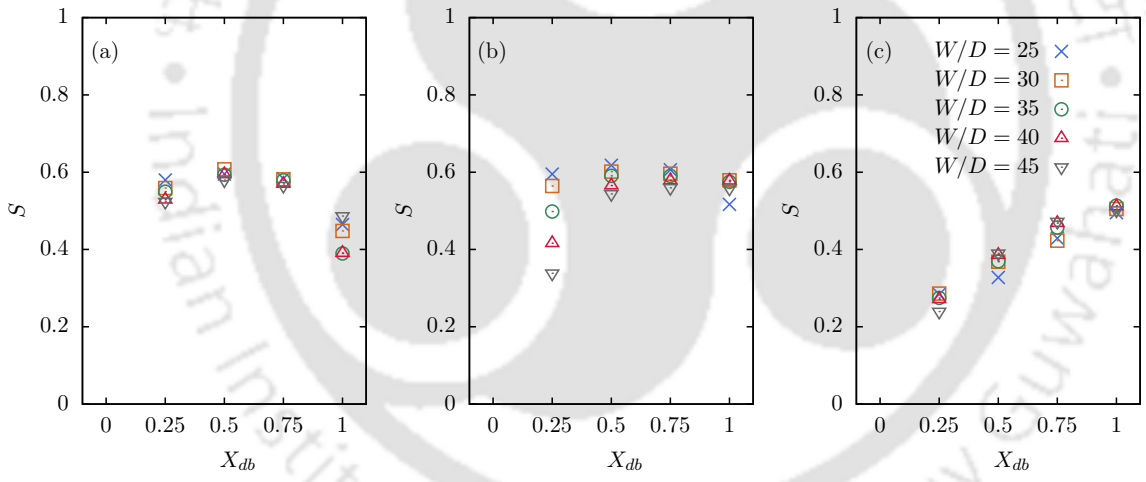

Figure 5.5: Orientational order parameter as a function of the fraction of dumbbells in the region a) $35 < x < 45$ and $10 < y < W - 5$, b) $15 < x < 25$ and $W - 5 < y < W + 5$, c) $5 < x < 15$ and $60 < y < 70$ at different orifice widths.

5.3.1.1 Flow fields at various lateral orifice widths W/d

We have generated continuous macroscopic flow fields by using discrete microscopic data like positions, velocities etc,. of the individual particles. Here we employeed coarse-graining technique as suggested by [35] for a two-dimensional silo. The area fraction $\phi(t)$, rotational velocity $\Omega(t)$, fluctuations in rotational velocity $\Omega_{fl}(t)$, velocity $\boldsymbol{v}(t)$, granular

temperature $T_g(t)$, stress tensor $\sigma_{ij}(t)$ and pressure $P(t)$ at any point of time t and at any position p having a position vector $\boldsymbol{r_p}$ is computed as follows:

$$\phi(t) = \left[\sum_{i=1}^{n} \frac{\rho\pi d_i^2}{4} \mathscr{W}(\boldsymbol{r_p} - \boldsymbol{r_i(t)})\right]/\rho \tag{5.1}$$

$$\Omega(t) = \left[\sum_{i=1}^{n} \frac{\rho\pi d_i^2}{4} \Omega_{z_i} \mathscr{W}(\boldsymbol{r_p} - \boldsymbol{r_i(t)})\right]/\rho\phi \tag{5.2}$$

$$\Omega_{fl}(t) = \left[\sum_{i=1}^{n} \frac{\rho\pi d_i^2}{4} (\Omega_{z_i} - \Omega)^2 \mathscr{W}(\boldsymbol{r_p} - \boldsymbol{r_i(t)})\right]/\rho\phi \tag{5.3}$$

$$\boldsymbol{v}(t) = \left[\sum_{i=1}^{n} \frac{\rho\pi d_i^2}{4} \boldsymbol{v_i} \mathscr{W}(\boldsymbol{r_p} - \boldsymbol{r_i(t)})\right]/\rho\phi \tag{5.4}$$

$$T_g(t) = \frac{\sum_{i=1}^{n} \frac{\rho\pi d_i^2}{4} |\boldsymbol{v_i} - \boldsymbol{v}|^2 \mathscr{W}(\boldsymbol{r_p} - \boldsymbol{r_i(t)})}{2\rho\phi} \tag{5.5}$$

$$\boldsymbol{\sigma_{ij}}(t) = \sum_{i=1}^{n} \sum_{j=i+1}^{n} (\boldsymbol{F^{ij}} \times \boldsymbol{r_{ij}}) \int_{s=0}^{1} \mathscr{W}(\boldsymbol{r_p} - \boldsymbol{r_i(t)} + s\boldsymbol{r_{ij}}) ds \tag{5.6}$$

$$P(t) = \frac{-tr(\sigma_{ij}(t))}{2} \tag{5.7}$$

$$\mathscr{W}(\boldsymbol{r}) = \frac{1}{\pi w^2} e^{-\boldsymbol{r}^2/w^2} \tag{5.8}$$

Here, ρ, d_i and $\boldsymbol{r_i}$ are density, diameter and position vector of the i^{th} particle and $\mathscr{W}(\boldsymbol{r})$ is the coarse-graining function which weighs the parameters over space from discrete data with $w = 1.414$. The parameters are evaluated only when $|\boldsymbol{r_p} - \boldsymbol{r_i}| < 3w$. Moreover, ϕ, Ω, Ω_{fl}, $\boldsymbol{v}$, T_g, σ_{ij} and P are the time-averaged quantities of the respective parameters. All the flow fields demonstrated in this subsection are averaged over 2500 frames and they corresponds to the region: $-38.5 \leq x \leq 48.5$ and $1.5 \leq y \leq 148.5$. For each parameter we have produced five flow fields each corresponding to a different lateral orifice width W/d ranging from 25 to 45. The fraction of dumbbells is $X_{db} = 0.5$ for all the flow fields demonstrated in this subsection.

Area fraction ϕ is found to vary slightly with an increase in the width W of the lateral orifice (figure 5.6). The area fraction is least in the region beside the orifice due to shear-induced dilation [36]. Moreover, with an increase of W, the region of dilation is

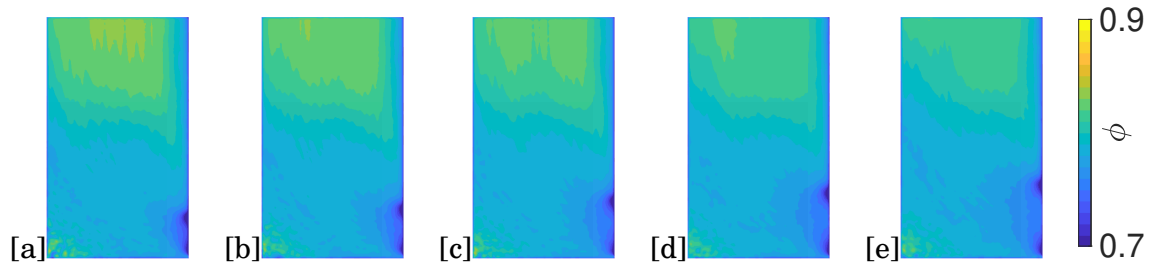

Figure 5.6: Spatial distribution of area fraction ϕ at an orifice width W/d = a) 25, b) 30, c) 35, d) 40 and e) 45 on the sidewall with fraction of dumbbells X_{db}=0.5.

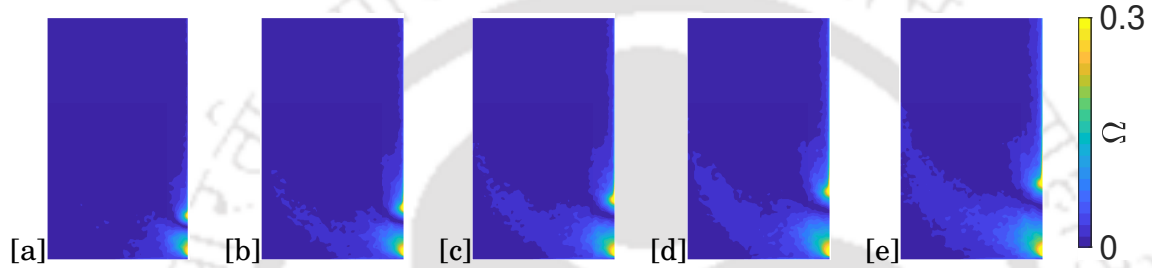

Figure 5.7: Spatial distribution of rotational velocity Ω at an orifice width W/d = a) 25, b) 30, c) 35, d) 40 and e) 45 on the sidewall with fraction of dumbbells X_{db}=0.5.

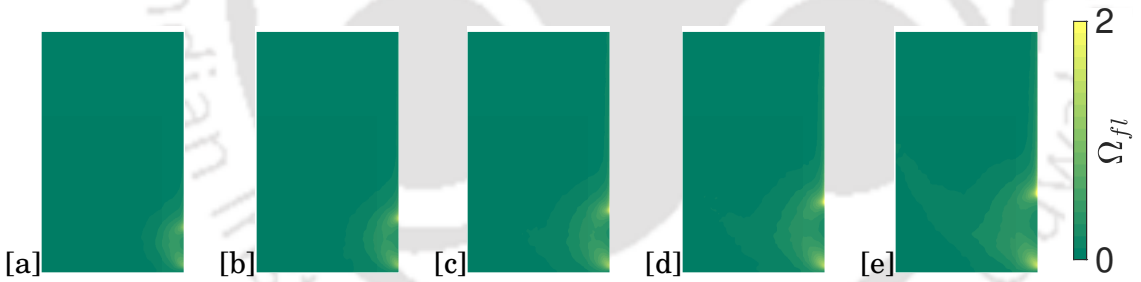

Figure 5.8: Spatial distribution of fluctuations in rotational velocity Ω_{fl} at an orifice width W/d = a) 25, b) 30, c) 35, d) 40 and e) 45 on the sidewall with fraction of dumbbells X_{db}=0.5.

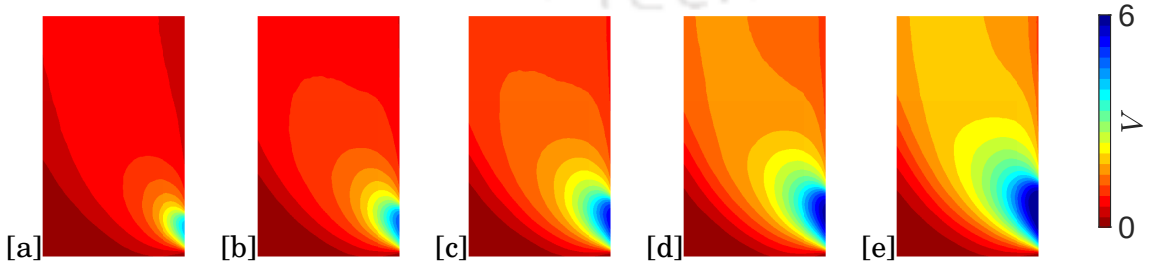

Figure 5.9: Spatial distribution of velocity V at an orifice width W/d = a) 25, b) 30, c) 35, d) 40 and e) 45 on the sidewall with fraction of dumbbells X_{db}=0.5.

noticed to increase. In the bulk as well as in the left side corner of the silo, ϕ is noticed to be slightly less than that of the random close packing (0.84) at all W. Figure 5.7 displays the spatial distribution of rotational velocity Ω at various lateral orifice widths. The flowing solid particles tend to rotate while crossing the edges [37], thus Ω is found to be maximum at both edges of the orifice for all the cases. In the bulk, as the particles are closely packed they hardly rotate resulting in a negligible Ω. However, in the region beside the orifice, the particles are loosely packed (figure 5.6) thus the particle collisions might yield in their rotations. Moreover, the particle collisions result in the fluctuations of rotational velocities Ω_{fl} in the region beside the orifice as seen in figure 5.8. This region is noticed to expand with the lateral orifice width due to an increase in the flowing zone of the particles. Figure 5.9 displays velocity V fields at various lateral orifice widths W. A stagnant zone is observed at the left side of the silo as well as on the base where velocity is found to be almost zero. This zone is found to vary slightly with an increase in the lateral orifice width. The stagnant zone hinders the movement of particles flowing adjacent to it. Thus velocity is found to increase as one moves away from it. Moreover, the flowing zone reaches the left wall at a certain height due to the presence of the stagnant zone. The presence of stagnant zone on the entire silo base as well as until a certain height of the left side wall was observed previously [17] though in their study they presented velocity fields at various widths of the silo. As particle velocities are almost constant in the bulk, granular temperature T_g or fluctuations in velocities are found to be almost negligible (figure 5.10) in the bulk. However, in the region beside the orifice, T_g is present due to two types of particle collisions. The first one is between the particles of the flowing zone and those present above the orifice. The other type is between the particles in the flowing zone and those present in the stagnant zone. Moreover, T_g is found to increase with an increase in W/d in the region beside the orifice due to an increase in the velocity fluctuations. This can be explained by an increase in the particle collisions as well as particle velocities (figure 5.9) due to an increase in the orifice width.

Pressure P flow fields are illustrated in figure 5.11. In granular media, force is transmitted through a network of contacts namely force chains [38]. In the region beside the orifice, the pressure is noticed to be least due to a low area fraction as seen in figure 5.6. With an increase in the orifice width, pressure varies slightly in the region beside the orifice. Towards the left side of the silo, the pressure is maximum due to the presence of a stagnant zone and the force exerted by the particles above it which corresponds to

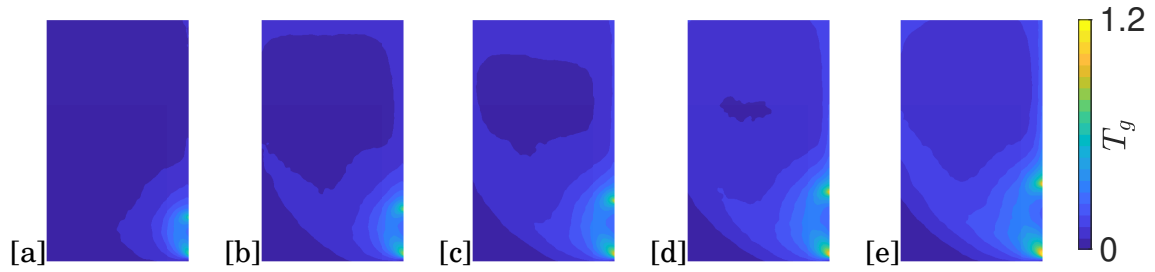

Figure 5.10: Spatial distribution of granular temperature T_g at an orifice width W/d = a) 25, b) 30, c) 35, d) 40 and e) 45 on the sidewall with fraction of dumbbells X_{db}=0.5.

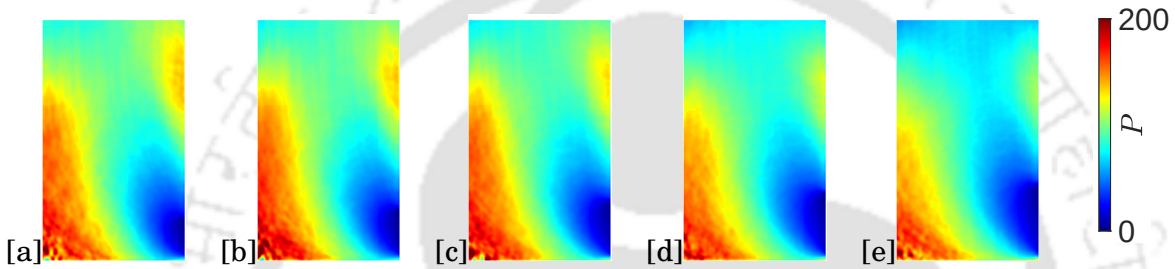

Figure 5.11: Spatial distribution of pressure P at an orifice width W/d = a) 25, b) 30, c) 35, d) 40 and e) 45 on the sidewall with fraction of dumbbells X_{db}=0.5.

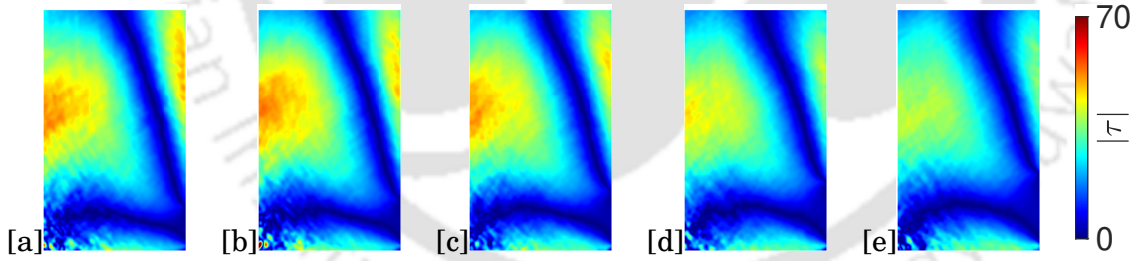

Figure 5.12: Spatial distribution of shear stress $|\tau|$ at an orifice width W/d = a) 25, b) 30, c) 35, d) 40 and e) 45 on the sidewall with fraction of dumbbells X_{db}=0.5.

the flowing zone. Figure 5.12 displays the shear stress $|\tau|$ and it is least in the region beside the orifice as it is flowing zone. $|\tau|$ is observed to be maximum for all the cases at the left side of the silo as it is the region that lies between the wall and the flowing zone. This kind of behaviour is similar to that observed in the liquids. Moreover, as there is hardly any flow in the region above the base of the silo, shear stress is the least in this region.

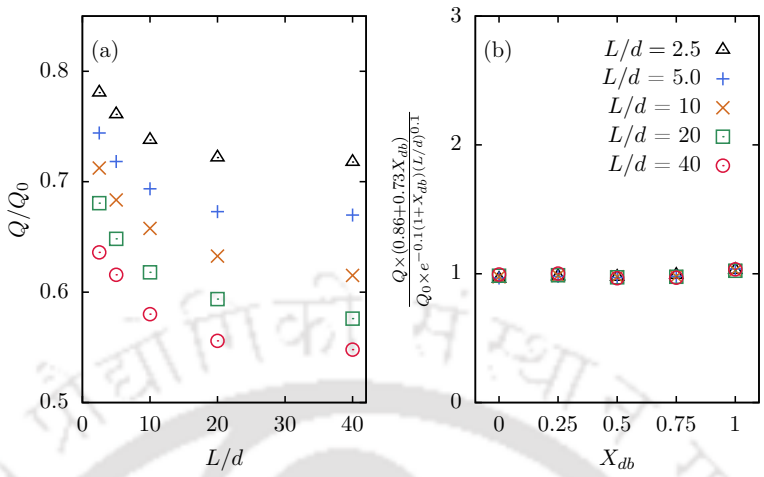

Figure 5.13: a) Normalized flow rate Q/Q_0 as a function of inter-orifice distances L/d at different fraction of dumbbells X_{db} and b) scaling of flow rate with inter-orifice distance L/d. Here, the width of each of the two orifices is $W/d = 20$ and Q_0 is the flow rate at $L/d = 0$.

5.3.2 Two orifices on a silo base

In this subsection, we are going to elucidate how the flow dynamics of a mixture of discs and dumbbells is affected by the separation distance between the two orifices that are placed on the silo base. In this regard, we have analysed the flow at six different separation lengths L/d ranging from 0 to 40 between the two orifices each of width $W/d = 20$. Moreover, we have considered five different fractions of dumbbells X_{db} from 0.0 to 1.0. When granular particles are discharging through an orifice on a flat bottomed silo base, a stagnant zone is present on either side of the orifice [36]. The stagnant zone usually hinders the movement of particles flowing adjacent to it. In the case of a silo with multiple orifices, an additional stagnant zone is present in between the orifices [21] along with the one that exists beside the sidewalls. As the distance between the orifices increases, the stagnant zone formed between them expands and the hindrance to the flow increases thus decreasing the flow rate Q. This is shown in figure 5.13a, where Q/Q_0 decreases with L/d for all fractions of dumbbells X_{db} until $L/d = 20$ and then it gets saturated. Here, Q is the flowrate of particles exiting through both the orifices and Q_0 represents flow rate when the inter-orifice distance is zero. Zhang *et al.* [21] reported a similar result to that of ours where they noticed a gradual decrease followed by saturation in Q with an increase in the inter-orifice distance for a system of spherical particles. We observed a decrease in the flow rate with an increase in the

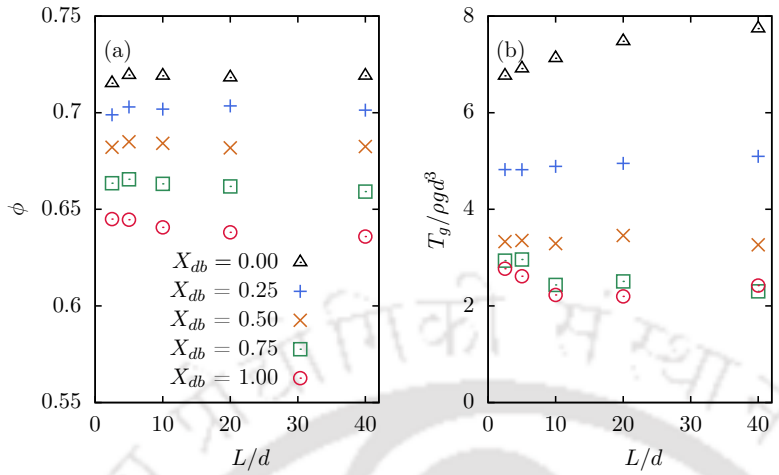

Figure 5.14: a) Area fraction ϕ and b) granular temperature T_g at different spacings L/d between the two orifices, each of width $W/d = 20$.

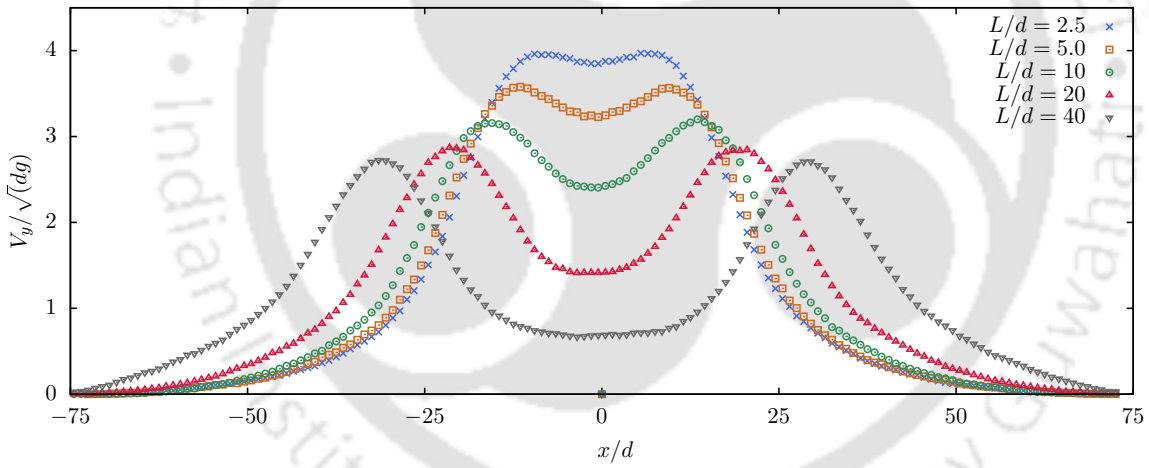

Figure 5.15: Vertical velocity V_y as a function of horizontal position x at various spacings L between the two orifices, each of width $W/d = 20$.

fraction of dumbbells X_{db}, similar to the result observed in figure 5.2a. The flow rates corresponding to different inter-orifice distances for various fractions of dumbbells are collapsed into a single curve. The flow rate Q scales with the inter-orifice distance L/d as $Q \propto Q_0 \times e^{-0.1(1+X_{db})(L/d)^{0.1}}$ and with the fraction of dumbbells as $Q \propto \frac{1}{0.86+0.73X_{db}}$ (figure 5.13 b).

Area fraction and granular temperature are computed in the region R_2 lying just above one of the orifices as shown in the figure 5.1b. Area fraction ϕ is found to vary

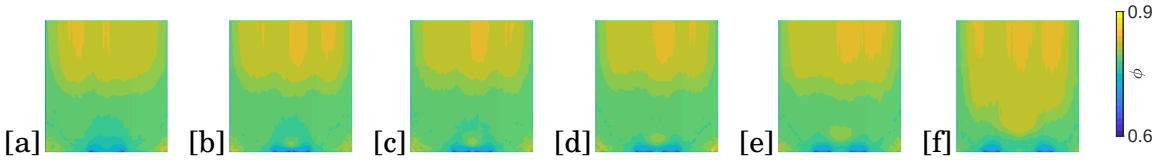

Figure 5.16: Spatial distribution of area fraction ϕ at different spacings L/d = a) 0.0, b) 2.5, c) 5, d) 10, e) 20 and f) 40 between the orifices, each of width $W/d = 20$, placed on the silo base. The fraction of dumbbells for all the cases is $X_{db} = 0.5$.

slightly with the inter-orifice distance L/d however it decreases with an increase in X_{db} (figure 5.14). Moreover, ϕ, in this case, is less as compared to that of the lateral orifice case because the particles lying above the lateral orifice flow into the region beside the orifice due to gravity and thus results in higher ϕ. Granular temperature T_g is found to increase with an increase in L/d for a system of discs $X_{db} = 0.0$ and it decreases with an increase in L/d for that of dumbbells $X_{db} = 1.0$. For the mixtures of dumbbells and discs, T_g is noticed to remain almost constant. Moreover, T_g is noticed to decrease with an increase in X_{db} at all L/d. With the addition of dumbbells, velocity fluctuations in the region above the orifice decrease due to a decrease in the particle collisions and particle velocities as dumbbells have more affinity to interlock due to their geometry. Figure 5.15 displays the vertical velocity profiles as a function of horizontal position. At a lower inter-orifice distance $L/d \leq 10$, the flow through an orifice is found to influence the flow of particles through another orifice. This interaction zone between the orifices is responsible for a significant difference in the magnitude of the particle velocities at $L/d = 2.5$ and $L/d = 20$ in the region above the orifice. The interaction zone is noticed to be almost absent at $L/d \geq 20$. As the distance between the orifices increases, the velocities of the particles lying between the two orifices decreases due to an increase in the stagnant zone. The silo flows are usually characterised by the spatio-temporal heterogeneities [39]. However, the two orifices are observed to have almost similar velocity profiles because V_y is averaged over a certain time. The maximum vertical velocity of the particles is noticed to decrease with an increase in L/d supporting the result of a decrease in the flow rate with L/d in figure 5.14a.

5.3.2.1 Flow fields at various L/d

We employed the coarse-graining technique as explained in section 5.3.1.1 to comprehend the influence of the separation distance between the two orifices on the flow dynamics.

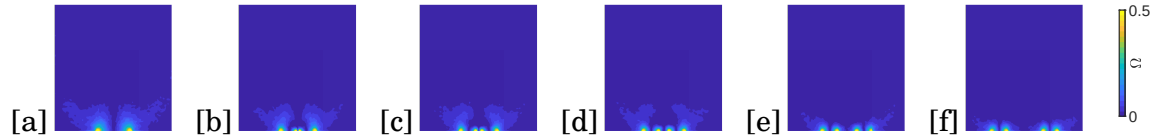

Figure 5.17: Spatial distribution of rotational velocity Ω at different spacings L/d = a) 0.0, b) 2.5, c) 5, d) 10, e) 20 and f) 40 between the orifices, each of width $W/d = 20$, placed on the silo base. The fraction of dumbbells for all the cases is $X_{db} = 0.5$.

Figure 5.18: Spatial distribution of fluctuations in rotational velocity Ω_{fl} at different spacings L/d = a) 0.0, b) 2.5, c) 5, d) 10, e) 20 and f) 40 between the orifices, each of width $W/d = 20$, placed on the silo base. The fraction of dumbbells for all the cases is $X_{db} = 0.5$.

Figure 5.19: Spatial distribution of velocity V at different spacings L/d = a) 0.0, b) 2.5, c) 5, d) 10, e) 20 and f) 40 between the orifices, each of width $W/d = 20$, placed on the silo base. The fraction of dumbbells for all the cases is $X_{db} = 0.5$.

Here, we demonstrated flow fields of area fraction ϕ, rotational velocity Ω, fluctuations in rotational velocity Ω_{fl}, velocity V, granular temperature T_g, pressure P and shear stress $|\tau|$. Each parameter is plotted at six different separation distances L/d ranging from 0.0 to 40.0 in the region: $-68.5 \leq x \leq 68.5$ and $1.5 \leq y \leq 148.5$. All the flow fields correspond to the fraction of dumbbells $X_{db} = 0.5$ and the width of each of the orifice is $W/d = 20$. The variation in L/d has little effect on ϕ in the bulk (figure 5.16) as the fraction of dumbbells is the same for all the cases. In the region above the orifice due to shear-induced dilation, the area fraction is noticed to be less. With an increase in L/d, the

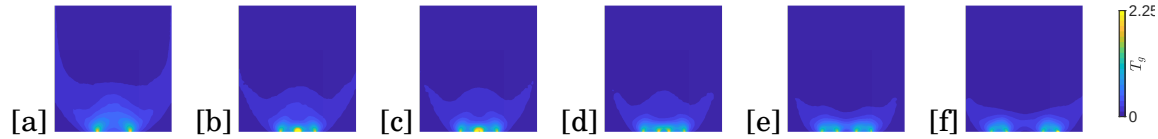

Figure 5.20: Spatial distribution of granular temperature T_g at different spacings L/d = a) 0.0, b) 2.5, c) 5, d) 10, e) 20 and f) 40 between the orifices, each of width $W/d = 20$, placed on the silo base. The fraction of dumbbells for all the cases is $X_{db} = 0.5$.

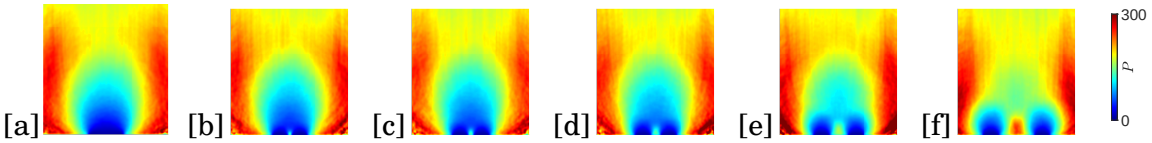

Figure 5.21: Spatial distribution of pressure P at different spacings L/d = a) 0.0, b) 2.5, c) 5, d) 10, e) 20 and f) 40 between the orifices, each of width $W/d = 20$, placed on the silo base. The fraction of dumbbells for all the cases is $X_{db} = 0.5$.

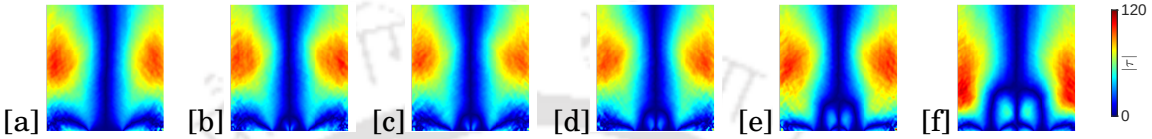

Figure 5.22: Spatial distribution of shear stress $|\tau|$ at different spacings L/d = a) 0.0, b) 2.5, c) 5, d) 10, e) 20 and f) 40 between the orifices, each of width $W/d = 20$, placed on the silo base. The fraction of dumbbells for all the cases is $X_{db} = 0.5$.

region of dilation decreases gradually and for $L/d \geq 10$, it is confined to small regions just above the orifices. Rotational velocity Ω is almost negligible in the bulk as the particle rotations are not possible because the particles are closely packed. As L/d increases, Ω is present on either side of the two orifices. Until $L/d = 10$, rotational velocity varied slightly from that of a single big orifice case ($L/d = 0$), however, at $L/d > 10$, the Ω at each orifice is found to be independent of the other orifice. Fluctuations in rotational velocity are almost negligible in the bulk (figure 5.18) as the rotational velocity is almost constant in the bulk as observed in figure 5.17. In the region above the orifice, Ω_{fl} is found to be less at inter-orifice distance $L/d = 0$ and $L/d \geq 20$. However, Ω_{fl} is found to be more in the region between the two orifices for $2.5 \leq L/d \leq 10$ as the particles present in between the orifices tends to discharge through either of the orifices.

Velocity fields of a mixture of discs and dumbbells at various inter-orifice distance L/d are displayed in figure 5.19. In the bulk, the velocities V of the particles are almost constant and V is found to decrease with an increase in L/d. The orifices are found to interact until $L/d = 20$ and then for $L/d = 40$, they cease to interact as they are wide apart. Qualitatively similar behaviour has been noticed in [21] while spherical beads are discharging through two orifices placed on the base of a flat-bottomed quasi-2D hopper. The stagnant zone is found to expand between the orifices from $L/d \geq 10$ forming an upward-pointed triangle due to the availability of a flat base. However, for $L/d < 10$, the stagnant zone is almost negligible as the base is so small that hardly two or three particles can stay on the base which would be discharged from either of the orifices. As

the stagnant zone hinders the flow, consequently velocity is found to decrease with an increase in L/d due to the expansion of the stagnant zone. Granular temperature T_g is found to be almost negligible in the bulk(figure 5.20) as the velocity is almost constant. However, T_g decreases with an increase in the inter-orifice distance L/d in the region above the orifice due to a decrease in the collisions resulting from a decrease in the particle velocities as noticed in figure 5.19. Pressure fields are illustrated in the figure 5.21 where the orifices are found to interact until $L/d = 10$ in the region above the orifice as if there is a single orifice. However, at $L/d = 20$, a weak interaction is noticed and at $L/d = 40$, it is completely absent as the orifices are wide apart. The pressure is more near the walls as compared to the bulk because the force chains are usually stronger near the walls as they can be supported by the walls. The pressure is found to be least in the region above the orifices due to dilation as noticed in figure 5.16. Moreover, due to the expansion of the stagnant zone as observed in figure 5.19, the pressure is found to increase in the region between the two orifices as the load from the particles flowing above is supported by the base wall between the two orifices. Shear stress seems to be almost independent of inter-orifice distance L/d in the bulk as shown in the figure 5.22 except at very large L/d. The areas of deep blue with the least $|\tau|$ in the bulk correspond to the flowing zone. Moreover, shear stress is noticed to be maximum near the walls, a behaviour reminiscent in the fluid flow. The stagnant zone developed at the centre of the silo base at $L/d \geq 10$ hinders the movement of particles discharging through each of the orifices thus resulting in higher shear stress. Figure 5.22 displays an increase in shear stress with an increase in the inter-orifice distance in the region between the orifices and the stagnant zone at the centre of the silo base due to an expansion of the stagnant zone as observed in the figure 5.19.

5.4 Conclusion

In this work, we studied the mixture of dumbbells and discs in a silo for two different situations: the first one is the flow through an orifice placed on the sidewall and the other one is flow through multiple orifices on a silo base.

5.4.1 Lateral orifice

Here, we studied the effect of the fraction of dumbbells on the mixture of dumbbells and discs flowing through an orifice placed on the sidewall. Flow rate is found to decrease with an increase in the fraction of dumbbells. This can be due to an increase in the dynamic friction with an increase in X_{db} resulting from the interlocking of the dumbbells. At any fraction of dumbbells, flow rate Q is found to scale with $(W/d)^{1.5+X_{db}/2}$ where W/d is the width of the lateral orifice. This is a modified Beverloo's law which includes not only orifice width but also the fraction of dumbbells. Moreover, at any orifice width, the flow rate is observed to scale with $1 - 0.65 \times X_{db}$. The ordering of dumbbells is found to decrease with an increase in the fraction of dumbbells near the lateral orifice. This results in a decrease in the area fraction and consequently a decrease in the flow rate. Moreover, the maximum velocity V_{max} is found to decrease with an increase in the fraction of dumbbells in the region beside the orifice thus complimenting the flow rate trends. The area fraction in the region beside the lateral orifice is found to be more as compared to the region above the orifice placed on a silo base as the particles lying above the lateral orifice slides into the region beside the orifice. Self-similar profiles of horizontal and vertical velocities are observed in the region beside the orifice for a mixture of dumbbells and discs. The pressure is noticed to be more towards the left side wall and least in the region beside the orifice. Shear stress is maximum in the region close to the left side wall as it lies between the wall and the flowing zone.

5.4.2 Multiple orifices on the silo base

Here, we analysed how the distance between the two orifices placed on the silo base influences the rheology of a mixture of dumbbells and discs. The flow rate Q is found to be maximum when the inter-orifice distance L/d is zero for all mixture concentrations. It decreases gradually with an increase in the inter-orifice distance and gets saturated when the distance between the two orifices is very large. Time-averaged velocity fields revealed an increase in the stagnant zone present in between the two orifices. The hindrance offered by this stagnant zone along with the one present besides the side walls might be the reason for a decrease in Q with an increase in L/d. The two orifices were found to interact until $L/d = 20$ and then they cease to interact for larger inter-orifice spacing. Inter-orifice distance has little effect on the area fraction. In the region above the orifices, shear stress is found to increase with an increase in the inter-orifice spacing

due to an expansion of the stagnant zone between the orifices.

BIBLIOGRAPHY

[1] L. E. Silbert, D. Ertaş, G. S. Grest, T. C. Halsey, D. Levine and S. J. Plimpton, *Phys. Rev. E*, 2001, **64**, 051302.

[2] C. Mankoc, A. Janda, R. Arévalo, J. M. Pastor, I. Zuriguel, A. Garcimartín and D. Maza, *Granular Matter*, 2007, **9**, 407–414.

[3] A. M. Lattanzi and J. J. Stickel, *AIChE Journal*, 2020, **66**, e16882.

[4] P. Cleary, *Second International Conference on CFD in the Minerals and Process Industries*, 1999.

[5] A. Ashour, S. Wegner, T. Trittel, T. Börzsönyi and R. Stannarius, *Soft Matter*, 2017, **13**, 402–414.

[6] I. Zuriguel, A. Garcimartín, D. Maza, L. A. Pugnaloni and J. M. Pastor, *Phys. Rev. E*, 2005, **71**, 051303.

[7] A. Vamsi Krishna Reddy, S. Kumar, K. Anki Reddy and J. Talbot, *Phys. Rev. E*, 2018, **98**, 022904.

[8] T. Börzsönyi, E. Somfai, B. Szabó, S. Wegner, P. Mier, G. Rose and R. Stannarius, *New Journal of Physics*, 2016, **18**, 093017.

[9] H. A. Janssen, *Zeitschr. d. Vereines deutscher Ingenieure*, 1895, **39**, 1045–1049.

[10] W. Beverloo, H. Leniger and J. van de Velde, *Chemical Engineering Science*, 1961, **15**, 260–269.

[11] P. Artega and U. Tüzün, *Chemical Engineering Science*, 1990, **45**, 205–223.

[12] F. Chevoir, F. Gaulard and N. Roussel, *Europhysics Letters (EPL)*, 2007, **79**, 14001.

[13] M. Benyamine, M. Djermane, B. Dalloz-Dubrujeaud and P. Aussillous, *Phys. Rev. E*, 2014, **90**, 032201.

[14] I. I. Bagrintsev and S. S. Koshkovskii, *Chemical and Petroleum Engineering*, 1977, **13**, 503–505.

[15] A. Medina, D. Cabrera, A. López-Villa and M. Pliego, *Powder Technology*, 2014, **253**, 270 – 275.

[16] D. A. Serrano, J. Hernández-Juárez, A. López-Villa, A. Medina, C. A. Vargas and M. Pliego, *Journal of Physics: Conference Series*, 2019, **1221**, 012034.

[17] Y. Zhou, P.-Y. Lagrée, S. Popinet, P. Ruyer and P. Aussillous, *Journal of Fluid Mechanics*, 2017, **829**, 459–485.

[18] C. Davies and M. Desai, *Powder Technology*, 2008, **183**, 436 – 440.

[19] A. Kunte, P. Doshi and A. V. Orpe, *Phys. Rev. E*, 2014, **90**, 020201.

[20] A. V. Orpe and P. Doshi, *Phys. Rev. E*, 2019, **100**, 012901.

[21] X. Zhang, S. Zhang, G. Yang, P. Lin, Y. Tian, J.-F. Wan and L. Yang, *Physics Letters A*, 2016, **380**, 1301 – 1305.

[22] C. Xu, F.-L. Wang, L.-P. Wang, X.-S. Qi, Q.-F. Shi, L.-S. Li and N. Zheng, *Powder Technology*, 2018, **328**, 7 – 12.

[23] L. A. Fullard, E. C. P. Breard, C. E. Davies, A. J. R. Godfrey, M. Fukuoka, A. Wade, J. Dufek and G. Lube, *Proceedings of the Royal Society A: Mathematical, Physical and Engineering Sciences*, 2019, **475**, 20180462.

[24] R. Maiti, G. Das and P. K. Das, *Physics of Fluids*, 2017, **29**, 103303.

[25] S. Kamath, A. Kunte, P. Doshi and A. V. Orpe, *Phys. Rev. E*, 2014, **90**, 062206.

[26] P. A. Cundall and O. D. L. Strack, *Géotechnique*, 1979, **29**, 47–65.

[27] N. V. Brilliantov, F. Spahn, J.-M. Hertzsch and T. Pöschel, *Phys. Rev. E*, 1996, **53**, 5382–5392.

[28] S. Plimpton, *Journal of Computational Physics*, 1995, **117**, 1 – 19.

[29] A. Stukowski, *Model. Simul. Mater. Sci. Eng*, 2010, **18**, 015012.

[30] S. Kumar, M. Dhiman and K. A. Reddy, *Phys. Rev. E*, 2019, **99**, 012902.

[31] K. A. Reddy, J. Talbot and V. Kumaran, *Journal of Fluid Mechanics*, 2010, **660**, 475–498.

[32] Y. Zhou, P. Ruyer and P. Aussillous, *Phys. Rev. E*, 2015, **92**, 062204.

[33] A. Janda, I. Zuriguel and D. Maza, *Phys. Rev. Lett.*, 2012, **108**, 248001.

[34] T. Weinhart, R. Hartkamp, A. R. Thornton and S. Luding, *Physics of Fluids*, 2013, **25**, 070605.

[35] B. J. Glasser and I. Goldhirsch, *Physics of Fluids*, 2001, **13**, 407–420.

[36] T. Börzsönyi, E. Somfai, B. Szabó, S. Wegner, P. Mier, G. Rose and R. Stannarius, *New Journal of Physics*, 2016, **18**, 093017.

[37] A. L. Dubov, T. Y. Molotilin and O. I. Vinogradova, *Soft Matter*, 2017, **13**, 7498–7504.

[38] R. Blanco-Rodríguez and G. Pérez-Ángel, *Phys. Rev. E*, 2018, **97**, 012903.

[39] A. Mehta, *Soft Matter*, 2010, **6**, 2875–2883.

CHAPTER 6

CLOGGING PHENOMENA IN A SYSTEM OF ASYMMETRIC DUMBBELLS

6.1 Introduction

A narrow road gets jammed when more automobiles simultaneously try to enter or exit through it. The entrance of any theatre or stadium gets blocked when a large crowd of enthusiasts wish to pass through it. Similarly, the flow of solid raw materials into a processing unit might get clogged if the outlet is slightly larger than the average size of the raw materials. Clogging is one of the major issues in industries as it halts processing. It is associated with the formation of an arch in a two-dimensional silo or a dome shape in a three-dimensional silo respectively. The clogged particles are mutually stabilized and can hold the weight of the entire bed. The clogged systems were termed as fragile matter by Cates *et al.* [1] as the entire bed collapses when the small external stress is applied on the arch particles at a particular point. The clogging phenomena can be quantified by using either clogging probability or avalanche size. Avalanche size is the number of particles discharged before the system gets clogged or the number of particles discharged between two consecutive clogged instances.

In a system of spherical particles, the ratio of orifice width and diameter of the particle is the prime factor that influences the clogging. When this ratio is beyond 5, the chances of clogging were found to be very less in a two-dimensional silo consisting of spherical

particles [2]. In a spherical particulate system, the aspect ratio (arch height/half of the orifice width) of the arch formed at the orifice in a clogged system was found to be 1.0 [3]. To and Lai [4] noticed that the clogged arch is convex in shape at all particle positions of an arch. However, Garcimartín *et al* [3] observed that some clogged particles might make an angle of more than 180^o with their two adjacent clogged particles and these are termed as defects. In another work [5], the maximum angle made by any clogged particle with its two adjacent particles was found to be the weakest portions of an arch. [6] noticed that the average normal force experienced by the particles in the arch is significantly larger than that of the surrounding particles. The authors further reported that the magnitude of the normal force on an arch particle strongly depends on the angle subtended by its centre with the contact points of the two neighbouring arch particles. Moreover, when this angle is more than 180^o, with an increase in the angle normal force was noticed to decrease whereas the tangential force was found to increase. The behaviour was vice versa when the angle is less than 180^o. Thomas and Durain [7] studied how the angle made by the hopper base with horizontal and the size of the aperture influences the clogging in a hopper. The authors reported that the chances of clogging increases with an increase in the tilt angle. Pournin *eta l.* [8] studied the influence of friction and polydispersity of spherical beads on the jamming behaviour. [9] reported that the clogging probability does not depend on the material properties but it depends on the shape of the particles.

Unlike spherical systems, in a system of non-spherical particles, along with the size ratio of orifice and particle, their orientation also plays a prominent role regarding clogging phenomena. The orifice width beyond which the chances of clogging is very less in a system of dumbbells (aspect ratio is 2) was found to be more than twice that of the one with spherical (aspect ratio is 1) particles [10]. The authors attributed the orientation of the particles as well as the geometrical interlocking among the particles to this behaviour. Parisi *et al.* [11] studied a system of self-propelled sphero cylindrical particles propelling with the desired orientation. The flow rate was found to be more when the small axis of the particles is oriented in the flow direction than that of the case where the large axis of particles is oriented in the flowing direction. The authors explained that the particles in the latter case are more prone to clogging than that in the former case. The importance of orientation in the case of non-spherical particles was reiterated in another work where the alignment of the elliptical particles was noticed to

enhance the stability of the arches [12]. Tamás Börzsönyi *et al.* [13] as well found that the elongated particles make small angles with the streamlines in the flowing zone of the three-dimensional silo. Yet in another study [14], the elongated particles were noticed to align in such a way that their longest axis is oriented towards the centre of the silo in a clogged state. Further, the authors reported that the clogging probability increases with an increase in the aspect ratio of the elongated particles. Moreover, they noticed that the number of particles required to form clog increases with an increase in the aspect ratio of the particles. At aspect ratios greater than 8, an extreme case namely “rat-holing" is observed which involves long vertical holes from silo base to the open surface of the granular bed.

A special case of elongated particles is the asymmetric dumbbell particles or snowman-shaped particles which are generated by fusing two different sized discs. Using Monte Carlo simulations and free energy calculations, Dennison *et al.* [15] illustrated a phase diagram of hard snowman-shaped particles. Han *et al.* [16] performed experiments as well as simulations on the dense random packing of snowman particles and observed strong correlations in orientation with the surrounding particles. To the best of our knowledge, there is no study on the clogging characteristics of a system of snowman particles or asymmetric dumbbells flowing through a two-dimensional silo. Most of the previous works on the clogging phenomena were confined to either spherical particles or in some cases with that of elongated particles. In this work, we probed how the clogging characteristics are affected by an increase in the asymmetry of the particles. The asymmetry is varied by increasing the diameter of one disc D_b of a snowman particle while keeping the diameter of the second disc D_s constant. Firstly, the average avalanche size is computed at different orifice widths and different D_b/D_s ratios. Further, we analysed the arch characteristics like the average number of particles required to form a clogged structure, arch morphology, the pressure experienced by clogged particles at various angular positions and the orientation of clogged particles. Moreover, we presented time-averaged flow fields of parameters like velocity, pressure, shear stress at various locations of the silo during the free flow of particles to analyse how the asymmetry of particles D_b/D_s affect the flow dynamics. The paper is organised as follows: the simulation technique is explained in the next section. In Section 6.3, results and their interpretations are elucidated.

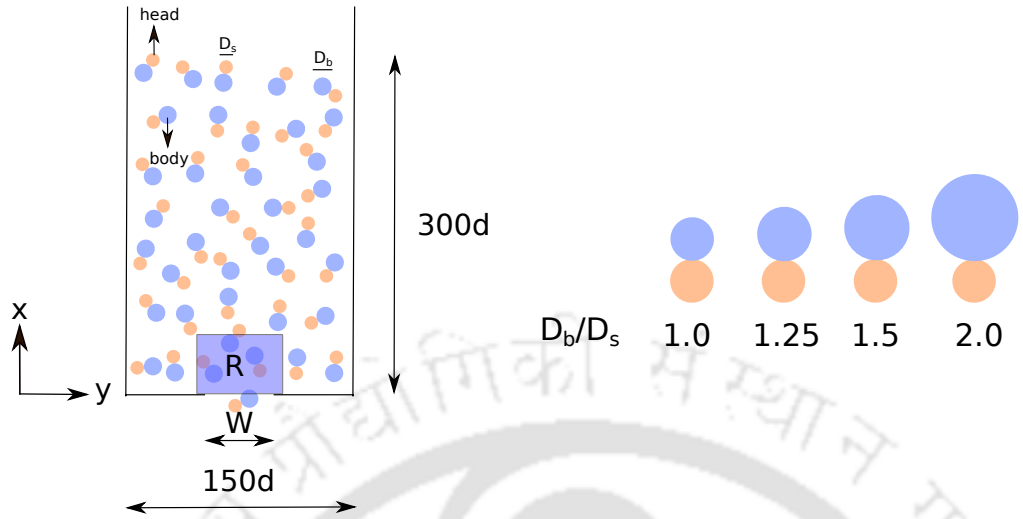

Figure 6.1: The schematic representation of snowman-shaped particles discharging through a flat-bottomed silo. Here, the orange ones indicate head or smaller part and the blue ones indicate body or larger part of snowman particles. D_s and D_b denote diameters of the smaller and larger parts of the snowman particles. The origin is located at the centre of the silo which is equidistant from both the side walls.

6.2 Simulation Methodology

The discrete element method (DEM) [17] is used in the study to comprehend the flow of snowman-shaped particles discharging through a two-dimensional flat-bottomed silo. The DEM technique is elucidated in chapter 2. Snowman particles are created by adjoining two discs of different diameter as shown in figure 6.1. The diameter of the smaller and larger particles are denoted by $D_s = d$ and D_b respectively. The initial configuration is generated by placing few snowman particles at arbitrary locations with random orientations in a silo confined by walls at $x = \pm 75d$ and $y = 0$. We ensured that there are no overlaps among the particles at any point in time. A gravity of magnitude g is applied in the negative y-direction. Once these particles get settled at the base, another set of particles are placed into the silo and they are allowed to settle and so on until the height of the bed reaches 300d. At time $t = 0$, an orifice of width W is opened on the silo base to let the particles discharge out of the silo. Periodic boundary conditions are applied in the y direction and the particles discharging out of the silo are placed at the top of the granular bed at random locations with reduced velocities. The simulation is stopped when the system gets clogged near the orifice. We have studied a minimum of 100 clogged states obtained from 100 different initial configurations for each of the cases. The values of the constants used in the simulations are shown in Table 6.1

Simulation parameters	Values
K_n	$2.00 \times 10^6 \rho d g$
K_t	$2.45 \times 10^6 \rho d g$
γ_n	$1000\sqrt{g/d^3}$
γ_t	$1000\sqrt{g/d^3}$
μ	0.5
$timestep$	$10^{-4}\sqrt{d/g}$

Table 6.1: The constants used in our numerical simulations

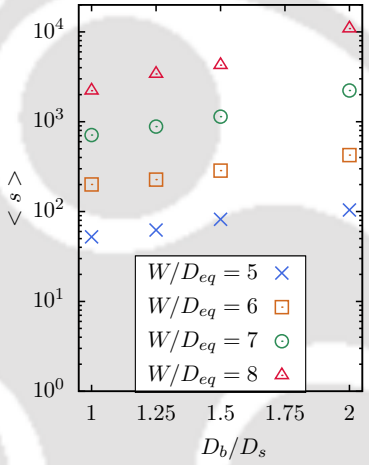

Figure 6.2: Average avalanche size $< s >$ as a function of D_b/D_s for various orifice widths W/D_{eq}. Here, D_b and D_s are diameters of larger and smaller parts of an asymmetric dumbbell and D_{eq} is the dumbbell equivalent diameter.

6.3 Results and Discussion

In this section, we will explain the results obtained for a system of snowman-shaped particles discharging through a two-dimensional silo. We elucidate the morphology of arches, the flow characteristics followed by the time-averaged flow fields. The flow is characterised by parameters like mass flow rate, area fraction, average velocity etc. Mass flow rate Q is obtained by computing the slope of the total mass of the particles discharged versus the time plot using the least-square fitting method. Area fraction ϕ and average velocity $< v >$ are computed in the region R which lies just above the orifice and having a size of $W + 2D_{eq}$ in the x-direction and $5D_{eq}$ in the y-direction as shown in figure 6.1. Area fraction is computed as the ratio of the total area occupied by particles in

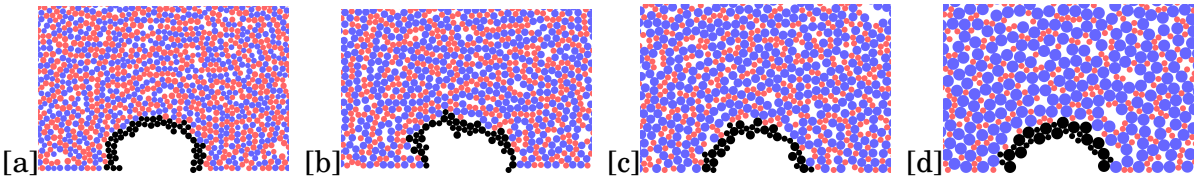

Figure 6.3: Representative clogging arches for $W/D_{eq} = 8$ and D_b/D_s = a) 1.0, b) 1.25, c) 1.5 and d) 2.0. Here, red and blue circles are used to represent the smaller and larger particle conforming the dumbbell respectively; except in a) where both dumbbell particles are equally sized and the color is assigned randomly. Black dumbbells are used to signal the particles conforming the clogging arch.

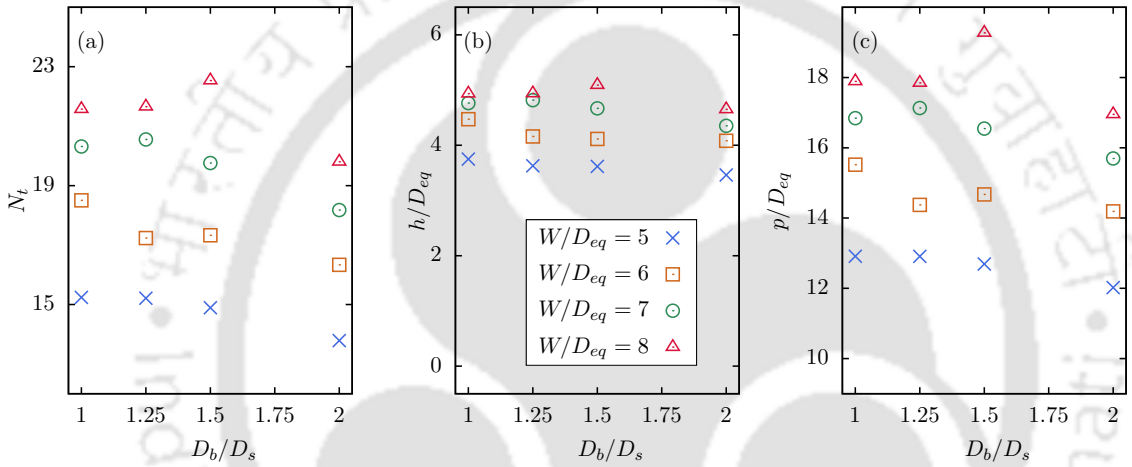

Figure 6.4: a) Number of clogged particles N_t, b) height h/D_{eq} and c) perimeter p/D_{eq} of the arches with respect to D_b/D_s.

the region R and the area of the region R. Finally, the flow fields of different parameters are presented.

We start by presenting the effect that an increase in the asymmetry of the snowman particles has on the appearance of clogging. To this end, we compute avalanche sizes, s, as the total number of particles discharged through an orifice before the system gets clogged. In particular, we use the mean avalanche size $< s >$, which is calculated by averaging over a minimum of 100 clogged states. In Fig. 6.2 the dependence of $< s >$ with the ratio D_b/D_s is reported for several orifice widths (W). Note that D_b/D_s somehow characterizes the asymmetry of the particles: 1.0 corresponds to symmetric dumbbells and 2.0, to the most asymmetric particles analyzed in this work. Also, it should be mentioned that the orifice width is normalized by D_{eq} which is the equivalent diameter of a disc D_{eq} with the same area as the snowman particle. The reason for using D_{eq} instead of, for example, D_b

or $D_s + D_b$, is based on the observation that the orientations of the particles when flowing out of the silo are not homogeneous. Indeed, if all the particles above the orifice were vertically orientated during the entire duration of flow, the best normalizing parameter for orifice width would be D_b, whereas if all the particles were horizontally oriented, then $D_b + D_s$ would be the best normalizing parameter. However, as the orientations of the particles generally lie between these two extremes, hence we chose D_{eq} as the normalizing parameter for orifice width.

Fig. 6.2a demonstrates that for all orifice widths, the average avalanche size $< s >$ increases with D_b/D_s; i.e. clogging reduces when the dumbbells become more and more asymmetric. This result, which may seem surprising at first, is rather reasonable if we consider that for $D_b/D_s >> 1$, the snowman particle becomes, basically, a disc. Thus, with an increase in D_b/D_s, the behaviour of the snowman particle shifts from a dumbbell-like (elongated particle) to that of a disc-like particle. Consequently, when increasing D_b/D_s, the role of the rotational degrees of freedom of the particles diminishes, as well as the characteristic interlocking among dumbbells. All these effects lead to a reduction of the ability of the particles to form clogs, and therefore, to an increase of the avalanche size. A similar result was noticed in [14], where the average avalanche size of a system of spherical particles was proved to be larger than that of elongated particles.

Next, we analyze some geometrical properties of the clogging arches (see Fig. 6.3 to see some examples for different D_b/D_s ratios). In particular, we measure the number of particles conforming the arch, as well as their height and perimeter. The height of the arch is the distance between the clogged particle whose centre of mass y position is maximum and the one lying on the silo base. The perimeter of an arch is computed as the sum of the distances between the centre of mass positions of adjacent clogged particles.

At any orifice width W/D_{eq}, the mean number of particles N_t averaged over all clogging arches, decreases with an increase in D_b/D_s (Fig. 6.4a). Again, this behaviour can be justified if we think that the particles tend to display more spherical or disc-like properties with an increase in D_b/D_s. Therefore, if the number of different geometrical configurations that can block the orifice is higher for the case of elongated particles than for discs, it follows that the average number of particles conforming these arches is also larger for the lower values of D_b/D_s. In other words, irregular arches that would not be stable with spherical beads can be found when using symmetric dumbbells. Also, the preferential orientation of elongated particles pointing to the orifice as noticed by Ashour *et al* [14], might be the reason behind the increase of N_t when D_b/D_s reduces. Incidentally,

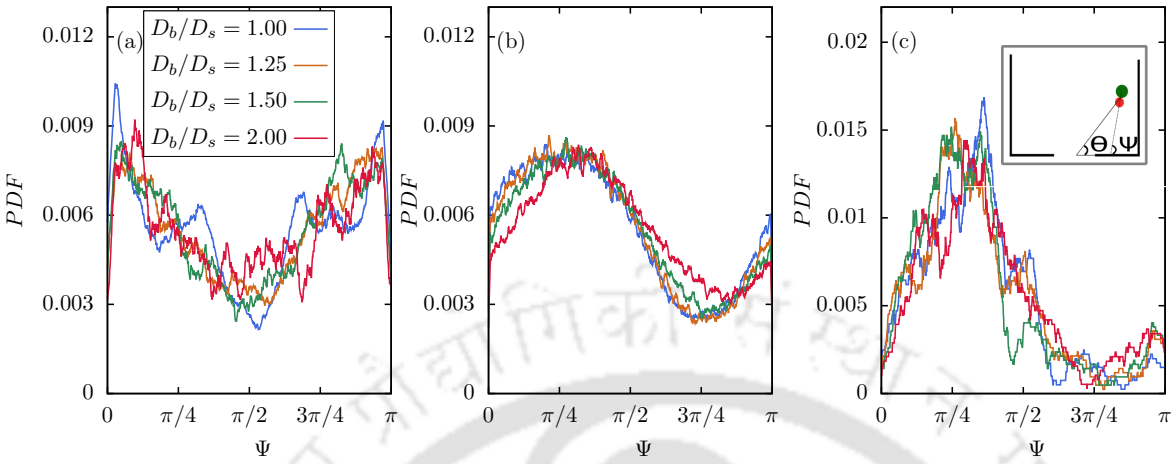

Figure 6.5: Probability distribution of the orientation Ψ of particles in different scenarios: a) in the stationary deposit formed before opening the orifice at the beginning of the simulation; b) during continuous flow ($W/D_{eq} = 8$); and c) particles conforming a clogging arch ($W/D_{eq} = 8$). In all cases, the region considered for computing Ψ is at an angular position $\theta = \pi/4$ at a radial distance of $10D_s$. In the inset of c) the definition of the dumbbell orientation (Ψ) and angular position of the particles (θ) is schematized.

let us note that in Fig. 6.4a, we can observe the expected effect that increasing W/D_{eq} must have in the obtained values of N_t: as the orifice size grows, more particles are required to span the entire width to form a clog.

The outcomes of the height and perimeter of the arches (Fig. 6.4b and 6.4c, respectively) are perfectly consistent with the ones in Fig. 6.4a: both magnitudes slightly decrease with an increase of D_b/D_s due to a decrease in the number of clogged particles. In summary, when D_b/D_s increases, it seems that to have an arch stabilized, its regularity should augment (N_t, h and p are reduced). This would reduce the number of arches that can clog the orifice, hence leading to an increase in the avalanche size. In other words, small values of D_b/D_s allow the stabilization of irregular arches that are never found for the case of isotropic particles (discs).

Once we have qualitatively related the arch geometry with the dependence of the avalanche size on D_b/D_s, we will focus on the role of the particle orientation in clogging. The particle orientation, Ψ, is measured as the angle made by the line joining the centres of the two discs in the asymmetric dumbbell with the horizontal axis ($y = 0$) as shown in the inset of figure 6.5c. As the orientation of anisotropic particles is known to depend on their position within the silo [14], we will perform a spatial analysis of the dumbbell

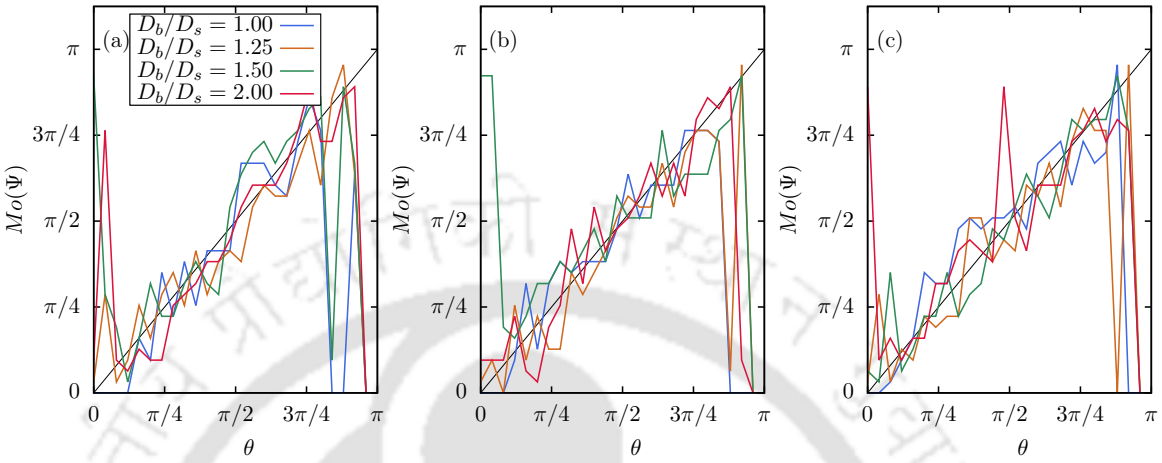

Figure 6.6: The mode of orientation of the clogged particles $Mo(\Psi)$ with respect to their angular positions θ. Results for orifice widths W/D_{eq}=6,7 and 8, are represented in a), b), and c) respectively. Black lines represent $Mo(\Psi) = \theta$.

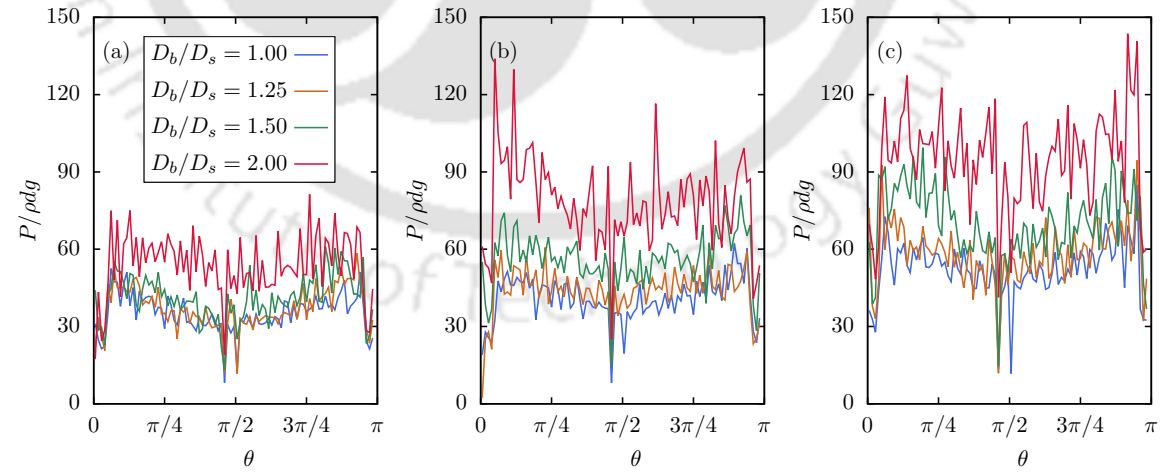

Figure 6.7: Pressure experienced by the clogged particles with respect to their angular positions θ. Results for orifice widths W/D_{eq}=6,7 and 8, are represented in a), b), and c) respectively.

orientation. Indeed, given the special geometry of our system, we will use cylindrical coordinates with the origin at the centre of the orifice to characterize the position of the particles. In particular, in the inset of figure 6.5c the definition of the angular position of the particles, θ, is schematized as the angle made by the line joining the centre of an orifice ($x = 0, y = 0$) and the centre of mass position of the particle with the horizontal axis ($y = 0$). As an example, in Fig. 6.5 we represent the probability distributions of the orientations Ψ of the dumbbells found at an angular position $\theta = \pi/4$. This is done in three different scenarios: a) immobile dumbbells in a static pile at a radial distance of 10 D_s, b) dumbbells at a radial distance of 10 D_s that are flowing out of the silo, and c) dumbbells conforming to a clogging arch. The particles prefer to orient horizontally irrespective of the D_b/D_s ratio in a static pile (figure 6.5a), a behaviour that is coherent with the one found in a static pile of elongated rods (aspect ratio 5) [21]. Dissimilarly, Fig. 6.5b reveals that, irrespective of D_b/D_s, the alignment distribution of flowing dumbbells displays a maximum at an angle close to $\Psi = \pi/4$ and a minimum for $\Psi = 3\pi/4$. This indicates that when flowing out of the silo, dumbbells have a certain tendency to align their long axis pointing towards the outlet. On the contrary, the perpendicular alignment of the dumbbell long axis with the outlet direction is disfavoured. Similar, but more pronounced behaviour, is observed for the particles conforming the clogging arch (Fig. 6.5c). Indeed, the peak at $\Psi = \pi/4$ displays almost twice the probability observed in Fig. 6.5b (note the different scale in both figures), and the probability of finding particles aligned at $\Psi = 3\pi/4$ is practically negligible.

Now, to see if the alignment of the clogging particles with their long axis pointing towards the outlet is robust and occurs for other angular positions, in Fig. 6.6 we represent the mode of the probability distributions of the orientation $Mo(\Psi)$ as a function of the angular position θ. To this end, we discretized the total range of angular positions $0 < \theta < \pi$ into bins, and we calculated the distribution of orientations of all the clogged particles with the centre of mass position lying within the bin limits; and then, the most probable orientation for each bin. This analysis is performed for several orifice widths and dumbbell aspect ratio, evidencing a robust behaviour: the most probable orientation of the dumbbells $Mo(\Psi)$ coincides with the angular position θ at almost all angular positions (see the continuous black lines representing $Mo(\Psi) = \theta$). This is due to the shear-induced alignment of the snowman particles to the flow direction as observed earlier [22] for a system of elongated particles. The only exception to this behaviour occurs for $\theta \approx 0$ and $\theta \approx \pi$, where the particles tend to align horizontally due to the

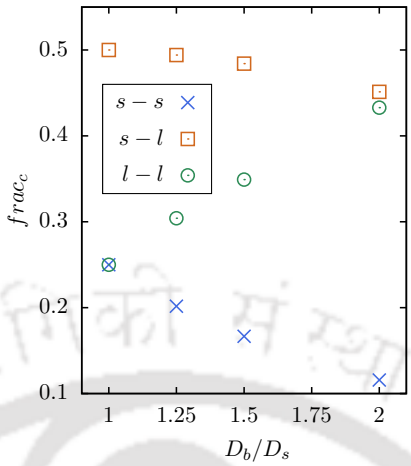

Figure 6.8: Average fraction of contacts between the different type of discs in the sample as a function of D_b/D_s. Fraction of contacts among smaller discs ($s-s$), the larger and smaller discs ($l-s$) and the larger discs ($l-l$), are calculated out of the total number of contacts that correspond to the particles in the entire system after the orifice gets clogged. The average fraction of contacts is obtained by averaging over a minimum of 100 clogged states. Note that, for $D_b/D_s = 1$, the represented proportion is obtained after randomly considering one of the two particles as large, and the other as small. Moreover, If a large disc of one snowman particle is in contact with both the small and large discs of another snowman particle, then the number of contacts is taken as one each in the smaller-larger and larger-larger contact

presence of a silo base. Interestingly, the orifice width W/D_{eq} and the dumbbells aspect ratio D_b/D_s have little effect on the preferred orientation of the clogged particles.

Next, the forces on the clogged particles are analysed in terms of stress tensor σ computed for each disc i of the dumbbells in the arch, considering only pairwise interactions as in [23]:

$$\sigma_{ab} = \frac{1}{2 \times V_i} \sum_{j=1}^{N_p} (r_{i_a} F_{i_b} + r_{j_a} F_{j_b}) \tag{6.1}$$

Here, a and b can take values x and y, N_p corresponds to the total number of neighbours and V represents the volume of the particle. Moreover, r_i and r_j are position vectors of particle i and its neighbouring particle j, F_i and F_j are the forces on the particles i and j due to their pairwise interaction. From the stress tensor, the pressure at each particle is computed as $P = -(\frac{\sigma_{xx}+\sigma_{yy}}{2})$. Then, following the idea of distinguishing among particles standing at different angular positions, in Fig. 6.7 we represent the average pressure of all particles that belong to a clogging arch and fall within the

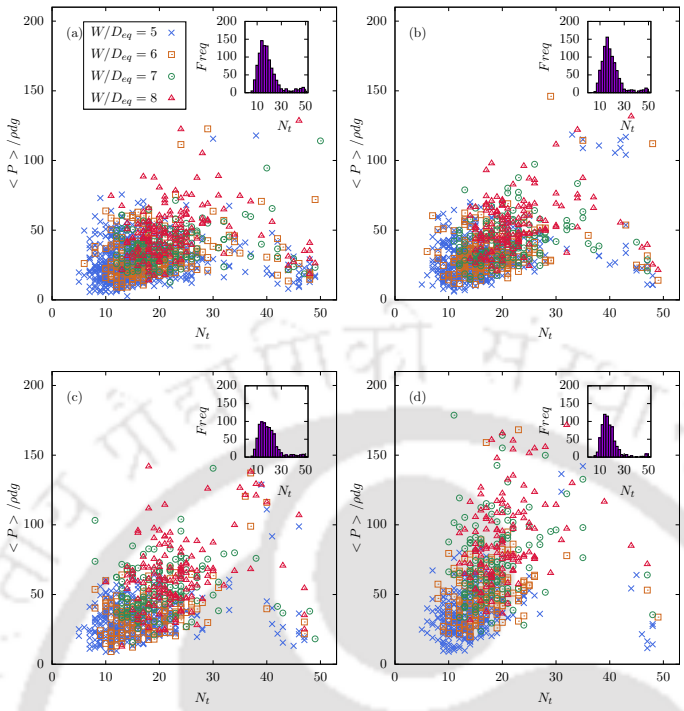

Figure 6.9: Average pressure $< P >$ of the particles conforming an arch as a function of its size (measured by its number of particles N_t). Results for dumbbell aspect ratios D_b/D_s= 1.0, 1.25, 1.5 and 2.0, are represented in a), b), c), and d), respectively. The insets in each of the plots display the histogram of the number arches found for each type of dumbbell.

regions (bins) defined by the same limits of θ established before. Again, this analysis is performed for three different outlet sizes and four dumbbell aspect ratios. Interestingly, three features can be distinguished in the plots: 1) the average pressure per particle grows with the aspect ratio D_b/D_s; 2) the average pressure per particle also increases with the outlet size W/D_{eq}; and 3) the particles above the centre of the orifice ($\theta \approx pi/2$) reveal a pressure slightly lower than in other angular locations (excluding $\theta \approx 0$ and $\theta \approx \pi$). The latter behaviour can be easily related to the lower overall pressure developed in the centre of the silo in comparison with the lateral sides reported by Hidalgo *et al* [6]. On the contrary, there is not a conclusive justification for the two former features; therefore, in the following, we will try to further investigate them and hypothesize some explanations.

The growth of the average pressure per particle with the aspect ratio D_b/D_s evidenced in Fig. 6.7 may be related to a progressive modification of the type of contact among dumbbells. Indeed, as D_b/D_s grows, the probability that two asymmetric dumbbells contact each other via their larger discs (instead of their smaller ones) also increases

(see Fig. 6.8). Therefore, as a larger disc can receive more pressure (from the force chains within the sample) than a smaller one, it seems reasonable that the pressure it exerts in the contact is also higher. Moreover, the fact that the larger disc in the dumbbell is heavier than the smaller one may play a role in the observed behaviour. Importantly, let us note that it seems to be a correlation between the pressure of the particles in the arch, and the probability of clogging: increasing D_b/D_s systematically leads to lower probabilities of clogging and higher particle pressures. We believe that these two phenomena may just be a consequence of a reduction of arch robustness when the conforming particles become more disc-like. Although this hypothesis should be confirmed, augmenting D_b/D_s will entail increasing the pressure necessary to get the arch stabilized and, consequently, a diminution of the number of arches that can get stabilized leading to a clog.

The increase of the average pressure per particle with the outlet size depicted in Fig. 6.7 was an unexpected result that suggests an increase of the average pressure per particle with the number of particles in the arch (as larger outlet sizes require arches with a larger number of particles). To confirm this, in Fig. 6.9 we represent, for each arch, the average pressure $< P >$ of the particles conforming it, as a function of its size (in the number of particles N_t). Overall, we can conclude that increasing N_t leads to an increase of the average pressure felt by the particles, at least up to $N_t \approx 35$. Above this size, a surprising reduction of the average pressure is appreciated in all the plots which could be related to the quite likely irregular shape that these arches should have. In any case, the relevance of these very large arches in the overall clogging behaviour observed in the system should not be important because they suppose a tiny fraction of the total number of arches, as it could be appreciated in the histograms displayed in the insets of Fig. 6.9.

The mass flow rate increases with an increase in the diameter of the larger disc D_b/D_s at all orifice widths (figure 6.10a). This is due to an increase in the area fraction as well as an increase in the velocity with an increase in D_b/D_s (figure 6.10b, c) in the region above the orifice. As D_b/D_s increases, the particle characteristics start to shift from that of an elongated particle to that of a spherical particle of diameter D_b. Thus with an increase in D_b/D_s, velocity increases at all W/D_{eq} as spherical particles can discharge more quickly than that of elongated particles through a given orifice width.

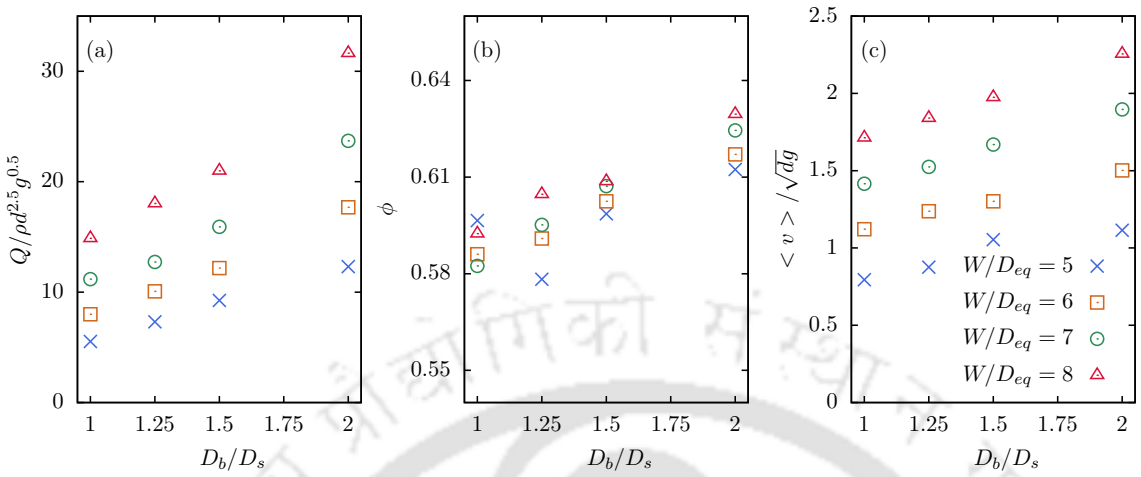

Figure 6.10: a) Flow rate Q, b) area fraction ϕ and c) average velocity $< v >$ with respect to D_b/D_s. Here, D_b,D_s are the diameters of the body, head of the snow-man particle and D_{eq} is the equivalent diameter.

6.3.1 Flow fields

In this subsection we demonstrated flow fields of various parameters obtained from coarse graining technique as suggested by Glasser and Goldhirsch [24]. The area fraction $\phi(t)$, velocity $\boldsymbol{v}(t)$, pressure $P(t)$ and stress tensor $\boldsymbol{\sigma_{ij}}(t)$ at any postion p with position vector $\boldsymbol{r_p}$ and at time t are computed as

$$\phi(t) = \left[\sum_{i=1}^{n} \frac{\rho\pi d_i^2}{4} \mathscr{W}(\boldsymbol{r_p} - \boldsymbol{r_i(t)})\right]/\rho \tag{6.2}$$

$$\boldsymbol{v}(t) = \left[\sum_{i=1}^{n} \frac{\rho\pi d_i^2}{4} \boldsymbol{v_i} \mathscr{W}(\boldsymbol{r_p} - \boldsymbol{r_i(t)})\right]/\rho\phi \tag{6.3}$$

$$\boldsymbol{\sigma_{ij}}(t) = \sum_{i=1}^{n}\sum_{j=i+1}^{n} (\boldsymbol{F^{ij}} \times \boldsymbol{r_{ij}}) \int_{s=0}^{1} \mathscr{W}(\boldsymbol{r_p} - \boldsymbol{r_i(t)} + s\boldsymbol{r_{ij}})ds \tag{6.4}$$

$$P(t) = \frac{-tr(\sigma_{ij}(t))}{2} \tag{6.5}$$

$$\mathscr{W}(\boldsymbol{r}) = \frac{1}{\pi w^2} e^{-\boldsymbol{r}^2/w^2} \tag{6.6}$$

In the above equations, ρ, d and $\boldsymbol{r}_i(t)$ are density, diameter and position vector of the i^{th} particle and $\mathscr{W}(\boldsymbol{r})$ is the coarse-graining function. Moreover, ϕ, $\boldsymbol{v}$, P, $\boldsymbol{\sigma}_{ij}$ are

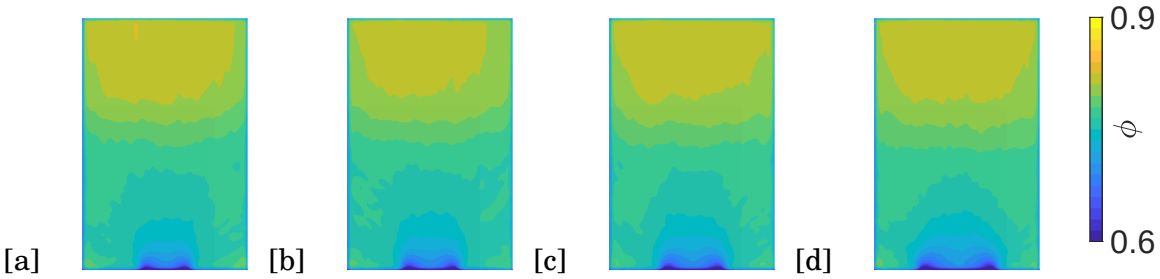

Figure 6.11: Spatial variation of area fraction ϕ at D_b/D_s = a) 1.0, b) 1.25, c) 1.5, d) 2.0 and width of the orifice is $W/D_{eq} = 20$.

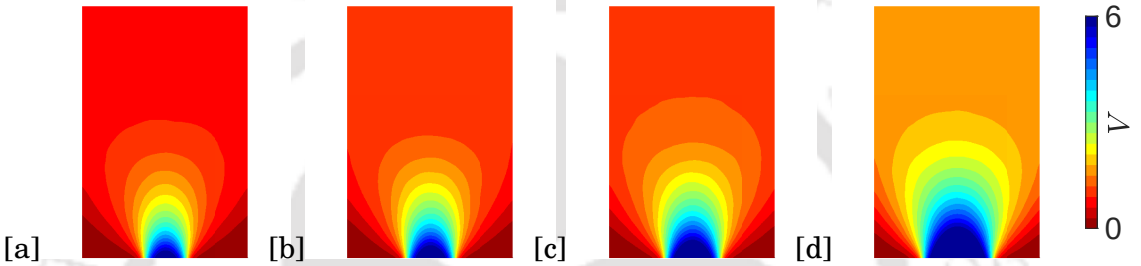

Figure 6.12: Spatial variation of velocity V at D_b/D_s = a) 1.0, b) 1.25, c) 1.5, d) 2.0 and width of the orifice is $W/D_{eq} = 20$.

time-averaged area fraction, velocity, pressure and stress tensor. For each parameter, four plots are illustrated each one corresponding to a different D_b/D_s ranging from 1.0 to 2.0 in the region: $-48.5 \leq x \leq 48.5$ and $1.5 \leq y \leq 148.5$.

Area fraction ϕ is noticed to vary slightly with an increase in the diameter of the larger disc of the snowman particles D_b/D_s. It is maximum in the bulk and minimum near the orifice due to shear-induced dilation close to the orifice. Velocity V is higher in the region above the orifice (figure 6.12) as the flow is less interrupted from the surrounded particles due to lower area fraction as noticed in the figure 6.11. A region of dark red beside the orifice signifies the presence of a set of almost immobile particles and this part of the silo is usually termed as the stagnant zone. A stagnant zone hinders the flow of particles adjacent to it which can be seen in the form of an increase in V at regions away from the stagnant zone. The stagnant zone is found to decrease with an increase in D_b/D_s thus the velocities of the particles increases with an increase in D_b/D_s. Pressure fields are demonstrated in figure 6.13 and the pressure is found to be maximum near the walls and it is least close to the orifice due to a low area fraction ϕ as observed in figure 6.11. With an increase of D_b/D_s, the pressure as well as shear stress $|\tau|$ increases because the stress transmission is more effective resulting from an

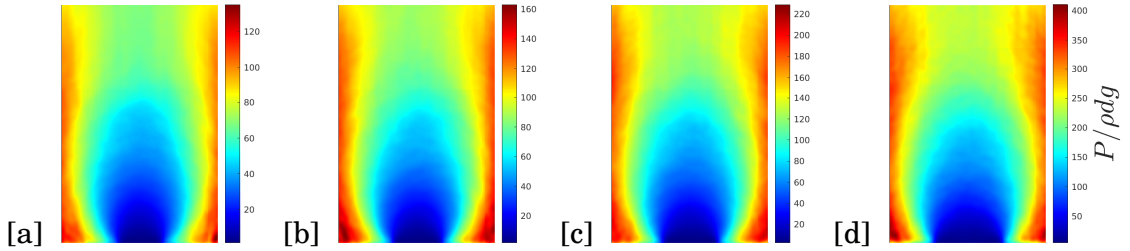

Figure 6.13: Spatial variation of pressure P at D_b/D_s = a) 1.0, b) 1.25, c) 1.5, d) 2.0 and width of the orifice is $W/D_{eq} = 20$.

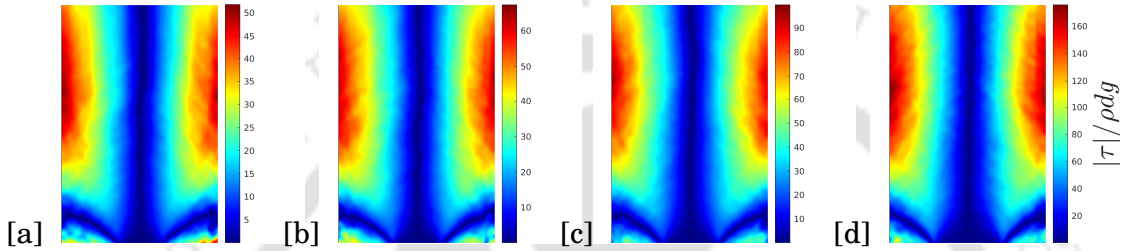

Figure 6.14: Spatial variation of shear stress $|\tau|$ at D_b/D_s = a) 1.0, b) 1.25, c) 1.5, d) 2.0 and width of the orifice is $W/D_{eq} = 20$.

increase in the area fraction. The spatial variation in shear stress $|\tau|$ is illustrated in figure 6.14. Shear stress is maximum towards the sidewalls and it slowly decreases as one moves away from the wall and it is least in the central part as it is the flowing zone. This behaviour is similar to that in the liquids which show maximum shear stress near the walls followed by a gradual decrease in the regions away from the wall.

6.4 Conclusion

We studied the clogging phenomena in a system of asymmetric dumbbells, also known as snowman particles, in a two-dimensional silo. An asymmetric dumbbell consists of two discs of different radii. We analysed the flow of these particles at four D_b/D_s ratios ranging from 1.0 to 2.0 and at four orifice widths W/D_{eq} ranging from 5.0 to 8.0. Here, D_b and D_s are the diameters of bigger and smaller discs of the dumbbell and D_{eq} is the diameter of a disc whose area is the same as that of the snowman particle. At $D_b/D_s >> 1$, the snowman particle is a disc and at $D_b/D_s = 1$, it is a symmetric dumbbell. With an increase in D_b/D_s, the characteristics of the snowman particles shifts from elongated particle to that of a disc and consequently, the average avalanche size is noticed to increase. This is because the chances of clogging are more in the case of dumbbells as

compared to that of a disc. The orientation of clogged particles vary neither with orifice width nor with D_b/D_s but it varies with the angular position of the clogged particles. The pressure experienced by the clogged particles increases with an increase in D_b/D_s because the force transferred between two heavier particles is larger than that of two lighter particles. Moreover, I noticed a dip in the pressure experienced by the clogged particles in the central region of a clog indicating that the weakest portion of an arch could be at the centre of the arch. The time-averaged flow fields revealed that with an increase in D_b/D_s, pressure and shear stress is found to increase because the force transmission is more among heavier particles than that of lighter particles.

BIBLIOGRAPHY

[1] M. E. Cates, J. P. Wittmer, J.-P. Bouchaud, and P. Claudin. Jamming, force chains, and fragile matter. *Phys. Rev. Lett.*, 81:1841–1844, Aug 1998.

[2] A. Janda, I. Zuriguel, A. Garcimartín, L. A. Pugnaloni, and D. Maza. Jamming and critical outlet size in the discharge of a two-dimensional silo. *EPL (Europhysics Letters)*, 84(4):44002, 2008.

[3] Angel Garcimartín, Iker Zuriguel, Luis A. Pugnaloni, and Alvaro Janda. Shape of jamming arches in two-dimensional deposits of granular materials. *Phys. Rev. E*, 82:031306, Sep 2010.

[4] Kiwing To and Pik-Yin Lai. Jamming pattern in a two-dimensional hopper. *Phys. Rev. E*, 66:011308, Jul 2002.

[5] C. Lozano, I. Zuriguel, and A. Garcimartín. Stability of clogging arches in a silo submitted to vertical vibrations. *Phys. Rev. E*, 91:062203, Jun 2015.

[6] R. C. Hidalgo, C. Lozano, I. Zuriguel, and A. Garcimartín. Force analysis of clogging arches in a silo. *Granular Matter*, 15(6):841–848, Dec 2013.

[7] C. C. Thomas and D. J. Durian. Geometry dependence of the clogging transition in tilted hoppers. *Phys. Rev. E*, 87:052201, May 2013.

[8] L. Pournin, M. Ramaioli, P. Folly, and Th. M. Liebling. About the influence of friction and polydispersityon the jamming behavior of bead assemblies. *The European Physical Journal E*, 23(2):229, Jun 2007.

[9] Iker Zuriguel, Angel Garcimartín, Diego Maza, Luis A. Pugnaloni, and J. M. Pastor. Jamming during the discharge of granular matter from a silo. *Phys. Rev. E*, 71:051303, May 2005.

[10] A. Vamsi Krishna Reddy, Sonu Kumar, K. Anki Reddy, and Julian Talbot. Granular silo flow of inelastic dumbbells: Clogging and its reduction. *Phys. Rev. E*, 98:022904, Aug 2018.

[11] Daniel R. Parisi, Raúl Cruz Hidalgo, and Iker Zuriguel. Active particles with desired orientation flowing through a bottleneck. *Scientific Reports*, 8(1):9133, Jun 2018.

[12] Junyao Tang and R. P. Behringer. Orientation, flow, and clogging in a two-dimensional hopper: Ellipses vs. disks. *EPL (Europhysics Letters)*, 114(3):34002, may 2016.

[13] Tamás Börzsönyi, Ellák Somfai, Balázs Szabó, Sandra Wegner, Pascal Mier, Georg Rose, and Ralf Stannarius. Packing, alignment and flow of shape-anisotropic grains in a 3d silo experiment. *New Journal of Physics*, 18(9):093017, sep 2016.

[14] A. Ashour, S. Wegner, T. Trittel, T. Börzsönyi, and R. Stannarius. Outflow and clogging of shape-anisotropic grains in hoppers with small apertures. *Soft Matter*, 13:402–414, 2017.

[15] Matthew Dennison, Kristina Milinković, and Marjolein Dijkstra. Phase diagram of hard snowman-shaped particles. *The Journal of Chemical Physics*, 137(4):044507, 2012.

[16] Youngkyu Han, Juncheol Lee, Siyoung Q. Choi, Myung Chul Choi, and Mahn Won Kim. Shape-induced chiral ordering in two-dimensional packing of snowmanlike dimeric particles. *Phys. Rev. E*, 88:042202, Oct 2013.

[17] P. A. Cundall and O. D. L. Strack. A discrete numerical model for granular assemblies. *Géotechnique*, 29(1):47–65, 1979.

[18] Steve Plimpton. Fast parallel algorithms for short-range molecular dynamics. *Journal of Computational Physics*, 117(1):1 – 19, 1995.

[19] Alexander Stukowski. Visualization and analysis of atomistic simulation data with ovito–the open visualization tool. *Model. Simul. Mater. Sci. Eng*, 18(1):015012, 2010.

[20] Nikolai V. Brilliantov, Frank Spahn, Jan-Martin Hertzsch, and Thorsten Pöschel. Model for collisions in granular gases. *Phys. Rev. E*, 53:5382–5392, May 1996.

[21] M. Acevedo, I. Zuriguel, D. Maza, I. Pagonabarraga, F. Alonso-Marroquin, and R. C. Hidalgo. Stress transmission in systems of faceted particles in a silo: the roles of filling rate and particle aspect ratio. *Granular Matter*, 16(4):411–420, Aug 2014.

[22] Tamás Börzsönyi, Ellák Somfai, Balázs Szabó, Sandra Wegner, Pascal Mier, Georg Rose, and Ralf Stannarius. Packing, alignment and flow of shape-anisotropic grains in a 3d silo experiment. *New Journal of Physics*, 18(9):093017, sep 2016.

[23] Aidan P. Thompson, Steven J. Plimpton, and William Mattson. General formulation of pressure and stress tensor for arbitrary many-body interaction potentials under periodic boundary conditions. *The Journal of Chemical Physics*, 131(15):154107, 2009.

[24] B. J. Glasser and I. Goldhirsch. Scale dependence, correlations, and fluctuations of stresses in rapid granular flows. *Physics of Fluids*, 13(2):407–420, 2001.

CHAPTER 7

CLOGGING REDUCTION AT AN ORIFICE DUE TO FLOW THROUGH AN ADJACENT LARGER ORIFICE

7.1 Introduction

Flow of granular particles through a multi orifice silo has been a topic of interest due to its wide variety of applications in industries. Kamath *et al.* [1] reported that a multi-orifice silo can be very useful in the effective mixing of the particles. The transverse motion of the particles is enabled by a random opening and closing of orifices. The authors suggested that the degree of mixing was can be altered by controlled opening and closing of orifices or by letting the orifice jam and unjam intermittently by keeping smaller orifices. Moreover, they indicated that the stagnant zone can be eliminated, a feature that can't be found in a flat-bottomed single orifice silo. The effect of inter-orifice distance and the coefficient of friction between the particles on jamming and unjamming behaviour in a multi-orifice silo is studied by [2]. The mean jamming time and flowing time was observed to increase and decrease with an increase in the inter-particle friction coefficient. However, the frequency of unjamming instances was noticed to behave non-monotonically with friction-coefficient. Cheng *et al.* [3] proposed an empirical equation relating the flow rate and inter-orifice distance for a two-dimensional multi-orifice system. The authors attributed the relation to the velocity above the orifices and the interaction between the orifices. Moreover, Zhang *et al.* [4] as well proposed a relation

between flow rate and inter-orifice distance in a multi-orifice silo. The authors noticed that the velocity field above an orifice is influenced by the other orifice thus decreasing the stagnant zone but doesn't influence the packing fraction field. Spontaneous jamming and unjamming behaviour at an orifice thus increasing the overall amount of particles discharged by an order of magnitude due to the presence of an adjacent orifice of the same outlet size were noticed by [5]. The authors reported that at large inter-orifice distances, only fluctuations from the flowing orifice is reason to unjam a jammed orifice. However, at small inter-orifice distances, along with fluctuations, flow is also a reason to unjam a jammed orifice. The flow of particles through a multi-orifice rectangular silo is studied by [6] using particle image velocimetry and DEM simulations. The flow rate was found to decrease with an increase in the inter-orifice distance reaches a minimum and then again increases until it reaches a saturated value which is roughly twice that of the flow through a single orifice.

Most of the two-orifice problems in a silo were dealt with spherical particles in a two or three-dimensional silo. There is hardly any work reported in the literature that investigated the flow of non-spherical particles in a two-dimensional silo with multiple orifices. In this work, we studied how the flow of dumbbells is affected by the inter-orifice distance and width of the smaller orifice. In the next section, we explained the simulation technique used and the simulation system. In section 7.3, results are discussed and in section 7.4 conclusions are reported.

7.2 Simulation Methodology

We used the discrete element method (DEM) [7] to study the flow of dumbbells flowing through a two-dimensional silo with multiple orifices on the silo base. Please see chapter 2 for the explanation of the DEM technique. A schematic diagram of our simulation system is shown in figure 7.1 consisting of dumbbell particles. A dumbbell is created by fusing two discs each of diameter d adjacent to each other. Initially, we placed a few randomly oriented dumbbells at arbitrary locations inside a silo confined by walls at $x/d = \pm 75$ and $y = 0$. The origin is located at the centre of the silo base. A gravity of magnitude g is applied in the negative-y direction which lets the dumbbells settle at the bottom of the silo. At regular intervals of time, the dumbbells are poured into the silo until the total number of dumbbells reach $N_t = 20000$. Thus, the height of the granular bed is noticed to reach $y/d \approx 250$. At time $t = 0$, two orifices of widths W_1 and W_2 placed

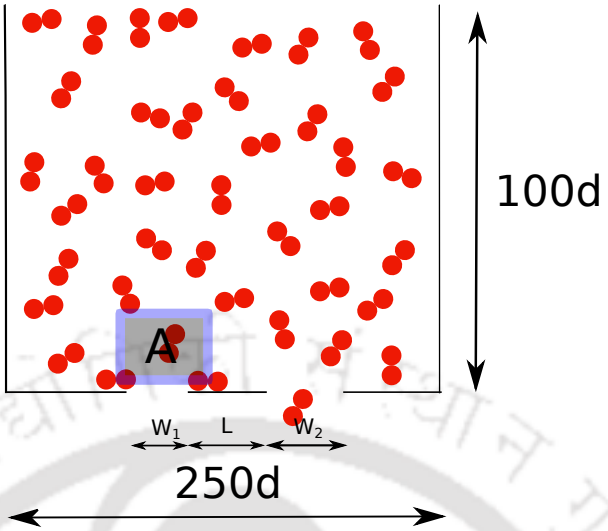

Figure 7.1: The schematic representation of a two-dimensional silo with multiple orifices on the silo base. Here, W_1 is the width of the smaller orifice which might get clogged whereas, W_2 is the width of the larger orifice through which there is an uninterrupted flow and the red ones indicate dumbbells. Moreover, L is the inter orifice distance. The origin is located at the centre of the silo which is equidistant from both the side walls.

Simulation parameters	Values
K_n	$2.00 \times 10^6 \rho d g$
K_t	$2.45 \times 10^6 \rho d g$
γ_n	$1000\sqrt{g/d^3}$
γ_t	$1000\sqrt{g/d^3}$
μ	0.5
$timestep$	$10^{-4}\sqrt{d/g}$

Table 7.1: The constants used in our numerical simulations

on the silo base are opened to let the particles flow out of the silo. We applied periodic boundary conditions (PBC) in the y direction and the particles flowing out of the silo are placed on the top of the granular bed. The values of various constants used in the simulations are displayed in Table 7.1.

7.3 Results and Discussion

In this work, we studied how the clogging characteristics at an orifice are affected due to the presence of a continuous flow of particles through an adjacent larger orifice. Firstly, the width of the larger orifice is set to $W_2/d = 20$ and the clogging phenomena

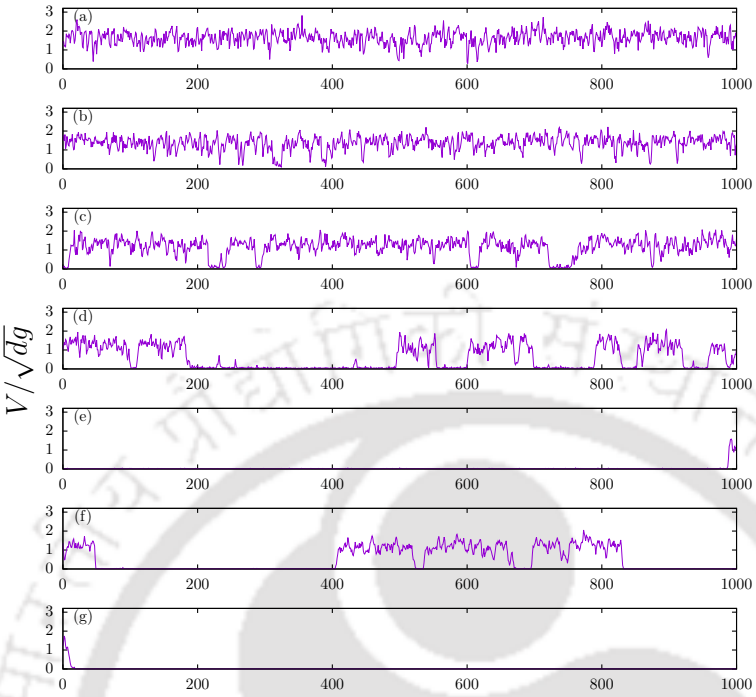

Figure 7.2: Time-evolution of average velocity in the region above the smaller orifice for an inter orifice distance L/d = a)5, b)10, c)20, d)25, e)50, f)100, g)150.

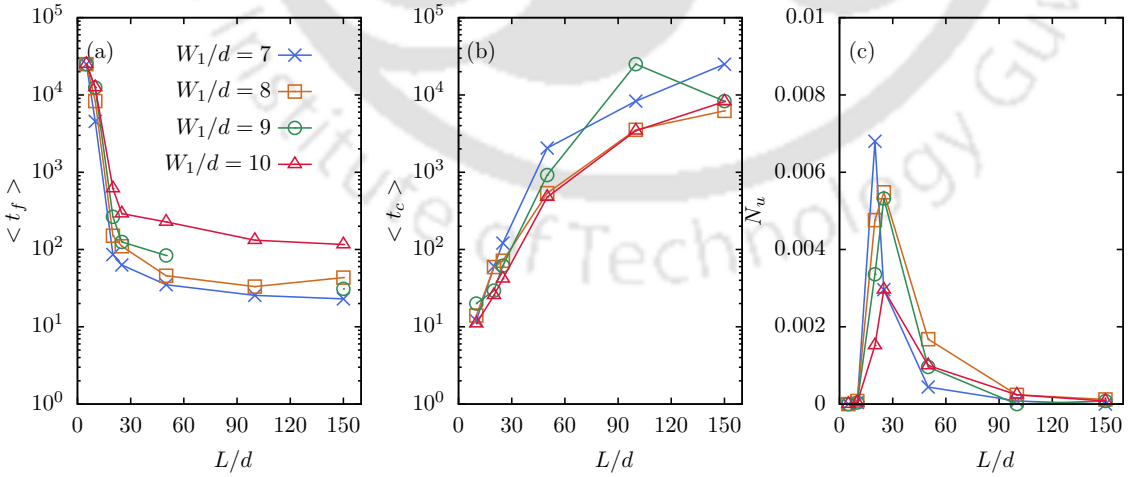

Figure 7.3: a) Average flowing time $< t_f >$ and b) average clogging time $< t_c >$ and c) the number of clogging instances per unit time N_u as a function of inter orifice distance L/d for different widths of the smaller orifice W_1/d.

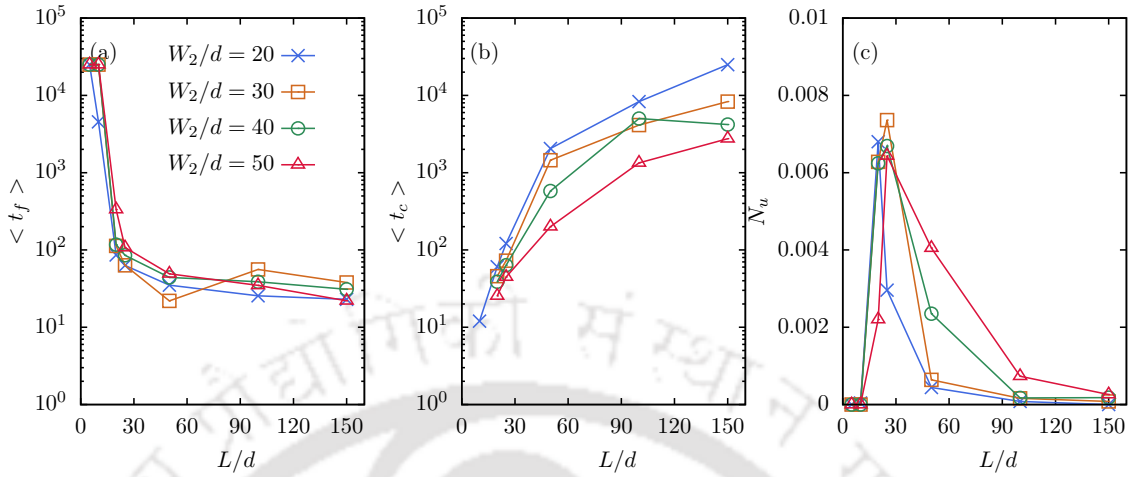

Figure 7.4: a) Average flowing time $< t_f >$ and b) average clogging time $< t_c >$ and c) the number of clogging instances per unit time N_u as a function of inter orifice distance L/d for different widths of the larger orifice W_2/d.

are analysed at four different widths of the smaller orifice $W_1/d = 7, 8, 9, 10$. Later, the width of the smaller orifice $W_1/d = 7$ is fixed and the effect of the driving force from the larger orifice is determined by varying the width of the larger orifice $W_2/d = 20, 30, 40, 50$. Moreover, at each above-mentioned cases, we considered seven different inter-orifice distances ranging from $L/d = 5$ to $L/d = 150$.

We have plotted the time evolution of average velocity in the region above the smaller orifice at different inter orifice distances (figure 7.2). When the plot is fluctuating, it implies a flow through the orifice whereas, a straight line showing $V \approx 0.0$ indicates a clogged state. At small inter orifice distances $L/d \leq 10$ the smaller orifice hardly gets clogged and at $10 < L/d < 50$, it gets clogged and automatically gets unclogged due to flow through the adjacent orifice. However, at large inter-orifice distances, $L/d \geq 50$, the time for unclogging is significantly high. Further, we investigated how the average flowing time and average clogging time and the frequency of unclogging instances are influenced by the inter orifice distance (figure 7.3). There is a sharp decrease in the average flowing time $< t_f >$ through the smaller orifice until $L/d = 20$ because there are hardly any clogging instances until $L/d = 20$ as noticed in figure 7.2. At $L/d > 25$, flowing time gets saturated with a slight decrease with an increase in L/d as the orifice gets clogged for longer durations of time. The average clogging time $< t_c >$ increases gradually with an increase in inter orifice distance. These two results suggest that the influence of flow

through the larger orifice decreases with an increase in the inter orifice distance. At small inter-orifice distances $L/d \leq 25$, both the orifices interact. I noticed maxima in the frequency of unclogging events per unit time N_u at $L/d = 25$ for all the smaller orifice widths. This is because at $L \leq 10$, there are hardly any clogging events and hence the frequency of unclogging is less. Moreover, at $L/d \geq 50$, the larger orifice is ineffective in unclogging the smaller orifice resulting in a decrease in N_u. This result indicates that the larger orifice is effective in unclogging the smaller orifice at an inter-orifice distance of $L/d = 25$. Further, I analysed how the width of the larger orifice W_2/d affects the clogging phenomena near the smaller orifice. To this end, I studied the system at four different widths of the larger orifice W_2/d ranging from 20 to 40 by keeping the width of the smaller orifice $W_1/d = 7$ and for different L/d. Flowing time is almost unaffected by the larger orifice width however, the clogging time is noticed to decrease with an increase in W_2/d as shown in figure 7.4.

To explore the reasons behind the interaction dynamics between the two orifices, I analysed the velocity v and velocity fluctuations v_{fl} inside the silo due to the particles flowing through the larger orifice. Firstly, I identified how the velocity and velocity fluctuations in the region of the arch formation above the smaller orifice are affected by variation in L/d (figure 7.5). With an increase in the inter orifice distance, I observed that both the velocity and fluctuations in velocities decreases. A decrease of two orders of magnitude in the velocity and a decrease of four orders of magnitude in the velocity fluctuations is noticed. This shows that the velocity fluctuations play a major role in the process of unclogging by the larger orifice. This is the reason for an increase in the clogging time or a decrease in the frequency of unclogging events with an increase in L/d as seen in figure 7.3. These fluctuations in velocity might cause the clogged structure to get destabilized. Further, I analysed the v and v_{fl} at different distances from the larger orifice to understand the effect of the larger orifice on its surroundings. Figure 7.6 shows velocity and its fluctuations at different distances x/d from the larger orifice of width $W_2/d = 20$ and $L/d = 150$. We noticed similar behaviour as that of figure 7.3. This further suggests that the velocity fluctuations play a major role in the process of unclogging the smaller orifice.

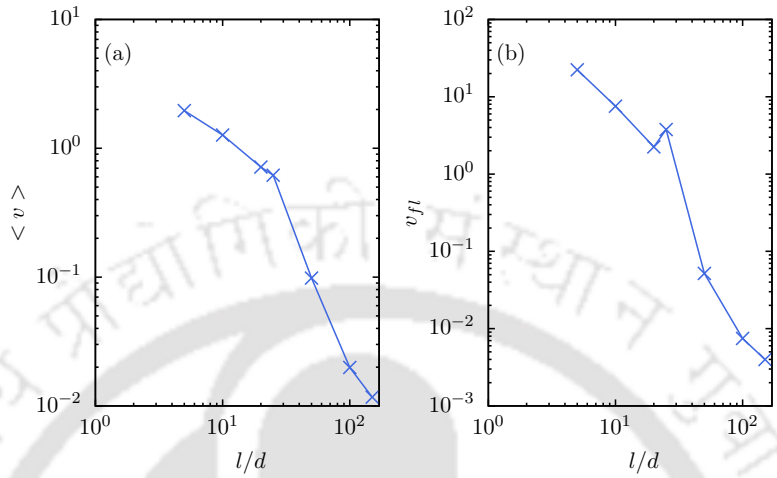

Figure 7.5: a) Velocity profiles and b) fluctuations in velocities v_{fl} in the region above the smaller orifice at different inter orifice distances L/d.

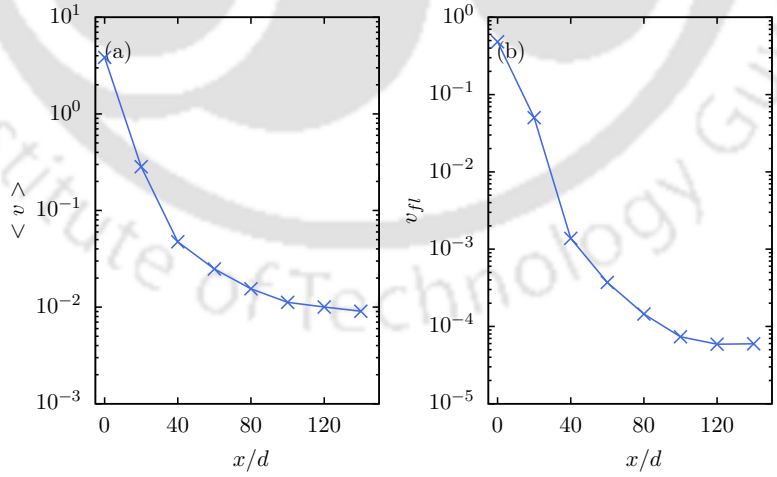

Figure 7.6: a) The velocity profile $< v >$ and b) fluctuations in velocity v_{fl} at different horizontal positions with $x = 0$ as the centre of the larger orifice.

7.4 Conclusion

Here, we studied the flow of non-spherical particles through a multi-orifice silo. Our main goal is to understand how the clogging behaviour at a smaller orifice is influenced by the presence of continuous flow through an adjacent larger orifice. We varied inter-orifice distance ranging from $5d$ to $150d$ and noticed how it affects the flowing and clogging events at the smaller orifice. The flowing time decreases sharply at lower inter-orifice distances L/d and get saturated at larger L/d. The average clogging time is close to zero at small inter-orifice distances and increases gradually with an increase in the inter-orifice distance. This can be attributed to the fluctuations emanating from the continuous flow through the larger orifice. Moreover, the frequency of unclogging instances per unit time is maximum at an inter orifice distance of 25. A decrease of four orders of magnitude in the velocity fluctuations with an increase in the inter-orifice distance suggests that it is the prime reason for a decrease in the efficiency of the larger orifice.

BIBLIOGRAPHY

[1] Sandesh Kamath, Amit Kunte, Pankaj Doshi, and Ashish V. Orpe. Flow of granular matter in a silo with multiple exit orifices: Jamming to mixing. *Phys. Rev. E*, 90:062206, Dec 2014.

[2] Ashish V. Orpe and Pankaj Doshi. Friction-mediated flow and jamming in a two-dimensional silo with two exit orifices. *Phys. Rev. E*, 100:012901, Jul 2019.

[3] Cheng Xu, Fei-Liang Wang, Li-Peng Wang, Xiao-Shuang Qi, Qing-Fan Shi, Liang-Sheng Li, and Ning Zheng. Inter-orifice distance dependence of flow rate in a quasi-two-dimensional hopper with dual outlets. *Powder Technology*, 328:7 – 12, 2018.

[4] Xuezhi Zhang, Sheng Zhang, Guanghui Yang, Ping Lin, Yuan Tian, Jiang-Feng Wan, and Lei Yang. Investigation of flow rate in a quasi-2d hopper with two symmetric outlets. *Physics Letters A*, 380(13):1301 – 1305, 2016.

[5] Amit Kunte, Pankaj Doshi, and Ashish V. Orpe. Spontaneous jamming and unjamming in a hopper with multiple exit orifices. *Phys. Rev. E*, 90:020201, Aug 2014.

[6] L. A. Fullard, E. C. P. Breard, C. E. Davies, A. J. R. Godfrey, M. Fukuoka, A. Wade, J. Dufek, and G. Lube. The dynamics of granular flow from a silo with two symmetric openings. *Proceedings of the Royal Society A: Mathematical, Physical and Engineering Sciences*, 475(2221):20180462, 2019.

[7] P. A. Cundall and O. D. L. Strack. A discrete numerical model for granular assemblies. *Géotechnique*, 29(1):47–65, 1979.

[8] Steve Plimpton. Fast parallel algorithms for short-range molecular dynamics. *Journal of Computational Physics*, 117(1):1 – 19, 1995.

[9] Alexander Stukowski. Visualization and analysis of atomistic simulation data with ovito–the open visualization tool. *Model. Simul. Mater. Sci. Eng*, 18(1):015012, 2010.

CHAPTER 8

CONCLUSIONS

In this dissertation, we studied the flow of granular particles discharging through a flat-bottomed silo. In our work, we studied systems of dumbbells or systems involving a mixture of dumbbells and discs.

The output of this dissertation is summarized as follows:

- The clogging probability of dumbbells (ar=2) is significantly higher than that of discs(ar=1). The size and position of the obstacle have a marked influence on the probability of clogging for a system of dumbbell particles. An important observation is the nonmonotonicity of the clogging index with the height of the obstacle.

- Flow rate of the mixture of dumbbells and discs decreases with an increase in the fraction of dumbbells X_{db}. Self-similar velocity profiles with horizontal positions are observed for all mixture concentrations. Mean flow fields are presented at various fractions of dumbbells. The temporal-averaged velocity fields revealed an expansion of the stagnant zone beside the orifice with an increase in the fraction of dumbbells. The stagnant zone hinders the flow thus resulting in a decrease in the flow rate with an increase in X_{db}. As X_{db} increases, the arch shape deviates from semi-circle.

- Flow rate decreases with an increase in the fraction of dumbbells for the case of lateral orifice due to an increase in the dynamic friction resulting from geometrical

interlocking. The area fraction at the lateral orifice is more as compared to that near an orifice on the silo base. Flowrates are scaled with orifice width using a modified Beverloo's law in the lateral orifice case. Flow rate decreases with an increase in the inter orifice distance L/d for the case of multiple orifices placed on the silo base. The flow fields revealed that the stagnant zone between the orifices expands with an increase in L/d resulting in higher pressure and higher shear stress in the region between the orifices.

- Avalanche size increases with an increase of D_b/D_s. There is a dip in the average pressure experienced by the clogged particles in the region close to the centre of the arch which possibly is the weakest portion of an arch. Flow rate is found to increase with an increase in D_b/D_s which is consistent with an increase in velocity as observed in flow fields. Pressure and shear stress increase with an increase in D_b/D_s as larger particles can transmit stress more effectively than smaller particles.

- With an increase in inter orifice distance l/d, the average flowing time of a smaller orifice is decreasing and the average clogged time is increasing in the presence of a continuous flow through an adjacent larger orifice. Fluctuations in velocity in the region of arch formation are decreasing with an increase in l/d.

8.1 Scope of future work

Some works which can be interesting for the future are summarized here:

- Clogging phenomena in a system of dumbbells flowing inside a silo with a rotatable obstacle placed just above the orifice.

- Reduction in clogging probability of elongated particles in a silo consisting of multiple obstacles.

- Flow characteristics of elongated particles with different aspect ratios flowing out of a silo.

- A mathematical relation for the flow rate of elongated particles discharging through a flat-bottomed silo.

- Flow rate scaling for a mixture of randomly shaped particles discharging out of a silo.
- Clogging mechanism for a system of non-spherical particles in a 3D silo.

List of Publications

.

Articles published

- A. Vamsi Krishna Reddy, Sonu Kumar, K. Anki Reddy and Julian Talbot. Granular silo flow of inelastic dumbbells: Clogging and its reduction. *Phys. Rev. E* **98**, 022904 (2018).
- A. Vamsi Krishna Reddy, Sonu Kumar and K. Anki Reddy. Granular particle-shape heterogeneous mixtures discharging through a silo. *J. Fluid. Mech* vol. 912, (2021).

Papers submitted

- A. Vamsi Krishna Reddy and K. Anki Reddy. Granular mixtures discharging through a silo with eccentric orifice location. *Soft Matter* (Revised version).
- A. Vamsi Krishna Reddy, K. Anki Reddy, Iker Zuriguel and Hiroaki Katsuragi. Clogging phenomena in a system of asymmetric dumbbells. *J. Stat. Mech* (Minor comments).

Manuscripts under preparation

- A. Vamsi Krishna and K. Anki Reddy. Clogging reduction at an orifice due to flow through an adjacent larger orifice.
- A. Vamsi Krishna Reddy, K. Anki Reddy, Iker Zuriguel and Hiroaki Katsuragi. Flow characteristics in a system of asymmetric dumbbells.